COUPLING ISOTACHOPHORESIS TO REACTION AND SEPARATION ASSAYS

A DISSERTATION

SUBMITTED TO THE DEPARTMENT

OF MECHANICAL ENGINEERING

AND THE COMMITTEE ON GRADUATE STUDIES

OF STANFORD UNIVERSITY

IN PARTIAL FULFILMENT OF THE REQUIREMENTS

FOR THE DEGREE OF

DOCTOR OF PHILOSOPHY

Charbel Eid

August 2016

This dissertation is online at: http://purl.stanford.edu/mz211tm5739

I certify that I have read this dissertation and that, in my opinion, it is fully adequate in scope and quality as a dissertation for the degree of Doctor of Philosophy.

Juan Santiago, Primary Adviser

I certify that I have read this dissertation and that, in my opinion, it is fully adequate in scope and quality as a dissertation for the degree of Doctor of Philosophy.

Beth Pruitt

I certify that I have read this dissertation and that, in my opinion, it is fully adequate in scope and quality as a dissertation for the degree of Doctor of Philosophy.

Lewis A. Marshall

Approved for the Stanford University Committee on Graduate Studies.

Patricia J. Gumport, Vice Provost for Graduate Education

This signature page was generated electronically upon submission of this dissertation in electronic format. An original signed hard copy of the signature page is on file in University Archives.

Abstract

Molecular diagnostics are rapidly growing with applications in disease detection, genetic profiling, forensic investigation, and various research purposes. These techniques include PCR, sequencing, antibodies, and hybridization assays, and offer exquisite sensitivity and multiplexity. However, widespread adoption of molecular diagnostics is constrained by a number of key challenges. Assay times often take 16 hours or more, due to slow second order hybridization kinetics as well as time-consuming sample preparation methods. Furthermore, sample preparation itself is laborious, requiring manual intervention by highly-skilled personnel at several steps in the workflow.

This dissertation discusses approaches that leverage isotachophoresis (ITP) and its coupling to at least one other assay step with an aim to significantly reduce analysis times and complexity of molecular detection assays. ITP is an electrokinetic technique which uses a heterogeneous buffer system to preconcentrate and separate ions based on their electrophoretic mobilities. In the first part of this dissertation, we present a simple analytical model to describe accumulation and reaction rates in ITP. This model is useful in the design of ITP experiments, and enables a user to make informed decisions regarding optimal sample placement in ITP assay design.

In the second part of this dissertation, we describe a novel approach that leverages ITP to accelerate chemical reactions and also use an ionic spacer to separate reaction products. We first demonstrate this approach using synthetic DNA targets, and show high-sensitivity detection in a 10 min assay. We then extend this technique and use high-

mobility probes to recruit typically non-focusing species (such as proteins) into ITP. We demonstrate this assay using C-reactive Protein (CRP) in buffer as well as in diluted serum. We also present a numerical and analytical model to describe ITP assays that involve non-focusing targets recruited into ITP.

The last part of this dissertation shows how ITP purification can simplify sample preparation protocols and integrate with downstream analysis methods. We first show size-based RNA fractionation using ITP in a 10 min assay. We use a commercial electrophoresis system to analyze resulting sample fractions. Finally, we show how ITP purification can extend the applicability of recombinase polymerase amplification (RPA) to whole blood samples. We demonstrate lysis, purification, and detection of inactivated *Listeria Monocytogenes* cells from whole blood using ITP and RPA.

Acknowledgements

Back in 2006, when I was still in Lebanon and in the process of applying to undergraduate programs in the US, I purposely did not apply to Stanford. Wisely, I realized at the time that I was a longshot to be accepted to a top American university. Less wisely, I thought that being rejected for undergrad would somehow blacklist me from being accepted later on, if I applied for graduate school. I was so blown away by Stanford, from oceans away, that it was the only university in the whole country that I treated with such reverence. As I reflect on my time here, I somehow feel even more reverence but also love for this place and all that it has given me. Completing a doctorate is no one's idea of fun, and certainly my particular path has not been without its twists and turns. But it has, without a doubt, been a wonderful journey.

I'd like to first thank Juan Santiago for accepting me into his lab in 2011, and for being my advisor ever since. His guidance and advice have greatly shaped me professionally and taught me a lot about how to be a good scientist and engineer. I also want to thank Ellen Kuhl who has been a fantastic advocate for me when I really needed one. It is almost certain that without her help, I would not have made it through some of the leaner times.

To my labmates, thank you for the mentorship, camaraderie, and collaboration that you've given me over the years. The Santiago lab is a special group of people, and I will miss you all tremendously. Special thank you to Giancarlo, Yatian, and Deni for the cherished friendships that came out of our time together in the lab.

I've been extremely fortunate to be part of some amazing groups and associations over my time here that have contributed as much as anything else to my personal and

professional growth. Being part of the Stanford Biodesign program has been one of the single best and most rewarding experiences of my life. I'd also like to thank InciteHealth, Patient Partners, Stanford EMT, and Biotech Connections Bay Area for igniting my love for healthcare and medical technology. As I move forward in my career, my primary goal is to create some value in those worlds. I'd also like to thank the Stanford community associate (CA) program for the opportunity to be a CA for several years. I learned the hard way what it's like to run events for hungry graduate students. A big thank you to Stanford VPGE for awarding me the Lieberman fellowship. This funding changed the path of my PhD and gave me a second life. Through VPGE I also had the opportunity to be a mentor in the EDGE program, and met amazing people along the way.

Like most experiences in life, this one is largely defined by the amazing friends I've made throughout my time here. To the following people, I love you all tremendously: Adam H., Adam M., Adrian, Alex Z., Andrea, Ann, Annika, Antoine, Apoorva, Avril, Brittany, Capella, Clara, Clement, Daniel , Daniela, Fadi Z., Greg , Hannah S., Henryk, Josh, Julien, Louis, Martin, Michel, Michele, Nicholas, Ralph, Si Tan, Thomas, Vicky, Yorgos, and everyone else I am invariably forgetting at this very moment (I'm very sorry, I'm on a deadline!)

There are a few people that have made a particularly indelible mark on my life and I want to recognize that. To Hannah D., French sister, you're kickass and always helped humble me (usually through mockery) and keep me in line. You supported me through some hard times early on, and helped get me through to a much better side. To Liliana, you might be the most unique person I've ever met in my life, and I admire that so much

about you. I feel so lucky to be your friend. To Maria, though you take so much joy in making fun of me, I take even more joy in returning the favor. You have been a wonderful friend, a go-to when I just want to talk (or rant) about anything. To Hardik, you're a silly, silly man, but you're a wonderful friend and a constant source of laughter and support.

To Lorenzo, I value your friendship like nothing else. I feel like you complete the missing parts of my personality. You're an amazing friend and just a fantastic person altogether. To Mike, I can't even imagine what this place would have been like without you. There has never and will never be someone who is exactly on the same wavelength as me. Thank you for giving me some of the best times of my life over these past 6 years. As the youths (of 2016) would say, you're my #bff.

To Diana, thank you for loving and sticking by me all these years. Your love of life and people is infectious. You inspire me to be a better (and more mature) person. There would be no PhD without you. You're the best.

Finally, and most importantly, I would like to thank my family. My brother is my favorite person in the world, plain and simple. My parents are my inspiration. I owe any good quality I have to their love and support. They have given me everything. I hope to one day be a fraction as loving, courageous, and supportive as they are.

As Bruce Springsteen (you knew it was coming) once said, "Talk about a dream, try to make it real". I'm eternally grateful for the wonderful memories and the amazing times I've had at this university. It's truly been an honor. This dissertation is dedicated to everyone who helped me get here.

Table of Contents

List of Tables

List of Figures

Figure 2.5. Ratio of sample accumulation rate into ITP zone from TE and LE, ϕ, as a function of several experimental parameters for values typical of DNA and RNA focusing using ITP. For all plots, we assumed Cl^- as LE species, with mobility of 79 x 10^{-9} $m^2V^{-1}s^{-1}$. a) ϕ as a function of the mobility difference between sample and TE for TE mobilities ranging from 5 x 10^{-9} to 25 x 10^{-9} $m^2V^{-1}s^{-1}$ and sample mobilities ranging from 26 to 38 x 10^{-9} $m^2V^{-1}s^{-1}$ results in essentially collapsed curves, indicating that this difference is a simple and predictive indicator of optimal initial sample loading. We set the ratio of initial LE and TE concentrations, γ, equal to 6 for demonstration purposes, though we note that the curves plotted largely collapse independently of γ value used. Unity (dashed red line) is a threshold value for ϕ. For ϕ > 1, sample ions should be loaded in the TE. For ϕ < 1, they should be loaded into the LE. b) ϕ is plotted as a function of TE mobilities, again ranging from 5 x 10^{-9} to 25 x 10^{-9} $m^2V^{-1}s^{-1}$, and values of γ ranging from 1 to 10. For higher values of γ, placing sample in TE results in significantly greater sample concentration in ATE zone, which in turn leads to much higher flux rate from the TE compared to LE. We set sample mobility as 30 x 10^{-9} $m^2V^{-1}s^{-1}$, an approximation of free-solution mobility of DNA. c) Here we plot ϕ for TE mobilities ranging from 5 to 25 x 10^{-9} $m^2V^{-1}s^{-1}$ and sample mobilities ranging from 26 x 10^{-9} to 38 x 10^{-9} $m^2V^{-1}s^{-1}$. Similarly to a), we set γ = 6 for demonstration purposes.

1 Introduction

1.1 Introduction to molecular detection assays

Molecular diagnostics are increasingly ubiquitous in both clinical and research settings. The term encompasses techniques that detect the presence of and may quantify the presence of molecular biomarkers (including nucleic acids and proteins) associated with various functions and pathologies. Nucleic acid assays, for example, have been used in disease detection, forensic sciences, genetic profiling, and food analysis.[12-14] The proteome, particularly the plasma proteome, which contains plasma proteins as well as tissue proteins and a variety of immunoglobulins, transmits immediate information about phenotype and is especially attractive in medical diagnostics.[15,16]

The most commonly used techniques for nucleic acid detection are amplification techniques and microarray and other hybridization techniques. Among nucleic acid amplification techniques, PCR is the most established and clinically-adopted. PCR is exquisitely sensitive, capable of detecting even a single copy. However, it requires extensive sample preparation, suffers from different levels of biases, and generally requires highly skilled technicians to perform sample preparation.[17,18] Microarrays are gaining popularity, and offer the potential for multiplexing, but they suffer from long hybridization steps, high cost, and difficulty in interpreting and quantifying results.[19-21]

Currently, the two leading techniques for protein detection are mass spectrometry and antibody assays.[22] Mass spectrometry is able to resolve complex samples with high fidelity. However, it is a time-consuming and laborious approach which requires several manual steps. Mass spectrometry is also highly sensitive to a large number of detergents

and polymers commonly used in sample preparation and results can be adversely affected by high salt concentration.[23] Antibody-based assays, on the other hand, offer high sensitivity and specificity, and have been accepted as a 'gold standard' in protein biomarker detection and quantification. However, immunoassays are limited by the availability and quality (e.g., affinity) of available antibodies targeting specific proteins. Furthermore, antibodies are very sensitive to factors like temperature and pH, and can undergo irreversible denaturation.[24]

Despite many advances made in the field, a number of common challenges remain that are inhibiting more widespread adoption of molecular diagnostic tools:

- *Long assay times:* All molecular detection assays include hybridization and reaction steps, with incubation times that are often up to 16-24 h long. Molecular diagnostic assays are characterized by second-order reaction kinetics, which at clinically-relevant target concentrations can lead to very slow reaction rates and increase assay time. Time-consuming sample preparation methods also contribute to long assay times. This is particularly true in infectious disease diagnostics, as well as assays from whole blood samples, where sample preparation may take hours or days.[25]
- *Complexity:* Another important limitation of current molecular detection techniques is laborious sample preparation methods.[25] Though recent development of high-quality commercial kits for nucleic acid extraction has reduced the sample preparation time in moderately complex samples, the workflow remains very laborious. Typical sample preparation methods involve multiple steps of mixing, centrifugation, separation, and buffer exchange, and

wash steps. All these steps require manual intervention as well as highly-skilled and trained personnel.

- *High costs:* Cost of highly-skilled labor, costs of maintaining specialized facilities and equipment to perform these assays, and high prices for many commercial kits and reagents all contribute to an overall large cost burden in these assays.

In this dissertation, we present and discuss approaches to significantly reduce assay times and complexity. Our work also lays the platform for automation and miniaturization of workflows, which is a first step towards reducing costs.

1.2 Introduction to isotachophoresis (ITP)

1.2.1 Fundamentals of ITP

Isotachophoresis (ITP) is a simple and robust electrophoretic technique that can preconcentrate, purify, and separate a wide range of chemical and biological species. For example, the Santiago group has shown that ITP can achieve million-fold preconcentration in a matter of minutes.[26] Similar to other electrophoretic methods, species in ITP electromigrate and separate based on their electrophoretic mobility. Electrophoretic mobility is given by

$$U_i = \mu_i E, \tag{0.1}$$

where U_i is the drift (relative to solvent) velocity of the species, E is the local electric field, and μ is the electrophoretic mobility of the species, with units of $m^2V^{-1}s^{-1}$. ITP uses a discontinuous buffer consisting of a high-mobility leading electrolyte (LE) and a low-mobility trailing electrolyte (TE). LE and TE have the same charge sign, so ITP

buffer systems typically contain a counter ion species of an opposite charge sign, such that solutions are well-buffered during the process. The LE and TE zones have respectively high and low conductivity, which gives rise to a sharp electric field gradient at the interface. This strong electric field gradient makes ITP robust to disturbances like pressure-driven flow, rough channel surfaces, and sudden changes in channel geometry. TE ions that diffuse into the LE zone experience a significantly lower electric field, and are thus overtaken by the LE ions and fall back into their original TE zone.

For an sample species to ocus in ITP, its mobility must satisfy two conditions:[27]

$$\begin{cases} \mu_S^{TE} > \mu_{TE}^{TE} \\ \mu_S^{LE} < \mu_{LE}^{LE}, \end{cases} \tag{0.2}$$

where μ_j^X represents the mobility of species *j* (TE, LE, or sample) and *X* represents the zone the species is migrating in (TE or LE). In Figure 1.1, we demonstrate the self-sharpening feature of ITP. If a sample ion diffuses into the TE zone, it experiences the same electric field as the TE ions, but has a greater mobility in that zone, and thus has greater velocity. Similarly, a sample ion in the LE experiences a similar electric field to LE ions but has mobility, and is thus be overtaken by LE ions. As a result, sample ions with mobilities intermediate to those of the LE and TE will focus at the TE-LE interface. For a rigorous analytical and experimental study of focusing dynamics in ITP, we refer to Khurana et al.[28]

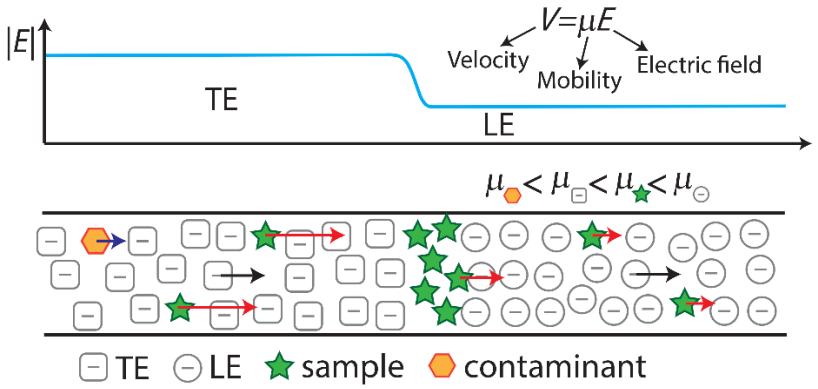

Figure 1.1. Schematic representation of selective focusing in ITP. Sample species with intermediate mobilities that are migrating in the TE zone overspeed TE ions, while those migrating in the LE zone are overtaken by LE ions. Sample species will therefore focus at the TE-LE interface, where their velocity will match that of the LE and TE zones. Species that have a mobility lower than that of the TE electromigrate but fall behind the ITP interface, whereas species with higher mobility than the LE overtake the LE.

1.2.2 Classifications of ITP assays

In this section, we briefly review various classifications of ITP assays. We emphasize discussion of peak and plateau-mode ITP, as that is fundamental to the work we present in Chapters 3 and 4. A more comprehensive discussion of dichotomies in ITP is given by Rogacs et al.[29] We here follow the presentation structure of Rogacs et al.[29] including descriptions of several relevant dichotomies associated with ITP methods.

Peak-mode vs. Plateau-mode ITP

Peak-mode ITP occurs when sample ion concentrations are several orders of magnitude smaller than those of the LE and TE buffers. Sample ions focus at a sharp interface between the LE and TE, and have negligible effect on the local ionic conductivity in the channel.[30] Multiple sample ions can co-focus within the same sharp ITP interface in largely overlapping, Gaussian-like peaks. The width of the ITP peak here is determined

by the balance of diffusion (which acts to mix species and broaden the peak) and electromigration (which acts to sharpen the interface) and is theoretically given by[31]

$$\delta_{theory} = \frac{RT}{FU_{ITP}}\left(\frac{\mu_{LE}\mu_{TE}}{\mu_{LE}-\mu_{TE}}\right), \tag{0.3}$$

where R is the universal gas constant, T is the temperature, F is Faraday's constant, and U_{ITP} is the velocity of the ITP interface. Theoretically, the interface width is constant, and sample concentration in the peak grows linearly with time. Experimentally, however, we often observe the peak growing with time. Peak-mode ITP is the predominant mode of migration for biomolecules during ITP, since species of interest are typically present in relatively low concentrations (nanomolar or less, compared with millimolar or higher, typical for buffers).

Above a certain threshold concentration, sample ions segregate into a plateau-like zone of constant concentration and increasing length.[32] For fully-ionized species (i.e., strong electrolytes), this threshold is determined by the Kohlrausch regulating function (KRF).[33] For weak electrolytes, it is given by the Alberty[34] and Jovin[35] functions instead. Plateau-mode ITP has been leveraged for many applications, including separation and indirect detection of toxins, amino acids, and others.[36-38]

In short, peak-mode ITP is well-suited for mixing and driving reaction kinetics due to co-focusing of sample ions in a high-concentration peak, whereas plateau-mode ITP is better-suited for separation of species into distinct zones. Peak and plateau-mode ITP is shown in Figure 1.2 below.

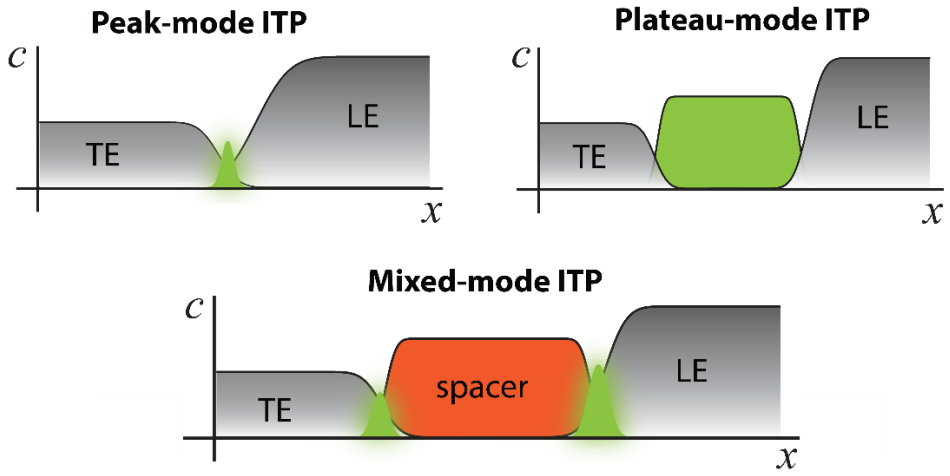

Figure 1.2. Schematic of peak and plateau-mode ITP. Dilute sample ions focus in a Gaussian-like peak. Multiple sample ions can co-focus in partially or entirely overlapping peaks, depending on their relative mobilities. The ITP peak is exaggerated considerably for visualization purposes. Sample ions at sufficiently high concentration form plateaus of constant concentration, and contribute significantly to local conductivity. Finally, it is potentially advantageous to mix peak and plaeaut-modes in the same assay, in order to drive reactions and separate products, as we discuss in Chapters 3 and 4.

Anionic vs. Cationic ITP

Another way to categorize ITP is by the sign of charge of the LE, TE, and sample ions being focused. Anionic ITP is predominantly used for assays with nucleic acid samples, owing to the negative charge present in nucleic acids above pH 3. We use anionic ITP in all experiments presented in the following chapters. Cationic ITP is commonly used for assays with proteins samples, particularly proteins with high isoelectric points.[39,40] Bidirectional ITP refers to assays that include both cationic and anionic ITP zones migrating in opposite directions.[41,42] Bidirectional ITP has been used to preconcentrate and separate reaction products,[43,44] and for simultaneous extraction of DNA and proteins from serum.[45]

Finite vs. semi-infinite injection

Semi-infinite injection refers to a configuration in which the sample is placed in the TE reservoir. In semi-infinite injection, sample accumulates continuously, though it is subject to limits on extraction efficiency due to limited buffering capacity of the reservoirs. In finite injection experiments, sample is loaded into the channel, bound on either end by the LE and TE. It is theoretically possible to extract all sample ions loaded into the channel, but a smaller volume of sample is typically loaded.

Constant voltage vs. constant current

In constant voltage experiments, voltage is held constant between the electrodes, and current decreases over time as low-conductivity TE replaces high-conductivity LE. As a result, velocity of ITP decreases in time. Constant current mode ensures a constant velocity, though voltage increases in time. We used constant current in the following chapters, in part because constant ITP velocity facilities analysis and modeling of ITP assays.

1.3 Isotachophoresis for acceleration of nucleic acid and protein reactions

An early (and perhaps earliest) demonstration of ITP to accelerate chemical reactions was by Kawabata et al.[5] Kawabata used ITP type process to focus a DNA/antibody complex, mix, and react it with a serum sample. We discuss Kawabata's work in more detail in Section 1.3.3.

Since the work of Kawabata and co-workers most work using ITP in reaction acceleration has used nucleic acid reactants. Nucleic acids hold key genetic information, and thus have widespread applications in both research applications and medical

diagnostics. In ITP assay design, nucleic acids offer a number of attractive features: they have relatively high and largely size-independent mobilities in free solution,[46] and they readily focus in ITP. Protein mobilities, on the other hand, cover a wide range of mobilities, and hard to model and predict *a priori*. Nevertheless, there have been recent attempts at accelerating reactions involving specific proteins with well-known mobilities. In this section, we trace the evolution of ITP-aided reaction assays for both nucleic acid and proteins, and highlight the primary contributions that these papers have made. We summarize these works and their contribution in Table 1.1.

1.3.1 Homogeneous NA reactions

Homogeneous nucleic acid hybridization involves reactants suspended in solution. Such assays are attractive due to their simple design and implementation. However, excess signal removal and clean-up steps are harder to incorporate into the workflow, and multiplexing is harder to achieve in this context. The first discussion of using ITP to mix reagents in the context of ssDNA hybridization came from Goet et al.[47] in 2009. This analysis came in the greater context of using ITP to bring sample zones into well-controlled contact. However, they did not demonstrate this concept experimentally.

Two years later, Persat and Santiago[1] were the first to experimentally demonstrate ITP-based hybridization with molecular beacons, using them for sequence-specific profiling of microRNA (miRNA) in total RNA samples. Molecular beacons are single-stranded DNA (ssDNA) probes with a unique hairpin structure that puts a fluorophore and quencher in close proximity.[48] Upon binding to a specific target, the structure of the probe loosens, separating the fluorophore from its quencher, and increasing observed

fluorescent signal. The authors improved assay sensitivity and specificity by using regions with different sieving matrix concentrations, to defocus long RNA and promote more stringent binding conditions. Figure 1.3 shows a schematic of their multi-stage assay. They achieved a 10 pM limit of detection in kidney and liver total RNA samples.

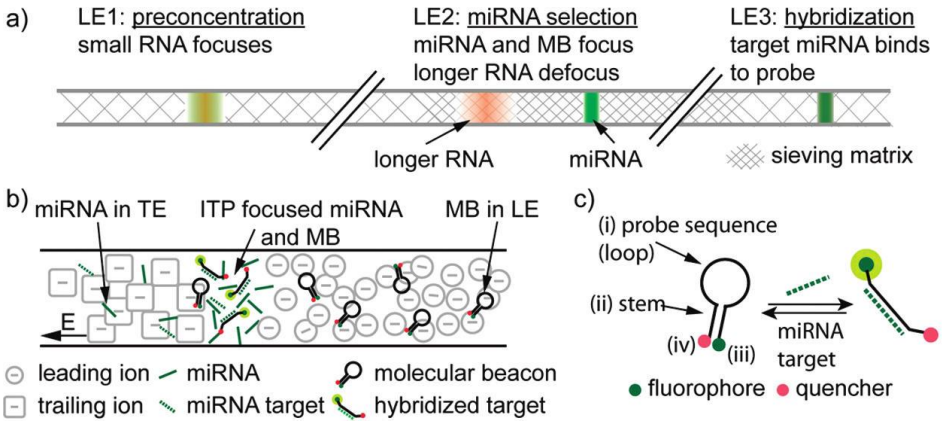

Figure 1.3. Schematic of the first assay to demonstrate ITP for nucleic acid reaction acceleration by Persat and Santiago.[1] The assay leveraged molecular beacon probe hybridization due to increased fluorescence upon binding to its target. The assay had three stages: the first used ITP preconcentration to collect all RNA. In the second, due to high-concentration sieving matrix, longer RNA defocus and allow purification of miRNA. Finally, the third region is designed to promote highly specific hybridization between molecular beacons loaded in the LE and miRNA focused in ITP. Molecular beacons were used in several subsequent ITP-aided reaction assays.[2,3]

Bercovici et al.[2] applied the same principle of ITP-based molecular beacon hybridization for the detection of a different and much larger target, 16S rRNA from bacteria in cultures and patient urine samples. In addition to demonstrating the applicability of this approach in a complex sample, the authors designed a photomultiplier tube (PMT) system for high sensitivity fluorescent signal quantification. They achieved a limit of detection of 10^6 cfu/mL, or 30 pM, of *E. Coli* in urine. Both assays were constrained by the structural limitations of molecular beacons. While the hairpin secondary structure bestowed increased specificity to the

probe, it reduced sensitivity and limited the dynamic range due to the comparatively large background signal present even in unbound beacons. These limitations highlighted the need for removal of background signal following hybridization.

Building on these two papers, Bercovici et al.[3] developed the first analytical model for nucleic acid hybridization using ITP, along with experimental validation of their model. Their work revealed a new characteristic timescale for ITP-aided reaction kinetics, inversely proportional to square-root of initial concentration (compared to standard incubation, where timescale is inversely proportional to initial concentration). As a result, they found that ITP-aided hybridization is increasingly beneficial at lower reactant concentration (14,000-fold reduced reaction time at 500 pM target concentration), as shown in Figure 1.4. Though their work nominally focused on DNA hybridization, it is theoretically applicable to any ITP-aided reaction assay in which both reactants are preconcentrated in ITP.

Bahga et al.[44] introduced an approach for removing excess background signal in (homogenous reaction) molecular beacon assays. They devised a post-reaction clean-up step by coupling ITP-based DNA hybridization with the high-resolving power of capillary electrophoresis (CE) using bidirectional ITP. Following ITP-aided hybridization, CE separated unbound molecular beacons from the beacon-target complex. They successfully demonstrated sequence-specific detection of a 39 nt ssDNA target, with a 3 pM limit of detection. Though Bahga et al. improved sensitivity of ITP and molecular beacon assays in this approach, CE resulted in more diffuse peaks, which hindered further improvements to sensitivity and limited downstream analysis of reaction products.

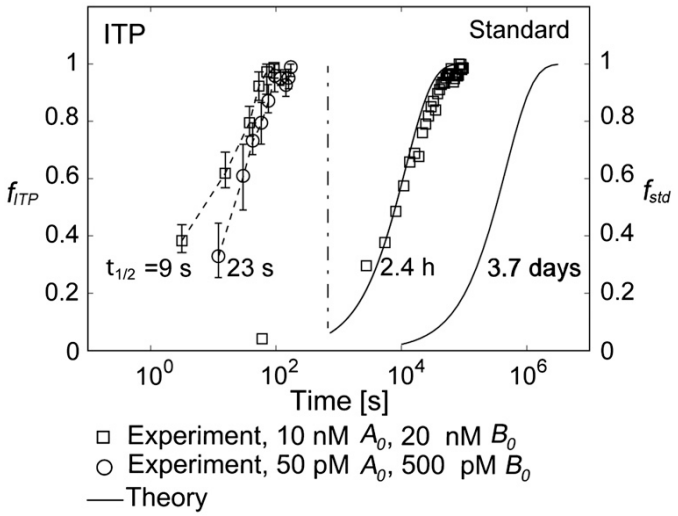

Figure 1.4. Bercovici et al.[3] predicted and experimentally demonstrated up to 14,000-fold reduction in reaction time in ITP-based DNA hybridization assays (reaction half-time from 3.7 days in standard incubation compared with 23 s in ITP assay).

1.3.2 Heterogeneous NA reactions

Heterogeneous assays offer high multiplexing capability, with the possibility of detecting hundreds of targets simultaneously. A second important feature is the easy integration of wash steps following hybridization, enabling removal of excess signal and reducing nonspecific binding, crucial for highly multiplexed assays.

Garcia-Schwarz and Santiago[49,50] developed a two-stage assay that used ITP to enhance hybridization and photopatterned functionalized gel to remove of excess reactant. The first of their two publications on this subject[49] is notable for its integration of serial ITP reactions with gel capture. The authors demonstrated the selectivity of this technique for mature over precursor miRNA that are larger but contain the mature miRNA sequence. They achieved a 1 pM limit of detection with a 4 order of magnitude dynamic range using a linear DNA probe. In the second paper,[50] Garcia-Schwarz and Santiago built on their previous work by focusing on further improving assay specificity. They

demonstrate single-nucleotide specificity for detection of let-7a over other members of the let-7 family, an important requirement in miRNA detection. Furthermore, they explored optimal probe design to enhance thermodynamic and kinetic specificity, and used locked nucleic acid (LNA) probes as well as a hairpin-structured reporter. The tradeoff for this enhanced specificity was reduced sensitivity and dynamic range, as they sacrificed an order of magnitude in the former and two orders of magnitude in the latter. Finally, they successfully validated this approach using total RNA samples, and demonstrated comparable results to PCR quantification. Despite its advantages, a limitation of this method of signal removal is the laborious experimental preparation required to pattern and functionalize the gel, and the challenge of performing multiple experiments on a single device.

The year 2014 was particularly fruitful for work using ITP to enhance heterogeneous nucleic acid hybridization assays. Karsenty et al.[51] developed the first analytical model for surface-based hybridization assays using ITP. They used this model to predict ITP-aided surface reaction rates for reactions involving a single probe and target. An interesting insight from their modeling is that increase in surface signal is much lower than sample preconcentration factor. They attributed this to the fact that the relevant reaction is between the surface and the average sample ion concentration, not peak concentration. They performed validation experiments using a single target and probe, wherein they functionalized paramagnetic beads with molecular beacons, and manipulated the beads to a desired location in the chip using an external magnet. They then used ITP to transport sample containing target molecules, and allowed two minutes for ITP zone to pass over the immobilized molecular beacons. Unbound target

molecules continued migrating downstream. They demonstrated two order of magnitude improvement in sensitivity (1 nM) compared with continuous flow surface hybridization assays.

Soon after, Han et al.[4] extended ITP-accelerated reactions to DNA microarrays. They presented an analytical model for ITP-aided microarray hybridization, and demonstrated this technique experimentally by detecting 20 target sequences using 60 spots. This was the first demonstration of a truly multiplexed detection assay (more than 2 target) using ITP. They achieved a 100 fM limit of detection and a dynamic range of 4 orders of magnitude in their 30 min assay. Compared to traditional DNA microarrays with overnight incubation, they showed 8-fold higher signal. The authors designed a clever solution to the problem of Joule heating and electrokinetic instability by using a constriction in the channel geometry (shown in Figure 1.5) and turning off electric field to allow target to redistribute through diffusion. They leveraged the microarray format to introduce a clean-up wash step following hybridization.

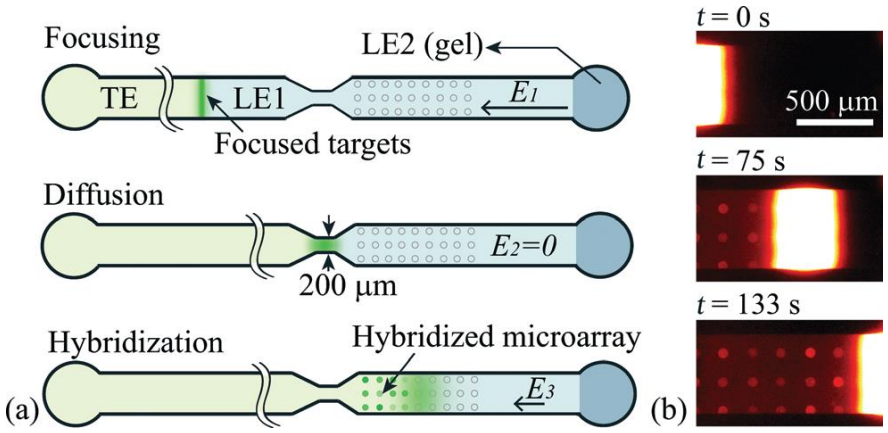

Figure 1.5. Schematic of Han et al.'s[4] ITP-aided microarray hybridization assay. The authors used the constriction to turn off electric field and allow diffusion to redistribute target DNA that was destabilized due to Joule heating, prior to surface reaction.

Shintaku et al.[52] used ITP to increase reaction rate and sensitivity of bead-based DNA hybridization assays. They demonstrated comparable sensitivity (100 fM) to standard reaction methods in 60-fold reduced reaction time, as well as 5-fold improvement in sensitivity at comparable reaction times. Furthermore, their multiplexed assay showed similar specificity as standard bead assays. All fluorescent signal was contained in the beads, and detection was performed using a Luminex 200 instrument, eliminating the need to integrate an additional clean-up step in assay design. The authors also discussed the idea of a quasi-equilibrium existing between reaction rate and target influx into the ITP zone. We analytically derive and discuss this concept further in Chapter 2.

Finally, in their two-part work, Shkolnikov and Santiago[53,54] presented a technique that couples ITP preconcentration with affinity chromatography for sequence-specific capture and purification of target DNA molecules. They developed an analytical model to describe spatiotemporal dynamics in this assay, identifying key process parameters that guide assay performance. Their analysis showed that various independent parameters collapse into three dimensionless parameters that concisely described reaction dynamics. To validate this technique experimentally, they synthetized a porous polymer monolith that is functionalizable, non-sieving, and compatible with ITP. They demonstrated the capability of this approach, purifying 25 nt target DNA from 10,000-fold more abundant background DNA in less than a minute.

1.3.3 Protein reaction assays

As previously mentioned, the very first demonstrated use of ITP to accelerate chemical reactions involved protein reactants. Kawabata et al.[5] leveraged ITP preconcentration to

accelerate reactions between a DNA-coupled antibody and target protein of interest, an isoform of α-fetoprotein (AFP). Conjugating the antibody with DNA molecule increased the electrophoretic mobility of the antibody and allowed it to focus in ITP. They coupled ITP concentration with capillary electrophoresis to separate the immune complex of interest from background fluorescent signal. They achieved a limit of detection of 5 pM with this assay. Kawabata et al. pioneered a number of ideas (such as the integration of ITP-aided reaction with subsequent separation and on-chip fluorescent detection) that subsequent works built and expanded upon. To the best of our knowledge, their work represents the only use of ITP for homogeneous reaction and detection of proteins.

Simultaneously (the papers were published within the same week), Park et al.[6] published a paper examining ways to improve reproducibility of the assay, shown in Figure 1.6. Their analysis showed that even small fluctuations in buffer concentrations and other assay conditions can lead to large differences in observed outcomes. They introduced automated handoff and timing mechanisms that relied on computer monitoring of voltage, in order to achieve highly precise control of signal intensity and peak separation.

Based on this work, Wako Diagnostics developed an automated system for quantitation of α-fetoprotein, and Kagebayashi et al.[55] describe its mechanism and performance in detail. They validated their assay in spiked serum samples, and achieved a limit of detection of 1 pM, with 2% coefficient of variation. The μTASWako i30 immunoanalyzer remains the only commercially available product using ITP.

Several years later, two groups published papers using ITP to accelerate heterogeneous immunoassays. Khnouf et al.[56] extended ITP-aided surface reaction assays to immunoassays using two different approaches: antibody-coated magnetic bead capture and antibody-functionalized microchannels. ITP was used to focus target proteins in free solution and drive enhanced surface reaction kinetics. They estimated a preconcentration factor of about 100 for the target protein. For both heterogeneous assays, they demonstrated improvement in sensitivity with ITP preconcentration.

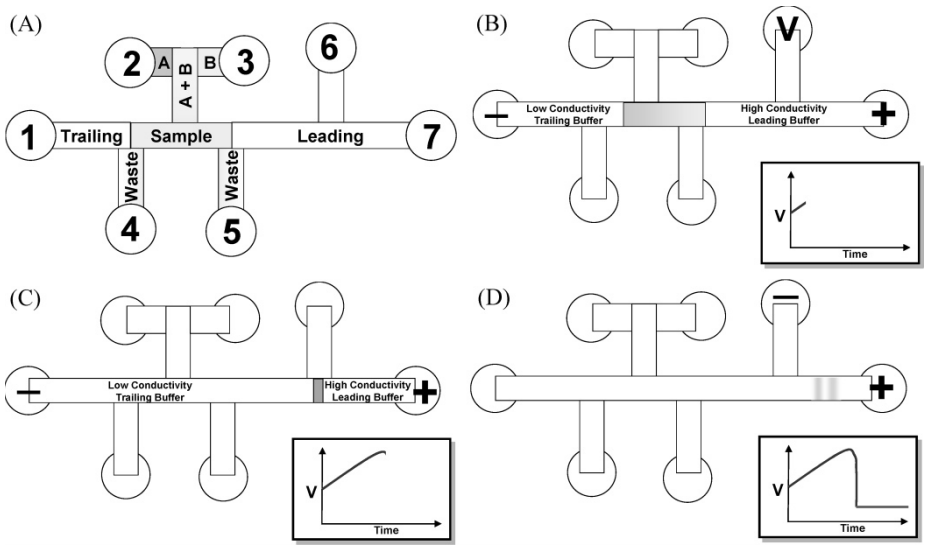

Figure 1.6. Schematic of first ITP-based reaction assay, developed by Kawabata et al. [5] and Park et al. [6] ITP here is used to accelerate an immunoassay reaction between an antibody and its target protein.

Moghadam et al.[57] further demonstrated the applicability of ITP to immunoassays, particularly the widely-used lateral flow assays. Using ITP preconcentration, they demonstrated two orders of magnitude improvement in sensitivity in detecting IgG from a clean buffer. This is due to substantially increased target extraction efficiency, 30% in ITP-enhanced lateral flow assays compared with less than 1% in conventional later flow assays. Furthermore, their work included a model that described different scaling

between conventional LFA and ITP-LFA assays. An interesting insight resulting from this work is the dependence of target captured in ITP-LFA on both antibody-specific binding parameters (k_{off} and K_D) as well as ITP preconcentration.

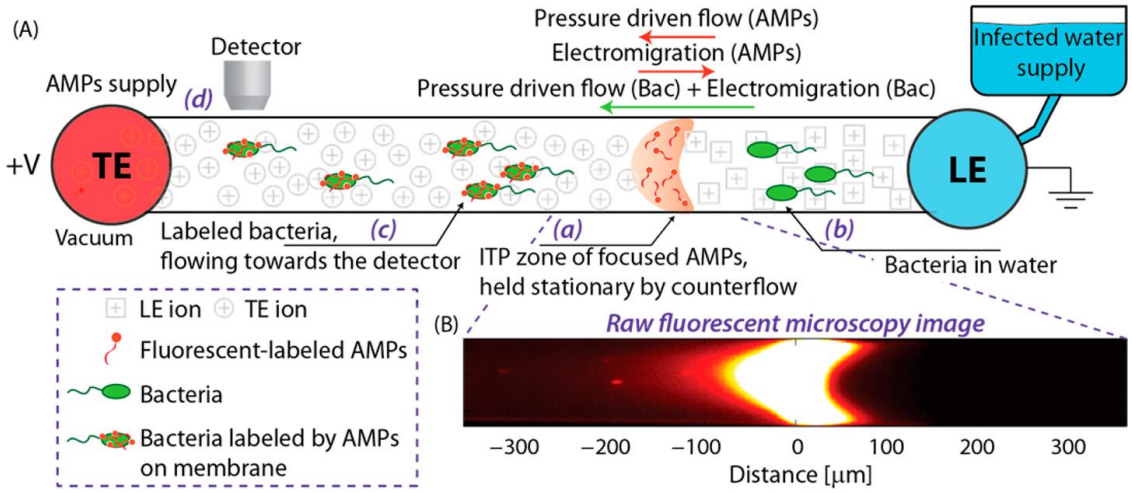

Figure 1.7. Schwartz and Bercovici's[7] device for labeling of bacteria using ITP and counterflow. To this day, this is the only use of ITP-aided reactions for the detection of whole cells.

To the best of our knowledge, there is only one work that applied ITP to accelerate reactions involving whole cells. Schwartz and Bercovici[7] combined free-solution, homogenous ITP-aided reactions and vacuum-driven counterflow to detect whole bacterial cells. Figure 1.7 shows the schematic of this assay and an image of the stationary ITP peak. They leveraged counterflow to hold antimicrobial peptides (AMPs) in a high-concentration zone. Meanwhile, ITP and pressure-driven flow acted unidirectionally on E. coli bacterial cells, resulting in continuous flow of bacterial cells reacting with and getting labeled by the stationary AMPs. Their assay was stable for the 1 hour of monitoring time, and used about 100-fold fewer reagents than comparable AMP-based methods.

Table 1.1 – Summary of publications using ITP to accelerate chemical reactions. We emphasize assay sensitivity as well as major contribution(s) of the work to the field.

Authors	Year	Sensitivity	Primary contributions
Homogeneous DNA reactions			
Persat and Santiago	2011	10 pM	- First demonstration of ITP-based enhancement of nucleic acid hybridization.
Bercovici et al.	2011	30 pM	- Extension of ITP-aided molecular beacon hybridization assays to large RNA detection.
Bercovici et al.	2012	--	- Physical model with experimental validation of ITP-based DNA assays.
Bahga et al.	2013	3 pM	- Coupling ITP-based reaction with capillary electrophoresis clean-up of background signal
Heterogeneous DNA reactions			
Garcia-Schwarz and Santiago	2012 2013	2 pM 10 pM	- ITP reaction coupled with gel-based excess reactant removal.
Karsenty et al.	2014	1 nM	- First experimentally-validated model for ITP-aided surface hybridization.
Han et al.	2014	100 fM	- Demonstration of ITP-aided DNA microarray hybridization. - First demonstration of multiplexed ITP detection.
Shkolnikov and Santiago	2014	--	- Coupling ITP preconcentration to affinity chromatography purification - Model describing spatiotemporal dynamics of ITP-AC.
Shintaku et al.	2014	100 fM	- Extension of ITP hybridization to bead-based assays.
Immunoassay and bacterial cell reactions			
Kawabata et al. Park et al. Kagebayashi et al.	2008 2008 2009	5 pM -- 1 pM	- To our knowledge, first demonstrated coupling of ITP with reactions. - Only work to use ITP in homogeneous immunoassays.
Khnouf et al.	2014	18 pM	- Demonstration of ITP enhancement for surface-based immunoassays
Moghadam et al.	2014	0.7 nM	- First demonstration of ITP accelerating lateral flow assays.
Schwartz and Bercovici	2014	2×10^4 cfu/mL	- Only work to use ITP to speed up reactions with whole cell reactants.

1.4 Nucleic acid extraction from whole blood using isotachophoresis

ITP has been most extensively used in extraction and purification of nucleic acids and proteins from complex samples. Many of the earliest applications of ITP involved

extraction and separation of proteins from serum samples.[58-60] Since then, several groups, most notably the Kondratova and Santiago groups, have demonstrated ITP's ability to extract nucleic acids and proteins from a variety of complex samples like cell culture,[61] urine,[2] milk,[62] and serum.[45,63,64] Whole blood, however, is among the most complex samples, and poses several challenges for ITP and other electrokinetic approaches. In this section, we will discuss the challenges that whole blood and serum pose, and review ITP-based nucleic acid extraction from whole blood.

1.4.1 Challenges of ITP assays from whole blood and serum samples

Blood is a uniquely difficult sample for ITP and many molecular diagnostic assays. It is highly dense with cells, proteins, electrolytes, and various other molecules, and is thus highly informative but challenging.

- *Cells:* Cells account for 45% of whole blood, by volume. Both red and white blood cells carry negative surface charge, which allows them to electromigrate under an applied electric field.[65,66] Additionally, the propensity of cells to coagulate and form clusters causes significant challenges in microfluidic platforms. When cells are lysed, as they are in many nucleic acid extraction assays, their contents are released into the channel or reservoir, creating further mix of potential contaminants.
- *Electrolytes:* The presence of high-concentration electrolytes alone poses difficulties in the design of ITP assays, requiring sample dilution or special pretreatment. In Table 1.2, we list some high-mobility species that are present in relatively large concentrations in serum. Chloride and sodium in particular, which are often used as LE ions in anionic and cationic ITP, respectively, are so

highly abundant that placing serum samples in TE reservoir would require a minimum of 10-fold dilution.

Table 1.2. Select high-concentration ionic species present in serum. This list is not comprehensive.

Species	Concentration
Chloride	100 mM
Sodium	40 mM
Bicarbonate	25 mM
Potassium	20 mM
Magnesium	5 mM
Lactic Acid	1.5 mM
Phosphorus	1.2 mM
Uric Acid	0.4 mM
Citric Acid	140 µM
Acetic Acid	40 µM
Aspartic Acid	20 µM

- *Proteins:* There are approximately 80 g/L of proteins in blood, approximately 65% of which is albumin and another 15% is IgG.[67] Proteins have a wide range of mobilities and isoelectric points, which makes them difficult to predict. Electrophoretic methods for protein extraction suffer from this heterogeneity. Compounding this issue is the high abundance of albumin, which obscures detection and identification of biologically-interesting proteins. Hemoproteins, which include hemoglobin, myoglobin, and other Fe^{2+}-containing proteins, are known inhibitors of PCR and other amplification methods.[68] Furthermore, proteins can inhibit nucleic acid detection by binding DNA, and thus have to be removed or degraded.[11]

1.4.2 Literature review of ITP-based nucleic acid extraction from whole blood

Persat et al.[11] were the first to successfully demonstrate ITP-based extraction of nucleic acids from whole blood. A very interesting insight from their work is the importance of using proteinase K, a broad-range protease, to digest nucleic acid-binding proteins. They theorized that these proteins lowered the electrophoretic mobility of nucleic acids significantly, and preventing them from focusing in ITP. Without proteinase K, they were unable to focus nucleic acids from 10-fold diluted blood lysate. In the work we describe in Chapter 6, we reach similar conclusions regarding the importance of proteinase K. They lysed the cells using high temperature (56 °C) and a detergent (Triton X-100). They performed this assay on a commercial deep crown glass chip from Perkin-Elmer to purify only 25 nL of sample. The low sample volume meant that only 45 pg of nucleic acids were extracted, which limited downstream analysis to amplification-based methods such as PCR.

Marshall et al.[69] later published a paper on the purification of malaria-infected whole blood samples. In it, they used a simple straight-channel geometry and used counterflow in order to hold the ITP zone stationary and increase extraction time. Using counterflow allowed them to detect parasite infection at a clinically-relevant parasite density of 0.5 parasites per nanoliter. The authors used the same approach of high temperature and a detergent as Persat et al.,[11] but found that 85 °C or higher was required for more effective lysis of malaria-infected cells, due to the parasites' higher thermal resistance.

Marshall et al.[8] built on their previous work on malaria-infected blood purification in a second effort, implementing their ITP-based assay and lysis chemistry on a printed

circuit board (PCB) device. The device contained heaters and temperature sensors integrated in the PCB layer. This allowed the authors to directly dispense a whole blood into the TE reservoir directly, as the heaters induced convective fluid flow to lyse and mix the sample. A schematic of their assay protocol is shown in Figure 1.8. Their assay's sensitivity with the PCB device was comparable to that of their previous work. Furthermore, this assay demonstrated ITP's robustness to different surfaces and its compatibility with a fully electrically-actuated sample preparation approach.

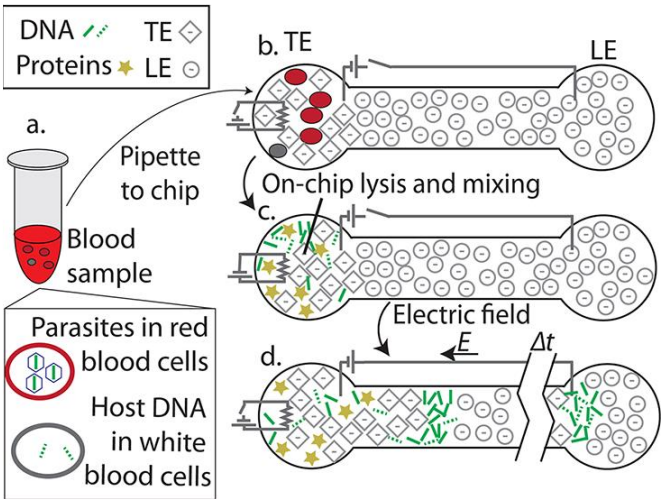

Figure 1.8. Schematic of ITP-based malaria extraction protocol by Marshall et al.[8] Whole blood is loaded into the TE reservoir. From there, mixing and lysis are performed in the reservoir, using asymmetrical heating. Electric field is then applied to initiate ITP, and target DNA is extracted from the LE reservoir for downstream processing.

Rogacs et al.[70] published the only work that we know of using ITP for extraction of bacterial RNA in whole blood. Bacterial cells, even Gram-negative species like the one shown in this work, are much more difficult to lyse due to their rigid cell wall. Furthermore, RNA, unlike DNA, degrades readily in whole blood and many lysing and extraction chemistry.[71] The authors overcame these challenges by designing an aggressive and ITP-compatible lysis chemistry that preserved RNA integrity. They

lysed the bacterial cells using high concentrations of NaOH, and included a reducing agent (DTT) and detergent (Triton X-100) to destroy and degrade RNAses. The authors also added high concentrations of carrier RNA to act as a competitive substrate for intact RNAses. With this well-crafted assay chemistry, they were able to detect 16S rRNA in approximately 10^4 cells/mL using PCR.

A common limitation to all these works is throughput and yield. Marshall et al.'s[8] work on the PCB device, which had the highest yield of the works above, still only processed less than 1 µL of sample. To address this limitation, Marshall et al.[10] designed an injection-molded device capable of processing 25 µL of sample. The device incorporated capillary barriers that enabled repeatable and robust sample loading. The authors overcame the challenge of increased susceptibility to pressure-driven flow by using Pluronic F-127. Pluronic F-127 is a polymer that is liquid at low temperature but solidifies at room temperature and higher. By pipetting it from a refrigerator into the TE and LE reservoirs, the authors were able to minimize pressure-driven flow in the channel. They then demonstrated extraction efficiency exceeding 80% over a wide range of initial DNA amounts, 250 pg to 250 ng. They also demonstrated purification of DNA from whole blood, and showed the compatibility of the ITP-purified sample with PCR.

Table 1.3. Summary of works using ITP for extraction of nucleic acids from whole blood samples

Authors	Year	Species extracted	Lysis method	Extraction efficiency
Persat et al.	2009	Nucleic acids from whole blood	Heat (56 °C) + Triton X-100 + proteinase K	0.25
Marshall et al.	2011	DNA from Malaria-infected RBCs	Heat (95 °C) + Triton X-100 + proteinase K	0.1
Marshall et al.	2012	DNA from Malaria-infected RBCs	Heat (95 °C) + Triton X-100 + proteinase K	10
Rogacs et al.	2012	Bacterial 16S rRNA	125 mM NaOH + Triton X-100	0.2
Marshall et al.	2014	DNA from whole blood	Triton X-100 + proteinase K	81

1.5 Scope of thesis and major contributions

The objective of this thesis is to improve the state of the art in nucleic acid and protein reaction assays, and in bacterial DNA extraction from whole blood. We leverage a microfluidic platform and electrokinetic focusing to extract species of interest, accelerate chemical reactions, and separate reaction products.

The dissertation's contributions may be summarized as follows:

1. Development of an analytical model for accumulation and reaction rates that guides sample placement in ITP assay design.
2. Design of a highly-sensitive technique for ITP-aided DNA hybridization followed by separation of reaction products using an ionic spacer.
3. Development of an assay in which non-focusing protein target is recruited into ITP mode by binding to a high-speed probe, followed by on-chip separation and target quantitation.

4. Development of a rapid approach to perform size-based RNA fractionation on a custom-designed microfluidic chip capable of processing 10 µL of sample.
5. Integration of ITP purification with recombinase polymerase amplification (RPA) for the detection of inactivated *L. Monocytogenes* cells from whole blood samples.

The thesis is composed of five main chapters. In Chapter 2, we present an analytical model describing the effect of sample loading on accumulation and reaction rates in ITP, and derive and identify key non-dimensionless parameters. In Chapter 3, we demonstrate a novel assay that combines peak-mode and plateau-mode ITP with an ionic spacer for accelerated DNA hybridization followed by separation of reaction products. In Chapter 4, we modify our ITP-spacer assay for simultaneous reaction and separation of a non-focusing protein target, C-reactive protein (CRP). We also present an analytical model that describes ITP reaction kinetics when one species does not focus in ITP. In Chapter 5, we extend our ITP-spacer assay approach to perform size-based RNA fractionation. We also present a laser-cut plastic microfluidic device capable of processing 10 µL of sample. In Chapter 6, we present an assay for the lysis, extraction, and detection of inactivated *L. Monocytogenes* cells in whole blood using ITP purification and recombinase polymerase amplification (RPA). We demonstrate our technique using both bacterial genomic DNA as well as chemically-inactivated bacterial cells. In Chapter 7, we summarize our work, summarize our main achievements, and present recommendations for future directions in ITP-aided reaction and extraction assays.

2 Accumulation and reaction rates in ITP

The contents of this chapter are adapted from a manuscript which is currently under review in *Analytical Chemistry*, and are reproduced here with minor modifications.

2.1 Introduction

We present an analytical model useful in the design of peak-mode isotachophoresis (ITP) experiments. The model quantifies sample accumulation rates and chemical reaction rates, the latter in applications of ITP toward acceleration of chemical reactions. We include analysis of the effect of initial sample placement location. We derive and identify key non-dimensional parameters for the general case of weak electrolyte buffer ions in terms of sample placement (injection mode), initial concentrations, fully ionized mobilities, and reaction kinetics constants. We then discuss how to use these parameters in the optimal design of peak-mode ITP assays, and highlight regimes of particular interest. We clearly identify a quasi-equilibrium regime wherein reaction rates increase until they equal the accumulation rates of reactants. The model and analysis are generally applicable to both cationic and anionic ITP assays and likely to a wide range of sample species.

Effective design of peak-mode ITP assays requires consideration several coupled phenomena. everal recent studies have analyzed sample distribution[72], focusing dynamics[28], and dispersive forces[73] influencing sample preconcentration. Rogacs et al.[29] recently discussed various design choices and parameters in the context of ITP nucleic acid purification. Several studies analyzed ITP assays for reaction acceleration and separation. Bercovici et al.[3] developed a reaction model for ITP-aided hybridization

assays for two reactants focused in ITP, while in Chapter 3, we will explore the design of assays in which a spacer molecule is used to separate reactants and products. Shkolnikov et al.[53] and Han et al.[4] analyzed ITP assays between a stationary probe and a focused nucleic acid species. We know of no engineering models useful in optimizing ITP accumulation and/or reaction rates as a function of sample properties and initial placement.

In Figure 2.1, we depict two loading configurations which we consider here. Sample ions with intermediate mobilities can be mixed initially with either TE or LE buffers, and will focus in ITP. However, the rate at which sample ions accumulate in the ITP zone can vary significantly. This rate depends on mobilities of the different ionic species, buffer concentrations and compositions, and channel and chip geometry.

In this chapter, present an analytical model that describes the effect of initial sample placement on accumulation and reaction rates in ITP. We concentrate on the case of negligible bulk flow and wherein sample is injected into a channel section prior to initiation of ITP. However, our analyses are extendable to other configurations including wherein sample is injected from a TE sample reservoir (see Section 2.2.3) We do not consider cases in which sample is loaded into both LE and TE (e.g., at same concentration), which is guaranteed to yield maximal accumulation and reaction rate and is thus less analytically interesting.

We begin with a simple formulation for sample concentration in the adjusted TE (ATE) zone. The ATE zone is the zone formed by TE ions as they migrate into a region formerly occupied by the LE. We then define a dimensionless parameter that relates the

rate of sample accumulation in ITP to initial sample placement. Finally, we discuss the effect of initial sample placement on ITP-aided reaction assays.

2.2 Theory

In addition to the simplifications discussed above, we will also here assume net charge neutrality in all zones.[74] In neglecting bulk flow, we also neglect advective currents. We will express ionic current in regions well away from the ITP interfaces(within TE, ATE, or LE plateaus) so we assume diffusive currents are negligible.[3] Further, we assume that charge relaxation timescale is negligibly small so we can obtain relations for electric fields in terms of conservations of ionic current.[74] We assume sample ions focusing in peak-mode ITP at constant current have negligible contribution to local conductivity due to their low concentration.[28]

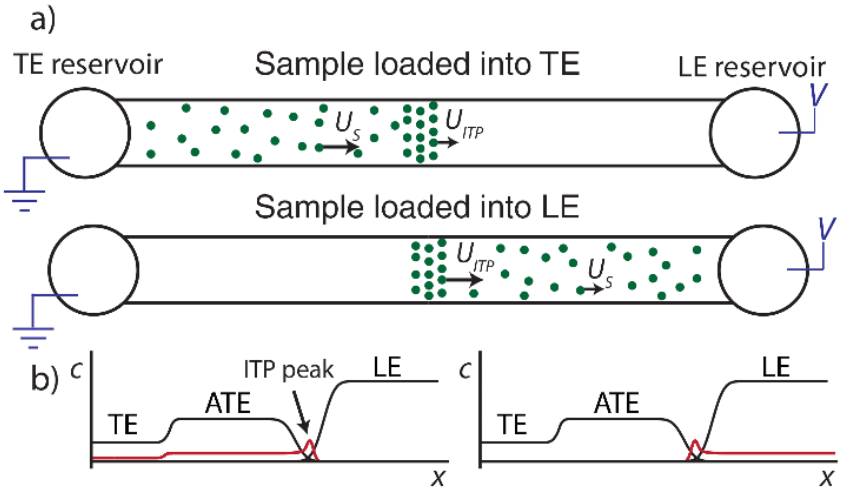

Figure 2.1. a) Schematic representation of an ITP assay showing two loading configurations. In the first, sample is loaded in the TE zone and overspeeds TE coions to focus at the ITP peak. In the second, sample is loaded in the LE, and is oversped by the LE coions. b) Plots of species concentrations in the different zones. We greatly exaggerated sample zone concentrations (red curve) versus typical initial values for clarity of presentation.

2.2.1 Derivation of effective mobilities and accumulation rates in ITP

Truly general explicit analytical expressions for ITP concentrations and accumulation rates are difficult (and cumbersome) for the general case of multivalent weak electrolyte mixtures (buffer and sample) ions[75] and with ionic strength effects.[76] Such generalized models are perhaps better addressed by accurate numerical simulations. For example, our group has published free, open source numerical tool called SPRESSO for non-linear electrokinetics problems (including ITP). SPRESSO uses a full chemical equilibrium formulation for weak electrolytes mixtures (including ampholytes) aided by a built-in data base of over 300 chemical species.[75] The code uses a compact 6^{th} order spatial discretization scheme for high resolution combined with adaptive grid refinement for fast solutions.

We here will concentrate on deriving compact relations which are nevertheless useful in designing ITP experiments and yielding actionable design criteria. We will concentrate on by far the most common application of ITP wherein LE and TE buffers are composed of ions of at most a singly ionized species. Examples include TE and LE buffers composed of a weak acid (base) titrated with strong base (acid), or alternately a weak base (acid) titrated with a weak acid (base). As stated earlier, we will also neglect ionic strength effects on mobilities and acid dissociation constants. These assumptions immediately let us use so-called regulation functions by which LE chemistry governs sample and adjusted TE (ATE) concentrations.

The first such function was derived by Jovin[35] and states that, for univalent species, and assuming "safe pH"[77] (i.e., that hydronium or hydroxyl ions do not carry significant current). Jovin's function is

$$\sum_i z_i c_i = \text{constant} \tag{2.4}$$

c_i here represents total (a.k.a. analytical) concentration for each species. Note Jovin's function is not a statement of charge neutrality, as the c_i is a sum concentration of all ionization states of a weak electrolyte species *i* (hence z_i is -1, 0, or 1). Alberty's function also assumes univalent species and safe pH and can be expressed as follows:

$$\sum_i \frac{c_i}{\mu_{i,z}} = \text{constant} \tag{2.5}$$

Here, $\mu_{i,z}$ represents a species' fully-ionized mobility at valence *z*, and c_i is total concentration. The constant is, of course, different than for eq 2.1. For the remainder of this formulation, we concentrate on anionic ITP, though note that our analysis can be extended to cationic ITP as well. We evaluate the Jovin function within the LE and set it equal to the Jovin function within the ATE. We formulate the Alberty function in a similar manner. Combining the two resulting equations, we derive TE ion concentration in ATE zone (for univalent electrolytes and anionic ITP)

$$c_{TE}^{ATE} = \frac{\mu_{TE,-1}^0}{\mu_{LE,-1}^0}\left(\frac{\mu_{CI,+1}^0 - \mu_{LE,-1}^0}{\mu_{CI,+1}^0 - \mu_{TE,-1}^0}\right) c_{LE}. \tag{2.6}$$

We note that all mobilities in the latter relation are fully-ionized mobilities. The superscript refers to the "absolute" mobility defined as the fully ionized mobility in the

limit of negligible ionic strength (since we neglect ionic strength). Since we neglect ionic strength effects, note that $\mu^0_{TE,-1} = \mu^0_{ATE,-1}$ even for a weak electrolyte.

We define β as the ratio of TE ion concentrations in the ATE and TE zones:

$$\beta \equiv \frac{c_{TE}^{ATE}}{c_{TE}^{TE}} = \frac{\mu^0_{TE}}{\mu^0_{LE}} \left(\frac{\mu^0_{CI} - \mu^0_{LE}}{\mu^0_{CI} - \mu^0_{TE}} \right) \frac{c_{LE}}{c_{TE}^{TE}}. \tag{2.7}$$

We see β is directly proportional to the ratio of initial LE and TE concentrations. The latter is an important, controllable parameter in the design of ITP assays[28]. We thus define:

$$\gamma = \frac{c_{LE}}{c_{TE}^{TE}}. \tag{2.8}$$

Combining eqs 2.3 and 2.4 we express the concentration of sample ions in the ATE zone as:

$$c_s^{ATE} E^{ATE} = c_s^{TE} E^{TE}, \tag{2.9}$$

$$c_S^{ATE} = c_S^{TE} \left(\frac{E^{TE}}{E^{ATE}} \right) = c_S^{TE} \left(\frac{\sigma^{ATE}}{\sigma^{TE}} \right) = c_S^{TE} \left(\frac{c_{TE}^{ATE}}{c_{TE}^{TE}} \right) = \beta c_S^{TE}. \tag{2.10}$$

This relation is useful when sample is initially loaded into the TE zone.

Effective mobilities of buffer ions. For univalent buffers, effective mobilities for weak electrolytes (which either accept or donate an arbitrary number of protons) are given by eqs 12 and 13 of Bercovici et al.:[75]

$$\mu_i = \sum_{z=z_i}^{z_n} \mu_{i,z} g_{i,z}, D_i = \sum_{z=z_i}^{z_n} D_{i,z} g_{i,z}, \tag{2.11}$$

where z is valence and D_i represents an effective diffusivity and g_i is given by

$$g_i = \frac{L_{i,z} c_H^2}{\sum_{z=z_i}^{z_n} L_{i,z} c_H^2} \ . \tag{2.12}$$

The summations above are over each "family"[75] of species; that is, the ionization states of the weak electrolyte *i*. As discussed above, we here consider only the case of univalent, negatively charged buffer ions, so eq 2.9 simplifies to

$$\begin{aligned} g_{i,0} &= \frac{1}{1 + K_{i,-1}/c_H}, \\ g_{i,-1} &= \frac{K_{i,-1}/c_H}{1 + K_{i,-1}/c_H}, \\ g_{i,+1} &= \frac{K_{i,+1}/c_H}{1 + K_{i,+1}/c_H}. \end{aligned} \tag{2.13}$$

As a result, we rewrite eq 2.8, the effective mobility of a monovalent species *i* as:

$$\mu_i = \mu_{i,0}^0 \underset{=0}{g_{X,0}} + \mu_{i,-1}^0 g_{X,-1} = \mu_{i,-1}^0 \frac{1}{1 + c_H / K_{i,-1}}. \tag{2.14}$$

For example, for anionic ITP (focusing of anionic samples), the effective mobilities of TE and sample ions in ATE zone are given by

$$\mu_{TE}^{ATE} = \mu_{TE,-1}^0 \frac{1}{1 + c_H^{ATE} / K_{TE,-1}}, \tag{2.15}$$

We will here preserve a general effective mobility of the sample in the formulation for now (e.g., to make the derivation applicable to polyionic DNA, RNA, etc.). Our expressions can then eventually be evaluated by inserting an effective (observable) mobility of the ion. For the special case of a singly ionized weak acid sample (with a single known dissociation constant $K_{S,-1}$), the sample's effective mobility in the ATE is then

$$\mu_S^{ATE} = \mu_{S,-1}^0 \frac{1}{1 + c_H^{ATE} / K_{S,-1}}. \tag{2.16}$$

Lastly, we will also make the common approximation that the concentration of protons (hydronium ions), c_H, can be directly related to pH as $\text{pH} = -\log(c_H)$.[77] We note also that while pH of LE and TE zone are known, pH of ATE zone is a function of the properties of the LE, TE, and the counterion species.

pH of ATE zone. Persat et al.[77] presents a derivation for pH of a buffer consisting of two weak electrolytes. We simply apply this two-weak-electrolyte-buffer result to the ATE zone which is composed of two weak electrolytes: The TE (weak acid) and the counter ion (CI) (weak base). The pH in the ATE zone for anionic ITP is then

$$c_H^{ATE} = \frac{K_{TE,-1}}{2}\left(\left(c_{TE}^{ATE} / c_{CI}^{ATE} - 1 \right) + \sqrt{\left(1 - c_{TE}^{ATE} / c_{CI}^{ATE} \right)^2 + 4 \frac{K_{CI,0} c_{TE}^{ATE}}{K_{TE,-1} c_{CI}^{ATE}}} \right), \tag{2.17}$$

where

$$K_{TE,-1} = \frac{c_{TE,-1}^{ATE} c_H}{c_{TE,0}^{ATE}}$$

and (2.18)

$$K_{CI,0} = \frac{c_{CI,0}^{ATE} c_H}{c_{CI,+1}^{ATE}}.$$

2.2.2 Accumulation rates in ITP

We can now derive accumulation rates in ITP. The accumulation rate (in moles per second) of sample from the ATE into an anionic ITP peak can be related to the drift velocity of sample ions in the frame of reference of the moving ITP zone as

$$\left(\frac{\mathrm{d}N_S}{\mathrm{d}t}\right)^{ATE} = \left(U_S^{ATE} - U_{ITP}\right) Ac_S^{ATE} = \left(\frac{\mu_S^{ATE}}{\mu_{TE}^{ATE}} - 1\right) U_{ITP} Ac_S^{ATE} = \left(\frac{\mu_S^{ATE}}{\mu_{TE}^{0}}\left(1 + c_H^{ATE} / K_{TE,-1}\right) - 1\right) U_{ITP} Ac_S^{ATE},$$

(2.19)

where U_S^{ATE} is the velocity of sample in the ATE zone, μ_i^0 is the absolute (fully ionized) mobility of species *i*, U_{ITP} is ITP velocity, and *A* is the cross-sectional area. U_{ITP} is simply equal to $\mu_{LE}^{LE} I / A\sigma^{LE}$, where *I* is applied current and σ^{LE} is the (known) conductivity of the LE buffer. μ_S^{ATE} is the effective (observable) mobility of the sample. Similarly, for sample ions initially loaded into the LE, accumulation rate into the ITP zone is given by:

$$\left(\frac{\mathrm{d}N_S}{\mathrm{d}t}\right)^{LE} = \left(U_{ITP} - U_S^{LE}\right) Ac_S^{LE} = \left(1 - \frac{\mu_S^{LE}}{\mu_{LE}^{LE}}\right) U_{ITP} Ac_S^{LE} = \left(\frac{\mu_S^{LE}}{\mu_{LE}^{0}}\left(1 + c_H^{LE} / K_{LE,-1}\right) - 1\right) U_{ITP} Ac_S^{LE}.$$

(2.20)

For interested readers, we here give the equivalent expressions for accumulation rates for *cationic* ITP (for singly ionized buffers):

$$\left(\frac{\mathrm{d}N_S}{\mathrm{d}t}\right)^{ATE} = \left(\frac{\mu_S^{ATE}}{\mu_{TE}^{0}}\left(1 + K_{ATE,+1} / c_H^{ATE}\right) - 1\right) U_{ITP} Ac_S^{ATE} \quad \text{(cationic ITP)}, \tag{2.21}$$

$$\left(\frac{\mathrm{d}N_S}{\mathrm{d}t}\right)^{LE} = \left(\frac{\mu_S^{LE}}{\mu_{LE}^{0}}\left(1 + K_{LE,+1} / c_H^{LE}\right) - 1\right) U_{ITP} Ac_S^{LE} \quad \text{(cationic ITP)}. \tag{2.22}$$

We don't show the derivation for the latter two equations but they can be derived by a procedure very similar to the anionic ITP case we have presented.

Accumulation rates for fully-ionized TE co-ion and sample ions.

The expressions of the preceding section can be simplified for fully-ionized TE co-ions and fully-ionized sample ions. For both anionic and cationic ITP, these expressions reduce to

$$\left(\frac{\mathrm{d}N_S}{\mathrm{d}t}\right)^{ATE} = \left(U_S^{ATE} - U_{ITP}\right) Ac_S^{ATE} = \left(\frac{\mu_S^0}{\mu_{TE}^0} - 1\right) U_{ITP} Ac_S^{ATE}, \tag{2.23}$$

and

$$\left(\frac{\mathrm{d}N_S}{\mathrm{d}t}\right)^{LE} = \left(U_{ITP} - U_S^{LE}\right) Ac_S^{LE} = \left(1 - \frac{\mu_S^0}{\mu_{LE}^0}\right) U_{ITP} Ac_S^0. \tag{2.24}$$

We will use these in further derivations presented in the rest of the chapter. The case of a fully-ionized TE co-ion is likely the most common (although not universal) in peak-mode ITP applications. It occurs when, for example, an anionic ITP process is buffered at a pH near the pK_a of a weak base counterion, so the LE and TE co-ions each act as local titrants to the cation. The case of fully ionized sample is common for peak-mode ITP focusing of weak acid species with pK_a significantly lower than the pH of the ATE. A salient example of the latter is the focusing of DNA or RNA using anionic ITP.

We define so-called separabilities, first introduced by Bocek[78] and then explored further by Marshall[79]

$$\begin{aligned} p_{S,TE} &= \frac{\mu_S^0}{\mu_{TE}^0} - 1, \\ p_{S,LE} &= 1 - \frac{\mu_S^0}{\mu_{LE}^0}. \end{aligned} \tag{2.25}$$

Separability quantifies the relative mobilities of the sample ion and surrounding TE or LE ions. So we recast eqs 2.20 and 2.21 as

$$\left(\frac{\mathrm{d}N_S}{\mathrm{d}t}\right)^{ATE} = \left(U_S^{TE} - U_{ITP}\right) A c_S^{ATE} = p_{S,TE} U_{ITP} A \beta c_S^0 \tag{2.26}$$

and

$$\left(\frac{\mathrm{d}N_S}{\mathrm{d}t}\right)^{LE} = \left(U_{ITP} - U_S^{LE}\right) A c_S^{LE} = p_{S,LE} U_{ITP} A c_S^0, \tag{2.27}$$

where c_S^0 is the initial sample concentration loaded into either TE or LE, respectively. The ratio of these two (steady) molar fluxes guides optimal initial sample placement; hence we define

$$\phi \equiv \frac{\left(\frac{\mathrm{d}N_S}{\mathrm{d}t}\right)^{ATE}}{\left(\frac{\mathrm{d}N_S}{\mathrm{d}t}\right)^{LE}} = \frac{p_{S,TE}}{p_{S,LE}} \beta. \tag{2.28}$$

Unity is a threshold value for ϕ. For $\phi > 1$, sample ions should be loaded in the TE. For $\phi < 1$, they should be loaded into the LE. Alternatively, we can define a threshold sample mobility:

$$\mu_S^{thres} = \frac{(1+\beta)\mu_{TE}^0 \mu_{LE}^0}{\beta \mu_{LE}^0 + \mu_{TE}^0}. \tag{2.29}$$

Sample ions with mobility greater than μ_S^{thres} should be placed in TE; those with lower mobility should be placed into LE zone.

2.2.3 Fraction processed when sample is loaded in TE reservoir

We consider the fraction of initial sample processed by ITP when sample is loaded into the TE reservoir. For simplicity, we assume that the contents of the reservoir are well-stirred. We first express the total moles of sample extracted with ITP:

$$N_S^{TE}(t) = \int_0^t \left(\frac{\mathrm{d}N_S}{\mathrm{d}t} \right)^{ATE} \mathrm{d}t = \left(\frac{\mu_S}{\mu_{TE}} - 1 \right) U_{ITP} A\beta \int_0^t c_S^{well}(t)\mathrm{d}t = p_{S,TE} U_{ITP} A\beta \int_0^t c_S^{well}(t)\mathrm{d}t. \quad (2.30)$$

Here, μ_i represents the effective mobility of species *i,* β the ratio of TE ion concentrations in the ATE and TE zones defined in eq 2.4,and $p_{S,TE}$ the dimensionless separability defined in eq 2.22. This formulation reflects the fact that the concentration of sample molecules present in the reservoir $c_S^{well}(t)$ changes as a function of time. We relate this concentration to the number of moles leaving the TE reservoir by

$$c_S^{well}(t) = c_S^{well,0} - \frac{N_S^{TE}(t)}{\forall_{well}} = c_S^{well,0} - \frac{p_{S,TE} U_{ITP} A\beta}{\forall_{well}} \int_0^t c_S^{well}(t)\mathrm{d}t. \quad (2.31)$$

Here, $\forall_{well}$ is the volume of the reservoir and $c_S^{well,0}$ is the initial sample concentration in the reservoir. For convenience, we first differentiate eq 2.27 and rewrite it as an initial value problem:

$$\frac{dc_S^{well}(t)}{dt} + \frac{p_{S,TE} U_{ITP} A\beta}{\forall_{well}} c_S^{well}(t) = 0, \quad (2.32)$$
$$c_S^{well}(t=0) = c_S^{well,0}.$$

We then solve this first-order homogeneous differential equation and obtain:

$$c_S^{well}(t) = c_S^{well,0} \exp\left(-\frac{p_{S,TE} LA\beta}{\forall_{well}} t \right). \quad (2.33)$$

Substituting this result into eq 2.27 and carrying out the integration yields:

$$N_S^{TE}(t) = \forall_{well} c_S^{well,0} \left(1 - \exp\left(-\frac{p_{S,TE} U_{ITP} A\beta}{\forall_{well}} t \right) \right) = \forall_{well} c_S^{well,0} \left(1 - \exp\left(-\frac{p_{S,TE} \beta AL(t)}{\forall_{well}} \right) \right), \quad (2.34)$$

where *L* is the length of the channel swept by ITP, defined by:

$$L(t) = U_{ITP} t. \tag{2.35}$$

The total moles of sample loaded into the TE reservoir is given by:

$$N_S^{well} = \forall_{well} c_S^{well,0}. \tag{2.36}$$

To relate the two, we define *x*, the fraction of sample loaded into the TE reservoir that is processed by ITP,

$$x \equiv \frac{N_S^{TE}}{N_S^{well,0}} = \frac{\forall_{well} c_S^{well,0} \left(1 - \exp\left(-\frac{p_{S,TE} \beta A L(t)}{\forall_{well}}\right)\right)}{\forall_{well} c_S^{well,0}} = 1 - \exp\left(-\frac{p_{S,TE} U_{ITP} \beta A L(t)}{\forall_{well}}\right). \tag{2.37}$$

At the end of the experiment, when the assay is completed and ITP has reached the extraction or LE reservoir, eq 2.34 can be rewritten as:

$$x = 1 - \exp\left(-p_{S,TE} \beta \frac{\forall_{ITP}}{\forall_{well}}\right), \tag{2.38}$$

where $\forall_{ITP}$ represents the volume swept by the ITP focus zone (the peak). From these expressions, we see that the fraction of sample processed is determined by three factors: channel-to-reservoir volumetric ratio, well-to-ATE concentration adjustment, and ratio of sample and TE mobilities. We further note that when a small fraction of the sample is processed, such as when using channels with small channel-to-well volumetric ratio, eq 2.35 can be simplified using a truncated Taylor series as

$$x = p_{S,TE} \beta \frac{\forall_{ITP}}{\forall_{well}}. \tag{2.39}$$

In Figure 2.2 we show the dependence of fraction of sample processed *x* on several experimental parameters. We note that we expect to see large deviation from this

predicted result at large channel-to-reservoir volume fractions. Significant depletion of TE ions from the TE reservoir results in large pH change (>0.5) in the TE reservoir, which consequently alters species' mobilities and interferes with ITP dynamics.

2.2.4 Reaction rate in ITP-aided reaction assays. ITP can be used to accelerate reactions between two reactants A and B, when one or both are focused in ITP. We here consider a second order chemical reaction between two ionic reactants where both are

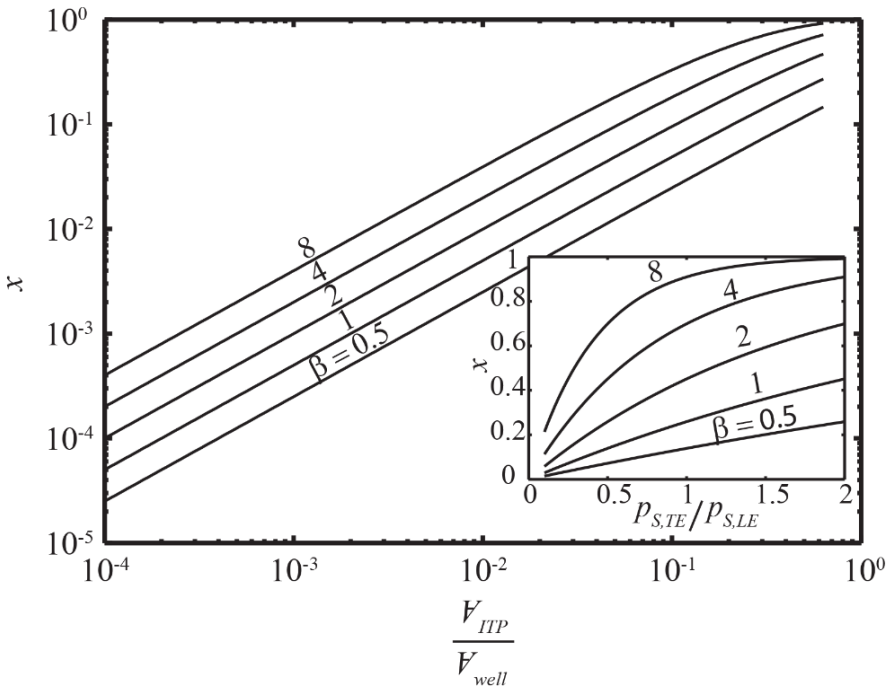

Figure 2.2. Fraction of sample loaded into a TE reservoir that is processed by ITP, x is shown against different experimental parameters. This fraction depends on volumetric ratio, adjustment in sample concentration upon entering adjusted TE zone, and separability between sample and TE ions. In the main figure, x is plotted against the ratio of the volume of the channel and the volume dispensed into the TE reservoir, at different values of β. For this figure, we assume $p_{S,TE} = 0.5$. Varying values of β, often by changing initial concentration of LE and TE ions, can result in processing significantly more sample, by up to an order of magnitude. Inset shows x plotted as a function of separability ratio and various values of β for a large channel with a volumetric ratio of 0.3. For such large-channels, sample depletion from the well-stirred TE reservoir is significant.

focused by ITP (e.g., RNA and cDNA in anionic ITP[1,3]), although our approach can be extended to other cases. We will here modify the mass-action reaction model first developed by Bercovici et al.[3] Bercovici presented volume-averaged conservation equations assuming overlapping Gaussian distributions for each reactant, resulting in the following ordinary differential equations:

$$\begin{cases} \dfrac{dc_A}{dt} = \dfrac{\left(\dfrac{\mathrm{d}N_A}{\mathrm{d}t}\right)^j}{\delta A} - \dfrac{3}{\sqrt{\pi}} k_{on} c_A c_B + k_{off} c_{AB} \\ \dfrac{dc_B}{dt} = \dfrac{\left(\dfrac{\mathrm{d}N_B}{\mathrm{d}t}\right)^j}{\delta A} - \dfrac{3}{\sqrt{\pi}} k_{on} c_A c_B + k_{off} c_{AB} \\ \dfrac{dc_{AB}}{dt} = \dfrac{3}{\sqrt{\pi}} k_{on} c_A c_B - k_{off} c_{AB}. \end{cases} \tag{2.40}$$

Here, j represents LE or ATE, depending on where each reactant is initially loaded. Here, c_A, c_B, and c_{AB} represents volume-averaged concentrations for A, B, and AB, respectively. Here, we will consider the configurations wherein both reactants are in the LE or both in TE. In Section 2.25, we consider the case where one reactant is placed in the TE and the other in the LE. For each of the two reacting species, the total amount at any time is related to the accumulation rate of that species in ITP, such that

$$\begin{aligned} c_A + c_{AB} &= \frac{\left(\dfrac{\mathrm{d}N_A}{\mathrm{d}t}\right)^j}{\delta A} t, \\ c_B + c_{AB} &= \frac{\left(\dfrac{\mathrm{d}N_B}{\mathrm{d}t}\right)^j}{\delta A} t, \end{aligned} \tag{2.41}$$

where δ is the characteristic width of the ITP zone (e.g. either an observed or predicted[72,73]). For simplicity, we make two further assumptions, following Bercovici et al.[3]:

$$\begin{aligned} &p_{A,i}c_A^j \gg p_{B,i}c_B^j, \\ &\frac{\left(\frac{\mathrm{d}N_A}{\mathrm{d}t}\right)^j}{\delta A}t \gg \frac{k_{off}}{k_{on}}, \end{aligned} \tag{2.42}$$

where *i* represents the LE or TE species and *j* represents LE or ATE zone, as above. The former inequality limit ensures that one species is in excess in ITP (we will call this reactant A; and the latter limit that the reverse (dissociation) reaction is negligible (low dissociation equilibrium constant). Under these assumptions, we substitute eq 2.38 into eq 2.37 and write:

$$c_{AB}^j = \frac{\left(\frac{\mathrm{d}N_B}{\mathrm{d}t}\right)^j t}{\delta A}\left(1-\frac{1}{2}\sqrt{\pi\tau_{rxn}^j t}\exp\left(-\frac{t}{\tau_{rxn}^j}\right)erfi\left(\sqrt{\frac{1}{\tau_{rxn}^j t}}\right)\right). \tag{2.43}$$

Here, we have defined τ_{rxn} as the reaction timescale for an ITP-aided reaction assay as:

$$\tau_{rxn}^j = \frac{\sqrt{\pi}}{3}\frac{\delta A}{k_{on}N_A^j}. \tag{2.44}$$

Again following Bercovici et al.[3], we expand the imaginary error function, erfi, as a Taylor series and truncate as $erfi(x) \simeq 2x/\sqrt{\pi}$ so approximate eq 2.40 as:

$$c_{AB}^j \cong \frac{N_B}{\delta A}\left(1-\exp\left(-\frac{t}{\tau_{rxn}^j}\right)\right). \tag{2.45}$$

Initial sample placement in an ITP-aided reaction assay is an important design parameter. To quantitatively capture this, we define

$$\varepsilon \equiv \frac{c_{AB}^{TE}}{c_{AB}^{LE}}, \tag{2.46}$$

where ε describes the ratio of product, AB, formation when both reactants are initially loaded into the TE (numerator) versus loading both into the LE (denominator). For the simplifying conditions listed in eq 2.39, ε can be written as

$$\varepsilon \cong \left(\frac{1-\exp\left(-\frac{t}{\tau_{rxn}^{TE}}\right)}{1-\exp\left(-\frac{t}{\tau_{rxn}^{LE}}\right)} \right) \phi_B. \tag{2.47}$$

Table 2.1. Key parameters defined and derived which characterize sample accumulation and reaction rate as a function of initial placement of sample in TE or LE.

Symbol	Interpretation	Definition
β	Ratio of sample concentration in ATE and TE zones	$\beta = \frac{c_{TE}^{ATE}}{c_{TE}^{TE}}$
γ	Ratio of initial LE and TE ion concentrations	$\gamma = \frac{c_{LE}}{c_{TE}^{well}}$
ϕ	Ratio of sample accumulation fluxes into ITP from TE and LE	$\phi = \frac{p_{S,TE}}{p_{S,LE}}\beta$
μ_S^{thres}	Threshold sample mobility for loading in LE or TE	$\mu_S^{thres} = \frac{(1+\beta)\mu_{TE}\mu_{LE}}{\beta\mu_{LE}+\mu_{TE}}$
τ_{rxn}^{j}	Reaction timescale in ITP-aided reaction	$\tau_{rxn}^{j} = \frac{\sqrt{\pi}}{3}\frac{\delta A}{k_{on}N_A^j}$
ε	Ratio of product formation in ITP-aided reactions for reactants loaded in TE and LE	$\varepsilon = \frac{c_{AB}^{TE}}{c_{AB}^{LE}}$

An important limiting condition for this ratio of reaction production rates is observed for process (reaction and ITP) times *t* which are significantly larger than, say, twice the value of both τ_{rxn}^{LE} and τ_{rxn}^{TE}. This regime is associated with long times (or distances to detector), high k_{on} values, and high species concentration. In this regime, the

concentration of AB grows linearly with time, so the problem is still unsteady but eq 2.44 simplifies to

$$\varepsilon \cong \phi_B. \tag{2.48}$$

Here reaction production rates are equal to net accumulation rates (c.f. eq 2.38).

2.2.5 ITP-aided reaction model for reactants loaded into different buffers

We here describe an assay that uses ITP to accelerate reactions between reactants A and B, where one is placed in the LE and another in the TE. We first consider the case wherein reactant A is placed in the TE and reactant B in the LE. The mass-action model would then look be

$$\begin{cases} \dfrac{dc_A}{dt} = \dfrac{\left(\dfrac{\mathrm{d}N_A}{\mathrm{d}t}\right)^{TE}}{\delta A} - \dfrac{3}{\sqrt{\pi}} k_{on} c_A c_B + k_{off} c_{AB} \\ \dfrac{dc_B}{dt} = \dfrac{\left(\dfrac{\mathrm{d}N_B}{\mathrm{d}t}\right)^{LE}}{\delta A} - \dfrac{3}{\sqrt{\pi}} k_{on} c_A c_B + k_{off} c_{AB} \\ \dfrac{dc_{AB}}{dt} = \dfrac{3}{\sqrt{\pi}} k_{on} c_A c_B - k_{off} c_{AB}. \end{cases} \tag{2.49}$$

For the same assumptions listed in eq 2.39 (reactant A is in excess of reactant B), we can derive concentration of product formed in this configuration,

$$c_{AB}^{TE-LE} \cong \frac{N_B^{LE}}{\delta A}\left(1 - \exp\left(-\frac{t}{\tau_{rxn}^{TE}}\right)\right). \tag{2.50}$$

Here, N_B represents ITP-focused moles of reactant B. Alternatively, if reactant A is initially placed in the LE and B in the TE and for the same assumptions listed above, c_{AB} (t) would be given by:

$$c_{AB}^{LE-TE} \cong \frac{N_B^{TE}}{\delta A}\left(1-\exp\left(-\frac{t}{\tau_{rxn}^{LE}}\right)\right). \tag{2.51}$$

In Table 2.2, we summarize c_{AB} (t) for the four possible configurations for the case of reactant A being in excess of B. When comparing two configurations that share placement of one reactant (e.g. placing both reactants A and B in the TE or reactant A in the TE and B in the LE), the ratio of c_{AB} (t) values, like ε from eq 2.44, simplifies. Either the accumulation rate prefactor, ϕ_B (when B is placed in the same buffer for both configurations), or the reaction timescale ratio involving τ_{rxn} cancels out (when A is placed in the same buffer for both configurations). Table 2.3 shows ratio of production ε, as function of ϕ, for the different reactant loading configurations. We note that since there are 4 such cases, only 3 independent ratios exist.

Table 2.2. Summary of product concentration, c_{AB} (t), for different reactant loading configurations. Reactant A is taken as the reactant in excess (which governs time to completion of reaction) and B is taken as the low abundance reactant (which limits maximum value of complex AB).

Initial placement	$c_{AB}(t)$
A in TE, B in TE	$\frac{N_B^{TE}}{\delta A}\left(1-\exp\left(-\frac{t}{\tau_{rxn}^{TE}}\right)\right)$
A in TE, B in LE	$\frac{N_B^{LE}}{\delta A}\left(1-\exp\left(-\frac{t}{\tau_{rxn}^{TE}}\right)\right)$
A in LE, B in TE	$\frac{N_B^{TE}}{\delta A}\left(1-\exp\left(-\frac{t}{\tau_{rxn}^{LE}}\right)\right)$
A in LE, B in LE	$\frac{N_B^{LE}}{\delta A}\left(1-\exp\left(-\frac{t}{\tau_{rxn}^{LE}}\right)\right)$

Table 2.3. Ratio of production, ε, as function of ϕ, for the different reactant loading configurations. ε is plotted for times below and above twice the value of τ_{rxn},

ε	$t \lesssim 2\tau_{rxn}$	$t \gtrsim 2\tau_{rxn}$
$\varepsilon \equiv \frac{c_{AB}^{TE-TE}}{c_{AB}^{TE-LE}}$	ϕ_B	ϕ_B
$\varepsilon \equiv \frac{c_{AB}^{TE-TE}}{c_{AB}^{LE-TE}}$	$\frac{1-\exp\left(-\frac{t}{\tau_{rxn}^{TE}}\right)}{1-\exp\left(-\frac{t}{\tau_{rxn}^{LE}}\right)}$	1
$\varepsilon \equiv \frac{c_{AB}^{TE-TE}}{c_{AB}^{LE-LE}}$	$\left(\frac{1-\exp\left(-\frac{t}{\tau_{rxn}^{TE}}\right)}{1-\exp\left(-\frac{t}{\tau_{rxn}^{LE}}\right)}\right)\phi_B$	ϕ_B

2.3 Results and discussion

2.3.1 Accumulation rates in ITP assays

We first presented a simple formulation for the concentration of sample in the ATE (c.f. Figure 1b), the zone from which it can directly focus into the ITP peak. We also presented the ratio of initial LE and TE concentrations, γ, a critical initial condition for sample mixed with TE. We used these factors and the concept of (non-dimensional) separability to quantify the relative rates of accumulation as a function of initial sample location. In Figure 2.3 we plot ratio of accumulation rate for samples mixed with TE and LE, ϕ, as a ratio of the separabilities of sample in TE ($p_{S,TE}$) and sample in LE ($p_{S,LE}$), as per eq 2.25. ϕ is determined by the product of ϕ and $p_{S,TE}/p_{S,LE}$. The proportionality to ϕ (and therefore β) shows the value of the field-amplified-type stacking of the sample as it migrates from TE to ATE. The magnitude of this stacking is achieved by establishing a high initial γ, and so leveraging the strict regulation of the ATE imposed by the LE. The proportionality to $p_{S,TE}/p_{S,LE}$ shows the relative importance

of establishing a strong ratio of ion mobility to the *local* co-ion mobility. ϕ greater than unity implies superior accumulation rate by placing sample in the TE. Note that fairly aggressive (but experimentally achievable) combinations of β and $p_{S,T}/p_{S,LE}$ (e.g., β = 0.5 and $p_{S,T}/p_{S,LE}$ = 0.25 or conversely β = 8 and $p_{S,T}/p_{S,LE}$ > 2) there can be a 10-fold improvement in accumulation rate by LE vs. TE (or vice versa).

The accumulation rates of Figure 2.3 can be used as initial design guidelines, but we note these are neither precise nor the only consideration. Our formulation neglects the effects of pH and ionic strength on electrophoretic mobility, and this is particularly important for polyions.[76,80] In Section 2.2.1, we derived accumulation rates accounting for influence of pH on electrophoretic mobility of singly-ionized TE species. The practical range of viable values of γ is constrained to different limits by Joule heating, maximum achievable voltage (e.g., to drive current through a low concentration TE), and the buffering capacity of the TE buffer. The latter is important when using a separation channel volume that is not small relative to electrode reservoirs and low c_{TE} buffer in an electrode reservoir (see Persat et al.[81] for volume-specific estimates of buffering strength). See Marshall[79] for a discussion of various ITP design parameters.

Initial sample placement may also be driven by need to have highly pure sample, as in the peak mode focusing of nucleic acids from complex samples.[29] The latter can drive a designer to lower values of $p_{S,TE}$ to ensure TE ions overspeed a relatively high mobility contaminant (e.g., sodium dodecyl sulfide surfactant).

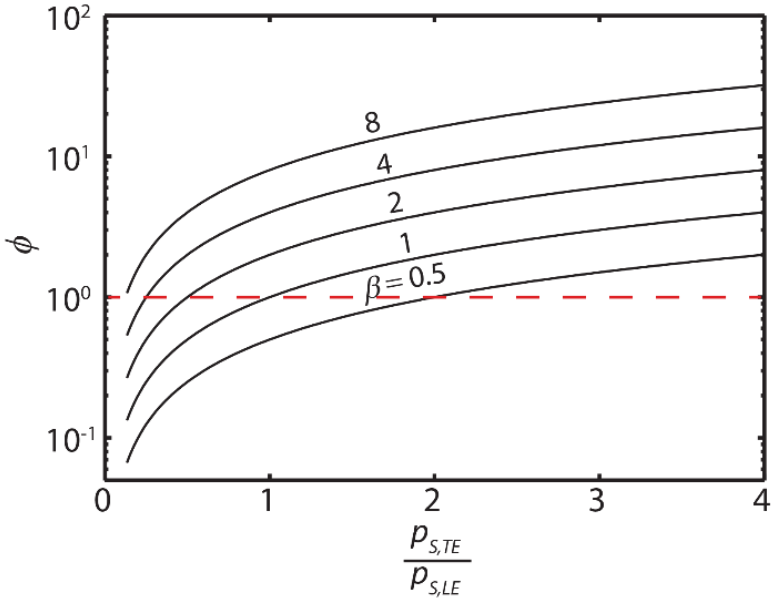

Figure 2.3. Ratio of accumulation rate from the TE and LE, ϕ, is plotted as a function of the ratio separabilites and β. ϕ is linearly depends on the relative mobility of sample ions and surrounding buffer ions, and the adjustment in sample ion concentration upon entering the ATE zone from the TE. Unity (dashed red line) is a threshold value for ϕ. For $\phi > 1$, sample ions should be loaded in the TE. For $\phi < 1$, they should be loaded into the LE.

ITP zone. However, $p_{S,TE}$ would likely be significantly smaller than $p_{S,LE}$, and the resulting ϕ less than unity. In such cases, $p_{S,TE}$ may be significantly smaller than $p_{S,LE}$, prompting mixing sample with LE. On the other hand, assays users aiming to extract a wide range of analytes, may choose high values of γ and $p_{S,TE}$ so placing the sample in TE would maximize accumulation. For example, designing a TE buffer with pH close to that of the isoelectric point of a protein drives very low sample mobility in the TE, prompting placing the sample in the LE. Type of contaminants is another important factor to consider, particularly in the presence of high-mobility, "LE-like" species such as NaCl. In such cases, the sample would either have to be diluted significantly in the TE or mixed with the LE.

2.3.2 Reaction rates in ITP assays

Finally, we explored reaction rates in ITP-aided reaction assays. Figure 2.4a presents the relationship between normalized concentration of product formed and normalized time, derived in eq 2.42 for the limiting assumptions listed in eq 2.39. We normalized c_{AB} by the concentration of the limiting species (reactant B) in ITP, $N_B/\delta A$, and time by a reaction timescale, τ_{rxn}, that incorporates association constant (k_{on}) and the accumulation rate of excess species (reactant A) in ITP. For t/τ_{rxn} ratio <2, we find that normalized product concentration increases with normalized time. For t/τ_{rxn} >2, however, the rate at which product is formed equals the rate at which the limiting species arrives at the ITP zone, and a quasi-equilibrium is established between the two rates. This regime represents optimal reaction rate in an ITP-aided assay, wherein the limiting species enters ITP and is immediately depleted through reaction. This analytical solution only applies when one reacting species exists in excess, a commonly encountered case in many reaction assays.

Figure 2.4b demonstrates how sample placement impacts reaction rate in ITP-aided reaction assays. We normalized ε, the ratio of product formed from TE and LE, by ϕ_B. We find the existence of different regimes where loading in LE is favorable over TE (high values of t/τ_{rxn}^{LE} and low values of t/τ_{rxn}^{TE}) and others where loading in TE is favorable (high values of t/τ_{rxn}^{TE} and low values of t/τ_{rxn}^{LE}). For large values of $t/\tau_{rxn}^{TE}$and t/τ_{rxn}^{LE} ε is equal to ϕ_B, a result we showed in eq 2.45. In such cases, optimal sample placement is independent of excess species and depends only on accumulation rate of limiting species.

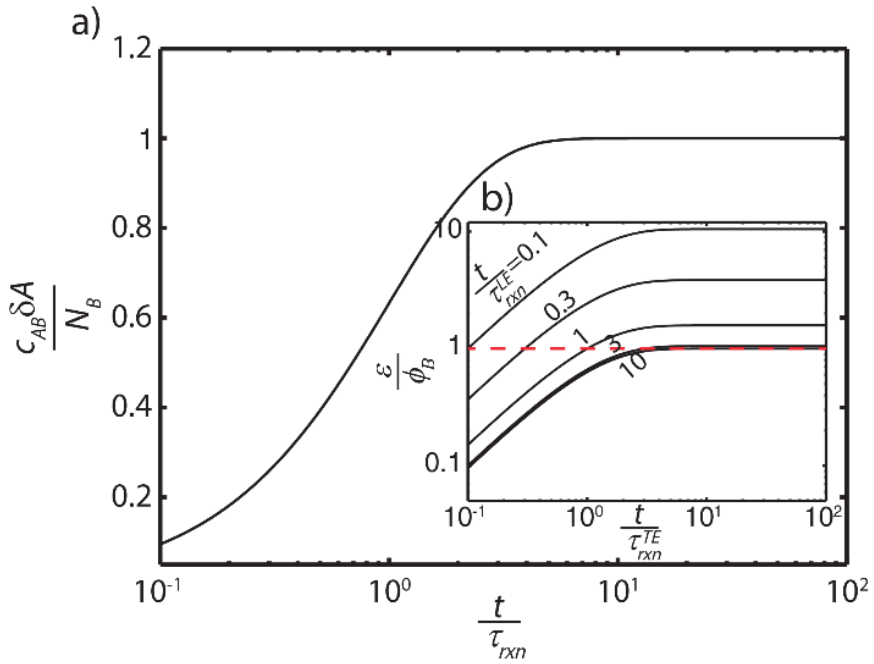

Figure 2.4. Reaction rates in ITP-aided assays. a) Plot of the analytical solution presented in eq 2.45. Concentration of reaction product, c_{AB}, is normalized by the concentration of limiting species (B) accumulated in ITP and shown versus time normalized by characteristic ITP-driven reaction time, t/τ_{rxn}. For large times, rate of product formation is equal to the accumulation rate of the limiting species, indicating a quasi-equilibrium regime. b) Inset shows dependence of product formation ratio ε on initial sample loading. We show the existence of different regimes favoring loading in the LE (below the red dashed line) or TE (above the red dashed line). We find that for large values of both $t/\tau_{rxn}^{LE}$and t/τ_{rxn}^{TE}, production rate ratio ε is determined solely by accumulation rate ratio ϕ_B.

2.3.3 Case study: ITP-based DNA extraction and reaction assay design

We consider sample placement in the design of DNA extraction and reaction assays using anionic ITP. We assume all species are fully-ionized in the following case study. Nucleic acids have largely similar, relatively high, mobilities in free solution, independent of their size.[46] Free-solution DNA mobility is approximated at 30 x 10^{-9} $m^2V^{-1}s^{-1}$.[46] We also here assume chloride ion, Cl^-, as LE species with mobility of 79 x 10^{-9} $m^2V^{-1}s^{-1}$. In Figure 2.5, we show how the accumulation ratio, ϕ, varies as a function

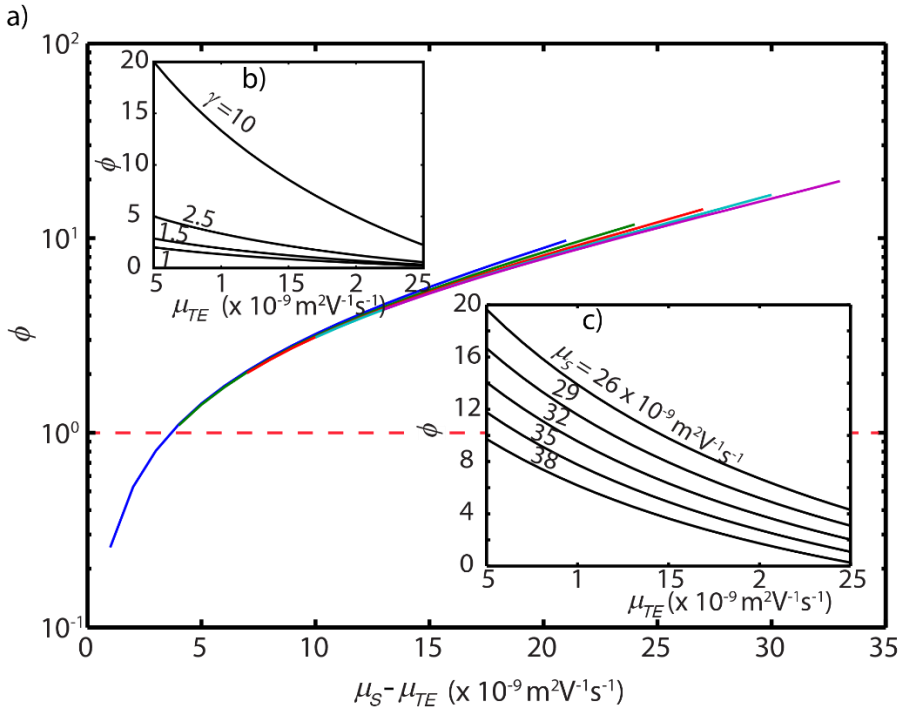

Figure 2.5. Ratio of sample accumulation rate into ITP zone from TE and LE, ϕ, as a function of several experimental parameters for values typical of DNA and RNA focusing using ITP. For all plots, we assumed Cl^- as LE species, with mobility of 79 x 10^{-9} $m^2V^{-1}s^{-1}$. a) ϕ as a function of the mobility difference between sample and TE for TE mobilities ranging from 5 x 10^{-9} to 25 x 10^{-9} $m^2V^{-1}s^{-1}$ and sample mobilities ranging from 26 to 38 x 10^{-9} $m^2V^{-1}s^{-1}$ results in essentially collapsed curves, indicating that this difference is a simple and predictive indicator of optimal initial sample loading. We set the ratio of initial LE and TE concentrations, γ, equal to 6 for demonstration purposes, though we note that the curves plotted largely collapse independently of γ value used. Unity (dashed red line) is a threshold value for ϕ. For $\phi > 1$, sample ions should be loaded in the TE. For $\phi < 1$, they should be loaded into the LE. b) ϕ is plotted as a function of TE mobilities, again ranging from 5 x 10^{-9} to 25 x 10^{-9} $m^2V^{-1}s^{-1}$, and values of γ ranging from 1 to 10. For higher values of γ, placing sample in TE results in significantly greater sample concentration in ATE zone, which in turn leads to much higher flux rate from the TE compared to LE. We set sample mobility as 30 x 10^{-9} $m^2V^{-1}s^{-1}$, an approximation of free-solution mobility of DNA. c) Here we plot ϕ for TE mobilities ranging from 5 to 25 x 10^{-9} $m^2V^{-1}s^{-1}$ and sample mobilities ranging from 26 x 10^{-9} to 38 x 10^{-9} $m^2V^{-1}s^{-1}$. Similarly to a), we set γ = 6 for demonstration purposes. Under these conditions, we find that placing sample in the TE is favorable for all but the highest mobility TE's (mobility near 25 x 10^{-9} $m^2V^{-1}s^{-1}$).

of LE and TE buffer concentrations, and sample and typical TE mobilities. We used values for buffer concentrations and mobilities commonly encountered in ITP experiments with DNA. Our fully ionized mobility values for TE co-ion range from 5 x 10^{-9} to 25 x 10^{-9} $m^2V^{-1}s^{-1}$. This range bounds the fully ionized (absolute) mobilities of, for example, the weak acids HEPES, TAPS, MOPS, and MES, which are common TE's for ITP (particularly peak mode focusing of DNA).[29] Also, we varied ratio of initial LE and TE concentrations, γ, from 1 to 10 which covers many applications (while respecting the requirement to buffer the TE reservoir).Interestingly, we find that for a wide range of sample and TE mobilities, the curves for ϕ vs. μ_S - μ_{TE} collapse, indicating that μ_S - μ_{TE} is in itself a good predictor of optimal sample placement in DNA assays. In Figure 2.6, we show the dependence of ε, defined in eq 2.43, on reactant and TE mobilities. We consider both free-solution and sieving conditions. For the latter case, we make the simplifying assumption that buffer ions are largely unaffected by the sieving matrix but that DNA mobility is size and matrix-dependent. We find that for experiments in free-solution, and using typical TE buffers and concentrations, placing reactants in TE is often favorable. In sieving matrices, using a typical TE buffer of Tris-HEPES (pH 8.2), we find that optimal sample placement depends on level of sieving and resulting DNA mobility.

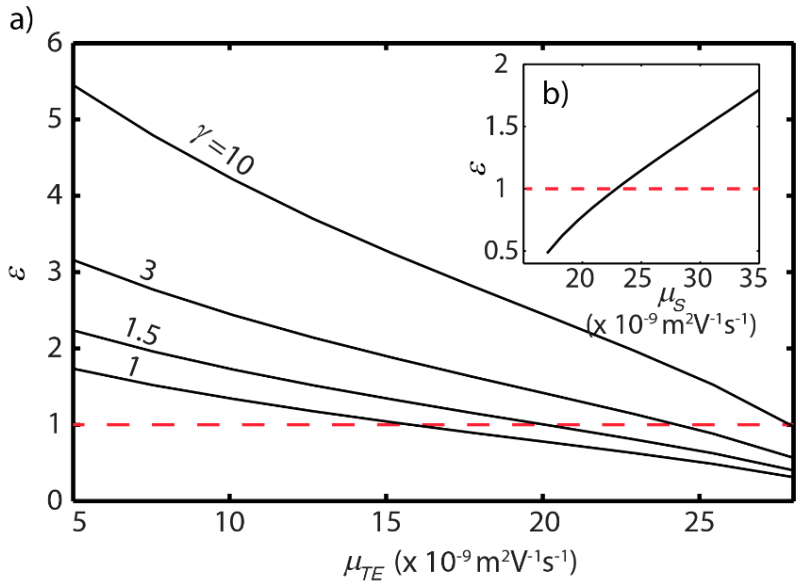

Figure 2.6. Reaction rates in ITP-aided DNA hybridization assays. For all plots, we assumed Cl^- as LE species, with mobility of 79 x 10^{-9} $m^2V^{-1}s^{-1}$. Unity (dashed red line) is a threshold value for ε. a) The ratio of product concentration, ε, is plotted for γ ranging from 1 to 10, and TE mobility ranging from 5 to 25 x 10^{-9} $m^2V^{-1}s^{-1}$, values commonly encountered in typical ITP experiments with DNA. Here mobility of probe and target molecules was assumed to be 30 x 10^{-9} $m^2V^{-1}s^{-1}$, consistent with approximate DNA mobility in free solution. We find that placing reactants in the LE is only favorable at low values of γ and high TE mobility. This indicates that for experiments using DNA and/or RNA as reactants in free solution, placing both reactants in TE is favorable for a majority of typical buffer concentrations and TE mobilities. b) Here we simulate sieving conditions, and vary sample mobility accordingly. We note that in sieving matrices, mobility of DNA is heavily size-dependent.[9] We plot ε for sample mobilities varying from 15 x 10^{-9} to 35 x 10^{-9} $m^2V^{-1}s^{-1}$, and set TE mobility to 15 x 10^{-9} $m^2V^{-1}s^{-1}$, that of HEPES, a widely-used TE ion, at pH 8.2. For this TE mobility, samples should be placed in the LE when sample mobility exceeds 25 x 10^{-9} $m^2V^{-1}s^{-1}$, and in the TE for lower sample mobilities.

2.4 Summary

In summary, we presented an analytical model examining accumulation and reaction rates in ITP. We identify a regime of quasi-equilibrium wherein reaction rate equals accumulation rate of reactants. We explored the role of sample placement in optimizing these rates. Our model enables a user to make informed decisions regarding optimal

sample placement. Finally, we delved into a case study of nucleic acid extraction and reaction in ITP. We believe that this model provides useful insight about a critical component of ITP assay design.

3 DNA detection using ITP and ionic spacer

Several sections of this chapter are based on a recent article published in *Analyst*, and are reproduced here with minor modifications.[†]

3.1 Introduction

We present an on-chip electrophoretic assay for rapid and high sensitivity nucleic acid (NA) detection. The assay uses isotachophoresis (ITP) to enhance NA hybridization and an ionic spacer molecule to subsequently separate reaction products. The technique offers a rapid and highly-sensitive alternative to traditional DNA hybridization assays, and can be multiplexed and extended to detect other biomolecules.

As discussed in Chapter 1, hybridization assays for trace target concentrations suffer from slow second-order kinetics that result in very long assay times.[4] Isotachophoresis (ITP)-based hybridization is one approach that offers enhancement of reaction kinetics and integration with fluorescent detection. Recently, ITP has been shown to achieve up to 14,000-fold reaction speed-up in NA-based hybridization systems.[5] A current limitation to assay sensitivity is background signal inherent to unreacted fluorescent probes. To our knowledge, two methods have been reported to physically separate unreacted probes and complexes in homogenous ITP assays. This separation improves signal-to-noise ratio (SNR) by reducing fluorescence background. The first method used a gel polymer functionalized with DNA target molecules that bind to unreacted probe

[†] C. Eid, G. Garcia-Schwarz, and J.G. Santiago, "Isotachophoresis with ionic spacer and two-stage separation for high sensitivity DNA hybridization assay," *Analyst*, 2013. **138**(11): p. 3117-20.

to remove excess reactant.[6] That technique demonstrated 2.8 pM sensitivity, which to our knowledge is the lowest limit of detection achieved using ITP-based DNA hybridization assays. However, sensitivity is limited by the remnant fluorescent reporter molecules following migration through the capture gel. The second method combined ITP with capillary electrophoresis (CE) to separate unreacted probe from the probe-target complex, and demonstrated 5 pM sensitivity.[7] The latter approach offers size-based separation, but the separated zones are subject to the dispersion effects of CE, thereby decreasing signal strength.

This chapter presents a new method of improving the SNR of ITP DNA fluorescence hybridization assays: We use two separation regions in series and an ionic spacer to separate reaction products from reactants. The assay consists of three main stages: incubation of reactants under ITP focusing, separation of probes from probe-target complex, and detection of independently focused reaction products and fluorescent probes. Through the use of the ionic spacer, we maintain the products and reactants each in a discrete ITP zone while still providing a rapid (40 to 45 s) transition from incubation to the fully separated state. Maintaining products and reactants in ITP mode is advantageous as it gives the designer flexibility as to where to place a detector (since signal is preserved over time) and facilitates further downstream manipulations (such as fractionation) without incurring dispersion losses. Further, creating two focused ITP zones allows for an internal control based on the ratio of the integrated signal of the two zones, making this method particularly robust to variations in injection amounts. Using this technique, we demonstrate a limit of detection of 220 fM in less than 10 min, with 3.5-decade dynamic range.

ITP is an electrophoretic technique that relies on a heterogeneous buffer system comprising a high mobility leading electrolyte (LE) and low mobility trailing electrolyte (TE) to achieve focus target analytes.[8] Here, we achieve probe DNA and target DNA preconcentration of order 10,000x and higher. Our assay includes a spacer ion with intermediate mobility which forms a plateau region between the LE and TE, thereby creating two sharp interfaces between the LE and spacer and between the spacer and TE. **Figure 3.1** demonstrates the steps in our reaction-separation assay. First, we leverage ITP to focus the probe and target molecules and accelerate second-order hybridization kinetics (time t_1). The second and third stages of the assay, denoted respectively by t_2 and t_3, employ a linear sieving matrix to separate the reaction products. The channel initially contains two LE regions in series, as shown **in Figure 3.1b**. LE1 includes no sieving matrix, while LE2 includes a sieving matrix. The sieving matrix primarily affects mobility of DNA molecules relative to small ions. In the LE1 region, spacer ions have an electrophoretic mobility lower than that of the probe, target, and probe-target complexes. This enables simultaneous rapid mixing and preconcentration of the probe and its target.[5] Upon entering LE2, the spacer ions overtake the now slower target and probe-target complex. The spacer has sufficient initial concentration to quickly form a plateau ITP region which separates excess probes from probes hybridized to target molecules. In this final stage, the excess probe molecules continue to focus between the LE and the spacer, while the probe-target complexes focus in a separate ITP zone between the spacer and the TE. This enables sensitive detection of the probe-target complexes in the absence of unhybridized fluorescent probe molecules.

3.2 Materials and methods

3.2.1 Materials and reagents

All experiments were performed on a 12 µm deep Crown glass NS-260 chip from Caliper Life Sciences (Mountain View, CA). We chose 100 mM chloride as our LE anion and 20 mM HEPES anion for our initial TE buffer mixture. The LE and TE buffers contained respectively 200 and 40 mM Tris cation, resulting in predicted pH of 8.1 in the LE zone and 8.6 in the TE zone. The spacer for all experiments was MOPS,

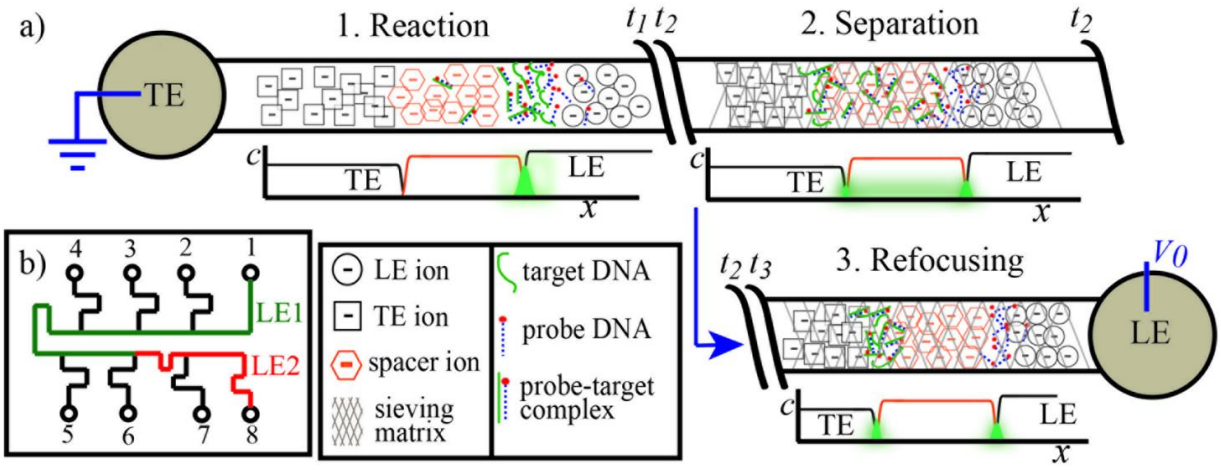

Figure 3.1. a) Schematic representation of the ITP-spacer assay, showing the three stages of the assay: (1) Reaction between the short (27 nt) DNA probe and the complementary (149 nt) target in free-solution conditions. In this stage, spacer molecules migrate at a mobility lower than that of the target DNA. (2) Upon entering the sieving matrix region (1.8% HEC), the ionic spacer molecules gradually overspeed the now slower target molecules and probe-target hybrids. (3) Following approximately 40 s of separation, the reaction products are fully separated and refocused among the two ITP interfaces. Excess probe molecules focus between the LE and spacer, whereas the probe-target hybrids focus between the spacer and the TE. b) Schematic of the Crown glass chip layout used for the assay. We initially load the microchannels with LE1 (no sieving matrix) and LE2 (1.8% HEC). We apply voltage between reservoir wells 1 (TE) and 8 (LE). The region containing LE1, which spans 5cm in length, allows for simultaneous mixing and preconcentration of the reactants in ITP mode. In the region containing LE2, spanning 3 cm in length, the reactant products separate and refocus.

which has an effective free-solution mobility of 18.5 x 10^{-9} m^2/V.s, higher than the 15.5 x 10^{-9} m^2/V.s effective mobility of HEPES in the adjusted TE zone. We chose the linear polymer hydroxyethyl cellulose (HEC) as our sieving matrix. At overly high HEC concentrations, the reproducibility of the experiments was compromised by the high viscosity of the HEC solution. We found that an HEC concentration of 1.8% (w/v) offered an effective compromise between fast resolution of the peaks and repeatability. In all buffers we included 1% (w/v) polyvinylpyrrolidone (PVP) for further electroosmotic flow suppression.[9] Interestingly, we have found that PVP does act as a sieving matrix at high concentrations (above 4%) but not significantly at 1%. We also included 5 mM magnesium chloride in the LE to improve DNA hybridization kinetics.[10] Finally, we use 4M urea in the LE1 region to improve selectivity and reaction completion by denaturing secondary structure. We note that we have optimized the assay to optimally separate 149 nt long DNA, but the chemistry and sieving matrix concentration can be optimized for targets of varying lengths. Denatured DNA have well-studied mobilities,[11] which facilitates such modifications of the assay.

We purchased 3-(N-morpholino)propanesulfonic acid (MOPS), 4-(2-Hydroxyethyl)piperazine-1-ethanesulfonic (HEPES), trizma base, and hydroxyethyl cellulose (HEC, MW = 250,000) from Sigma-Aldrich (St. Louis, MO). Pre-pared UltraPure 1M Tris-HCl (pH 8.0) and DNase/RNase-free distilled water were obtained from Invitrogen (Life Technologies, Carlsbad, CA). We purchased hydrochloric acid from J.T. Baker (Avantor Performance Materials, Center Valley, PA). Sodium hydroxide was procured from Mallinckrodt Chemicals (Avantor Performance Materials, Center Valley, PA). We purchased Urea and magnesium chloride from EMD Millipore

(Gibbstown, NJ). Polyvinylpyrrolidone (PVP, MW = 1,000,000) was obtained from Polysciences, Inc. (Warrington, PA).

We obtained the polyacrylamide gel (PAGE)-purified synthetic DNA oligonucleotides from Genelink (Hawthorne, NY). The sequences are shown in **Table 3.1**. We reconstituted the oligonucleotides in 10 mM Tris-HCl buffer. Further dilutions were prepared in 20 mM Tris-HEPES buffer. Stock solutions were stored in -20°C. DNA solutions were kept in 4°C for short-term usage. We purchased Crown glass microfluidic chips (model NS260) from Caliper Life Sciences (Mountain View, CA). Chip geometry and layout is detailed in **Figure 3.2.**

Table 3.1. Sequence of the synthetic DNA oligonucleotides used here as well as melting temperatures (T_m) as predicted by the manufacturer.. Both oligonucleotides are purified by polyacrylamide gel electrophoresis (PAGE).

Description	**Sequence**	**T_m (°C)**
27 nt probe	5-/Cy5/ CAT CGT TTA CGG CGT GGA CTA CCA GGG -3	66.9
149 nt target	5- ATT GGG AGT GGT TGA TGC TCT ATA CTC CAG TAG CAA GGC ACT TCC GGA CTC AAT GAA GGG CCG GGA CCC TGG TAG TCC ACG CCG TAA ACG ATG AAG GAG CCA ATA CAA AGG CTT CAT CCT CAC TCG CAT GGA GGC AAA CGC AGA ACA AT- 3	80.6

3.2.2 Experimental setup and apparatus

Experimental visualizations were performed on an epifluorescent microscopy setup. The components of the setup include an inverted epifluorescent microscope (Eclipse TE200, Nikon, Melville, NY) equipped with 4x and 10x objectives (PlanApo, Nikon, Melville, NY) and Cy5 filter cube (XF110-2, Omega, Brattleboro, VT). Illumination was provided by a 100 W short-arc mercury lamp (102DH, Ushio, Tokyo, Japan). The microscope was connected to a coupled charge device (CCD) camera (Coolsnap, Roper

Scientific, Trenton, NJ). We triggered the microscope with a function generator (Model 555, Berkeley Nucleonics, San Rafael, CA). We used a high-voltage sourcemeter (2410, Keithley Instruments, Cleveland, OH) and applied constant current (at 2.5 μA) to the chip. We controlled the sourcemeter and recorded data using a custom MATLAB (R2011a, Mathworks, Natick, MA) script.

Data acquisition was performed using a custom built point-confocal epifluorescent microscopy setup, described by Bercovici et al.[1] and Garcia-Schwarz and Santiago.[2] We refer to Garcia-Schwarz and Santiago. for a detailed schematic of the experimental setup (see their Supplemental Information document). Briefly, the setup consists of an inverted epifluorescent microscope (IX70, Olympus, Hauppage, NY) equipped with 60x water-immersion objective (LUMPlanFL, Olympus, Hauppage, NY) and Cy5 filter cube (Cy5-4040A, Semrock, Rochester, NY). An automated stage (ASI, Eugene, OR) was used to adjust chip location and focus. Illumination was provided by a 642 nm diode laser (Stradus-642, Vortran Laser Technologies, Sacramento, CA). The microscope was also connected to a photomultiplier tube (PMT) model (H6780-20, Hamamatsu Photonics, Hamamatsu, Japan) with data acquisition unit (C8908, Hamamatsu Photonics, Hamamatsu, Japan) for detection. The PMT was triggered by a function generator (E3631A, Agilent Technologies, Santa Clara, CA) and operated at a rate of 66.7 Hz (with 10 ms integration time). We used a high-voltage sourcemeter (2410, Keithley Instruments, Cleveland, OH) and applied constant current (at 2.5 μA) to the chip. We controlled both the PMT and sourcemeter and recorded data using a custom MATLAB (R2007b, Mathworks, Natick, MA) script.

3.2.3 Chip layout and assay protocol

Before each run, we rinsed the chip to clean and prepare the glass channel surfaces for experiments. By rinsing, we refer to the process of injecting a volume into the reservoirs, followed by applying vacuum at reservoir 6 to fill the rest of the channel. The process was carried out in the following steps:

1. Rinse with deionized (DI) water for 10 min
2. Rinse with 1M sodium hydroxide for 5 min
3. Rinse with 1M hydrochloric acid for 5 min
4. Rinse with DI water for 10 min

Immediately following this process, we loaded the chip and ran the assay as follows:

1. Pipette 10 µL of LE1 into reservoirs 1, 2, 3, 4, 5, 6 and 10 µL of LE2 into reservoirs 7 and 8.
2. Apply vacuum at reservoir 6 to fill the channel with the buffer solutions LE1 and LE2.
3. Quickly empty reservoirs 1 and 4, clean with a small amount of DI water, and pipette TE into reservoir 4 and TE+sample into reservoir 1.
4. Place the ground electrode in reservoir 1 and the high with reservoir 8. As soon as the sample zone reaches the pre-determined observation point, switch the ground electrode from reservoir 1 to reservoir 4. This process is described in **Table 3.2** below.

During the injection phase, we applied 1 mW of laser power. In the detection phase, however, the laser powered applied depended on the target concentration. For the negative control as well as at target concentrations of 220 fM and 760 fM, we used 110

Table 3.2. Electrode arrangement for injection and detection steps. Termination of the injection and detection phases was triggered by the arrival of the sample plug into a fixed observation point. We applied 2.5 μA constant current between ground (GND) and positive (HI).

Step	**Approximate Duration (s)**	**Reservoir**							
		1	2	3	4	5	6	7	8
Injection	190	GND	-	-	-	-	-	-	HI
Detection	380	-	-	-	GND	-	-	-	HI

mW of laser power. We used 1 mW for higher concentrations, including 76 pM, 760 pM, 7.6 nM, and 76 nM. At 7.6 pM, we used both 1 and 110 mW in order to compute a conversion factor between 1 and 110 mW laser powers. This conversion factor was necessary due to slight photobleaching that may occur at higher laser powers and any differences in quantum yield (e.g., due to saturation of the fluorescence rate). We found this conversion factor to be 37.75 (i.e., 1 fluorescence unit at 1 mW is equivalent to 37.75 units at 110 mW).

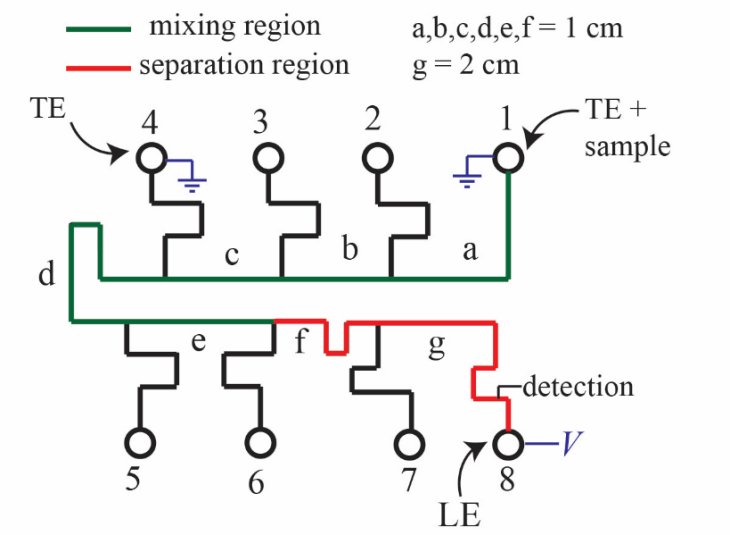

Figure 3.2. Layout of microfluidic Crown glass chip used for all experiments. The mixing region (green) contains LE with no sieving matrix present. The separation region (red) contains LE along with 1.8% HEC polymer. TE, TE + sample, and LE were all dispensed into their respective reservoirs prior to the application of electric field. The procedure for loading chip and applying voltage is described in Section S3 and Table S1. The first observation point was located a few millimeters beyond reservoir 4. When the sample plug reached that point, we observed a peak in the signal, attributed to the fluorescence of the probe molecules. At this point, the GND was switched from reservoir 1 to reservoir 4 for the remainder of the experiment.

3.3 Results and discussion

3.3.1 Visualization of separation

We performed experiments to visualize the reaction and separation processes using a charged coupled device (CCD) camera (Coolsnap, Roper Scientific, Trenton, NJ), as shown in **Figure 3.3**. To demonstrate experimentally the three stages of our assay, we constructed a spatiotemporal plot showing the signal intensity as a function of axial channel dimension (abscissa) and time (ordinance) (**Figure 3.3a**). We also show individual snapshots of the separation process at various times (**Figure 3.3b**). Initially, the analytes migrate together in a single peak in free solution (time t_1). Upon entering

the sieving matrix, the two peaks begin to separate, with a comet-shaped cloud migrating from the first ITP zone toward a second, newly formed ITP zone which trails the first by about 0.6 mm (t_2 and t_3) Eventually, the spacer ions overtake the slower probe-target complexes completely, and the reaction products are fully separated and focused in ITP mode (time t_4). The separation process takes approximately 40 s for a spacer concentration of 0.5 mM MOPS (included in the TE).

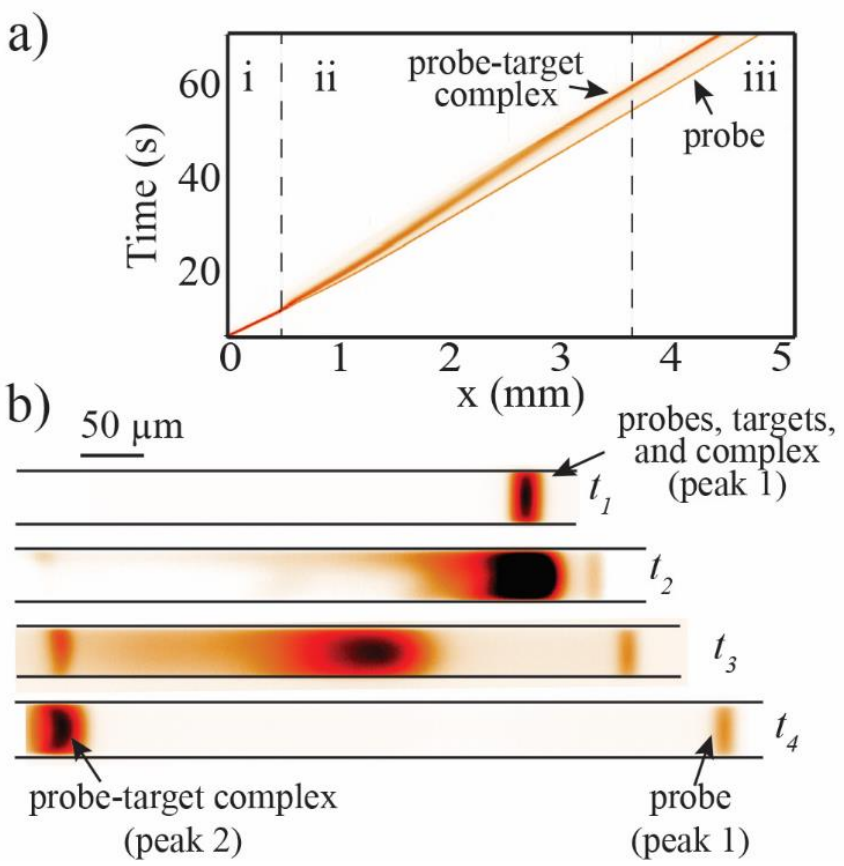

Figure 3.3. Experimental visualizations of reaction and separation regions of the ITP-spacer assay. a) Spatiotemporal plot demonstrating the three stages of the assay: (i) the two reactants co-focus between the LE and spacer, resulting in a single peak, (ii) upon entering the separation region, the spacer ions overtake the probe-target complex, and (iii) reaction products are fully separated by the spacer region and refocus at separate ITP interfaces. b) Images of the separation process at four times. Image intensities are scaled individually to optimize contrast. Times t_1 are the mixing/reaction stage, t_2 and t_3 show the separation, and t_4 shows the steady state after refocusing.

3.3.3 Estimating complex mobility

The mobility of the target-probe complex within the sieving matrix can be approximated by measuring the relative velocity of the target-probe complex peak relative to the ITP interface velocity, as follows:

$$\Delta V = V_{peak1} - \mu_{complex} E_{spacer} = \frac{L}{t} \tag{3.1}$$

where V_{peak1} is the velocity of the front peak containing unreacted probe, $\mu_{complex}$ is the mobility of the longer target, E_{spacer} is the electric field in the spacer region, L is the length of the spacer zone, and t is the time for transition from the first peak (right peak in **Figure 3.3b**) to the second peak (left peak). V_{peak1}, L, and t are determined experimentally. We estimate E_{spacer} using the electrophoresis solver SPRESSO software.[12] For the simulation, we assume that the mobility of small ions is unaffected by the presence of a sieving matrix (see the SI for further discussion.) We solve eq 3.6 for $\mu_{complex}$ in the separation region and obtain a mobility estimate of 15.6 x 10^{-9} m^2/V.s, higher than that of our TE anion and lower than that of the spacer (as calculated using SPRESSO).

3.3.2 Effect of sieving matrix on small ion mobility

In obtaining an estimate for the mobility of the probe-target complex based on eq 3.6, we stated the assumption that the mobility of small ions is unaffected by the presence of a sieving matrix. We use this assumption to obtain the electric field as computed in the SPRESSO software package. We set out to examine the impact of including a sieving matrix in the buffer on the mobility of the ions. We chose to infer the mobility indirectly by measuring the voltage using the same set-up described in the other sections. The relation between voltage and mobility can be shown briefly. Ohm's Law,

as well as the definitions of electrical resistance and conductivity yield the following equations:

$$V = RI \tag{3.2}$$

$$R = \frac{l}{\sigma A} \tag{3.3}$$

$$\sigma = \sum_i \sum_{z=n_i}^{p_i} z_i F c_{i,z} \mu_{i,z} \tag{3.4}$$

We chose to perform this evaluation of small ion mobility using potassium chloride (KCl). The two ions comprising the electrolyte, K^+ and Cl^-, are monovalent and have similar mobilities,[3] therefore making them suitable for this analysis. After some algebraic manipulation, eq 3.2 can be rewritten as:

$$V = \frac{LI}{FA} \frac{1}{(c_{K^+}\mu_{K^+} + c_{Cl^-}\mu_{Cl^-})} \tag{3.5}$$

In a solution of 100 mM KCl, the concentration of the ions is equal ($c_{K^+} = c_{Cl^-} = c$). The mobilities of K^+ and Cl^- are assumed approximately equal ($\mu_{K^+} = \mu_{Cl^-} = \mu$), which leads to the simplified version of eq 3.5:

$$V = \frac{LI}{FA} \frac{1}{c\mu} \tag{3.6}$$

Therefore, by using the same chip (*L* and *A* are constant), supplying the same amount of current (*I* is constant), and using the same concentration solution (*c* is constant), the change in voltage will be inversely proportional to the increase in mobility. We thus ran two sets of experiments, supplying 5.5 μA of current and using a 100 mM KCl solution. The first set included no HEC polymer, while the second one included 1.5%

HEC. Results of these experiments are shown in **Figure 3.4**, and indicate that HEC does not significantly affect mobility of these small ions.

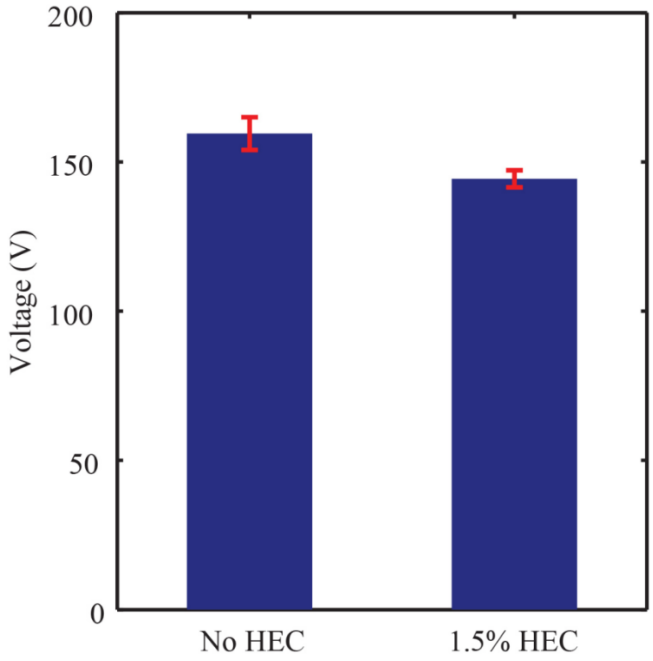

Figure 3.4. Measurements quantifying the impact of sieving matrix on the mobility of an electrolyte buffer. Measured voltage is inversely proportional to mobility, and thus provides a method to infer information about mobility. We performed two sets of experiments involving 100 mM KCl buffer in a microfluidic channel. In the first set the buffer contained no HEC polymer, while in the second we included 1.5% HEC in the buffer. We applied 5.5 μA of constant current in all experiments and measured mean voltages of 159.5 V and 144.3 V, respectively. A decrease in mobility corresponds to an increase in measured voltage. We see no indication of that, and instead observe a slight decrease in the voltage. We therefore assume that the sieving matrix does not significantly affect the mobility of these small ions.

To corroborate this result, we also measured the conductivity of KCl solutions with and without HEC directly using a conductivity meter (not shown). These experiments confirmed our initial findings. The results in **Figure 3.4** even indicate a minor increase in the conductivity, but we know of no physical basis to indicate that the mobility of ions increases in the presence of sieving matrix. We therefore attribute this difference

to incomplete surface equilibration and/or small temperature differences between experiments. In our ITP assay analysis, we made the assumption that the mobility of the LE ions was the same in free solution as is in the presence of a sieving matrix.

3.3.4 Evaluating assay performance

We chose to demonstrate and quantify the performance of this assay using synthetic DNA as a well-characterized model target. The experimental setup is detailed in the supplementary information section of Garcia-Schwarz and Santiago[6]. The probe was a 27 nt DNA with a sequence complementary to bacterial 16S ribosomal RNA (rRNA). 16S rRNA is closely associated with urinary tract infection (UTI).[13] Our target is a synthetic 149 nt DNA containing the 16S rRNA sequence complementary to the shorter probe. **Figure 3.7a** shows the titration curve we constructed to quantify the dynamic range of the assay. We held the probe concentration constant at 100 pM, and varied target concentration over approximately 5 orders of magnitude, from 220 fM to 73.6 nM. For each run, we divide the signal associated with the second peak, (attributed to the probe-target complex) by the total fluorescence signal in the two ITP peaks. We therefore normalize our measurement, and can account for variations in injection concentrations. Assay sensitivity is limited by fluorescence remaining in the second peak for a negative control run. We hypothesize this background signal is due to probe impurity. We therefore estimate hybridized product amount, N_{hyb}, by subtracting the background signal from the measured signal:

$$N_{hyb} = \frac{f_{peak2}}{f_{total}} - \frac{f_{c,peak2}}{f_{c,total}} \tag{3.7}$$

Here f_{peak2} and $f_{c,peak2}$ denote the fluorescent signal associated with the second peak (peak 2 in **Figure 3.3b**) in the data and control runs, respectively. f_{total} and $f_{c,total}$ denote the total fluorescent signal associated with both peaks (peak 1 plus peak 2) in the data and control runs, respectively. Based on the models of Bercovici-Han *et al*.[5] and Garcia-Schwarz and Santiago,[6] we expect this fraction to increase linearly with increasing target concentration. The assay has a 3.5-decade dynamic range, on the same order as that presented by Garcia-Schwarz, and higher than other ITP-hybridization assays.[14] Shown together with the experimental data is a plot of ITP hybridization reaction model developed by Garcia-Schwarz (a simplification of the more comprehensive Bercovici-Han model) using kinetic on-rate as a fitting free parameter.

3.3.5 Gaussian filtering using a seven point kernel

In order to eliminate high-frequency noise in the raw experimental data, we performed Gaussian filtering on all obtained data. Gaussian filtering convolves a Gaussian function with the raw data. The Gaussian function is characterized by a standard deviation width equal to double the 15 ms sampling period of the PMT), and is normalized in order to keep the sum of the values in the filter at unity. We used a seven point Gaussian kernel, and performed all processing using MATLAB. **Figure 3.5** shows the pre- and post-filtering data for a limit of detection (220 fM) experiment.

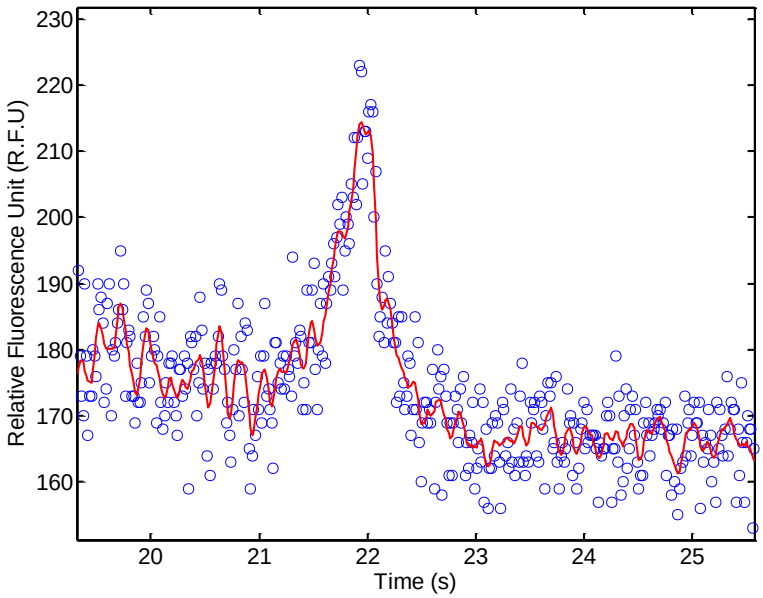

Figure 3.5. Raw fluorescence data (circles) plotted along with the Gaussian filtered signal (solid line) from an arbitrary run using 220 fM target. Gaussian filtering using a normalized Gaussian curve with width equaling twice the sampling period of the PMT. Note the difference in background noise levels preceding (19.5 – 21 s) and following (23 – 25.5 s) the peak. These data as shown here are not background adjusted.

3.3.6 Data analysis technique

In all experiments, we observed incongruence in the noise floor before and after the trailing peak. An example of this can be observed in **Figure 3.5**, as the noise floor up to 21 s and that after 23 s converge at different baseline values. The trailing peak is preceded by a leading peak, which is comprised of unreacted probe molecules. We hypothesized that the high noise level between the two peaks is due to probe impurity, as well as trace amounts of dimerized target or probe molecules. Optimizing the concentration of the sieving matrix aided in minimizing this noise, but we were unable to completely remove it. This issue was only relevant at the lowest concentrations, where the signal-to-noise ratio is relatively low. We thus chose to account for the discontinuous noise floor levels by modifying our peak integration method. We wrote a

script that locates the maximum value of the Gaussian filtered signal, and forms a fit of the five points on each side of the maximum. This results in an 11-point fit used for computing the integral. In this way, the fit includes information about the amplitude of the peak and its width but more strongly emphasizes the highest magnitude regions of the peak. **Figure 3.6** demonstrates this method, using an arbitrary run with 7.6 pM of target.

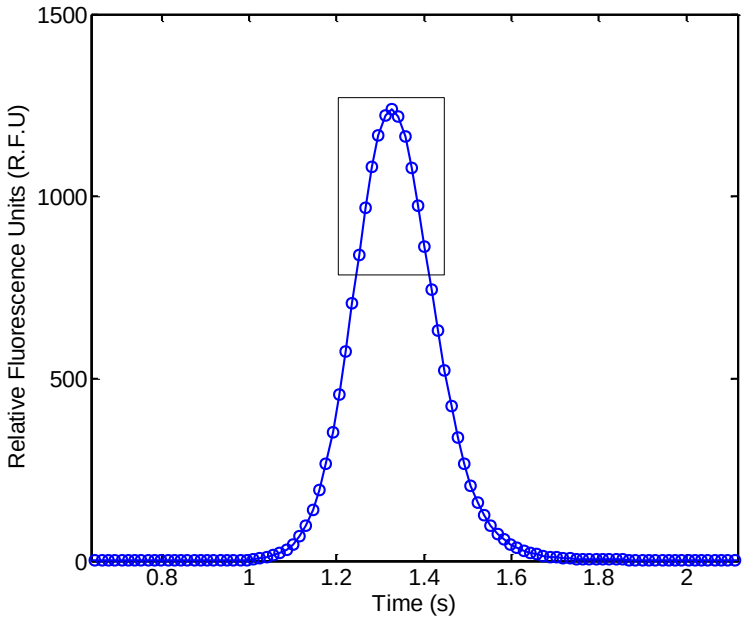

Figure 3.6. Demonstration of the data analysis used to integrate over the trailing peak in the signal data. The rectangular box indicates the 11 points that comprise the fit, consisting of point of maximum signal along with the adjacent 5 points preceding and following it. We then sum over the 11 points to compute the signal associated with the peak. We do this for both the leading and trailing peaks in all the runs. The above plot is taken from an arbitrarily-chosen, background-adjusted experiment containing 7.6 pM target.

3.3.7 Assay performance

We found an LOD of 220 fM, with a p-value of 0.03 (**Figure 3.7**). This result constitutes 100x lower detection limit than ITP assays using molecular beacons (MB),

and 12x improvement over the most sensitive NA hybridization assay with ITP thus far. In **Figure 3.8**, we overlay three representative runs of the negative control as well as the lowest two target concentrations, and demonstrate the combined Gaussian filtering and the chosen data analysis technique. We estimate that we are detecting approximately 0.1 fg of target DNA, which corresponds to 1300 target molecules. We hypothesize that further improvement in LOD can be obtained given probes of higher purity.

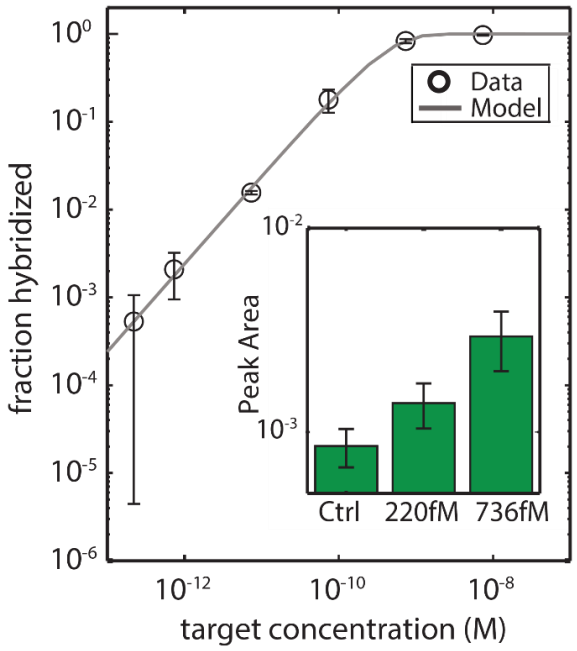

Figure 3.7. Experimental data demonstrating the sensitivity and dynamic range of the ITP-spacer assay for detection of a 149 nt DNA target. All error bars correspond to 95% confidence on the mean. a) Titration curve of target concentrations ranging from 220 fM to 7.36 nM, with probe concentration fixed at 100 pM. The assay has a linear dynamic range (R^2 = 0.99) of nearly four orders of magnitude. Along with the experimental data, we show results from a numerical reaction model with a single global fitting parameter. b) Limit of detection study showing the computed mean peak area for the lowest three target concentration values: c_T = 0 (negative control), 220 fM, and 736 fM.

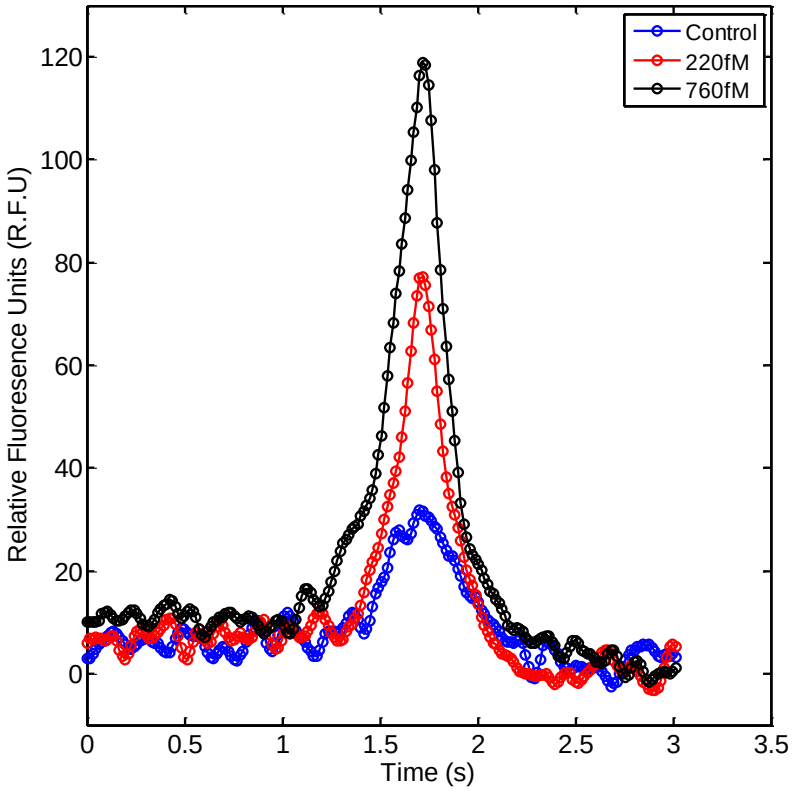

Figure 3.8. Plots of the Gaussian filtered data (as described in **Section S5**) for the trailing peak in the negative control as well as lowest target concentration cases (with 220 and 760 fM target). The peak signals are stacked on top of each other for easy comparison. The origin on the abscissa is set to the point at which the laser power is switched to 110 mW.

3.4 Summary

In summary, we introduced a rapid (~10 min), highly sensitive assay for sequence specific quantitation of a DNA target. The assay leverages ITP-enhanced hybridization and an ionic spacer ion and sieving matrix for background fluorescence removal. Our assay includes an initial mixing and reaction stage, and a subsequent separation stage. This results in two separate, focused ITP zones: the first zone containing unreacted probes and the second zone containing probe-target complexes. We demonstrated 220 fM LOD with a 149 nt target, a 12x improvement over previous ITP-based hybridization

assays, and 100x improvement over ITP-MB assays. We hypothesize this LOD can be improved with purer probes and longer channel lengths to allow more time for the hybridization reaction. Further, our technique has the advantage of producing two peaks, each focused in ITP mode, which allows for easy downstream manipulation and automation. We intend to extend this technique to detect other biomolecules (such as proteins) for use in biological and clinical applications.

4 Protein detection using ITP and ionic spacer

Several sections of this chapter are based on a recent article published in *Analyical Chemistry*, and are reproduced here with minor modifications.[‡]

4.1 Introduction

In this chapter, we present an on-chip electrophoretic assay for rapid protein detection with a SOMAmer® reagent. We used isotachophoresis (ITP) coupled with an ionic spacer to both react and separate SOMAmer–protein complex from free SOMAmer reagent. ITP accelerates the reaction kinetics as the ionic spacer concurrently separates the reaction products. We developed a numerical and analytical model to describe ITP spacer assays which involve low-mobility, non-focusing targets that are recruited into the ITP zone by higher-mobility, ITP-focused probes. We demonstrated a proof-of-concept of this assay using C-reactive protein (CRP) in buffer, and achieved a 2 nM limit of detection (LOD) with a combined 20 minute assay time (10 min off-chip preparation of reagents and 10 min on-chip run). Our findings suggest that this approach has potential as a simple and rapid alternative to other homogeneous immunoassays. We also explore the extension of this assay to a diluted serum sample spiked with CRP, where we observe decreased sensitivity (an LOD of 25 nM in 20-fold diluted serum). We describe the challenges in extending this assay to complex samples and achieving higher sensitivity and specificity for clinical applications.

[‡] C. Eid., J. W. Palko, E. Katilius, J. G. Santiago, "Rapid Slow Off-Rate Modified Aptamer (SOMAmer)-Based Detection of C-Reactive Protein Using Isotachophoresis and an Ionic Spacer," *Analytical Chemistry*, 2015. **87**(13): p. 6736-43.

Aptamers are synthetic nucleic acid (NA) ligands and a promising alternative to antibodies for protein detection.[82] Developed through several rounds of a process known as SELEX[83], aptamers are synthesized using solid state DNA synthesis methods allowing for reproducible replenishment of reagents, typically a problem with antibodies. DNA-based aptamers also tend to be more stable and can be reversibly denatured by heat. However, performance of traditional aptamers has been hamstrung by a number of issues, including relatively low affinity and high dissociation rates (k_{off}). In an effort to address these deficiencies of aptamers, SomaLogic, Inc. has developed SOMAmers (Slow Off-Rate Modified Aptamers)[84,85], which use modified nucleotide bases which offer expanded chemical diversity for interactions, in particular hydrophobic groups similar to amino acid residues. Modifications on nucleotides also dramatically improve ability to select SOMAmers for various protein targets with excellent (sub-nM) affinity. Standard on-chip capillary electrophoresis (CE)[86,87] and chromatography techniques[88,89] for aptamer-type detection have been used with some success, but are often impractical because they do not allow sample recovery and can require long separation times.

Recent work has been aimed at electrokinetic aptamer-based detection of proteins on microfluidic chips. Wang et al.[90] used transient-isotachophoresis (t-ITP) with a modified TE to detect thrombin-aptamer complexes at an intersection. Their assay had a 1 nM LOD. However, t-ITP is subject to significant dispersion effects, reducing signal-to-noise ratio. Cheow et al.[91] designed a chip in which conductivity gradients were created on the boundaries of ion depletion zones. Aptamer and protein targets were reacted off-chip, then continuously injected into the channel. Free aptamer and aptamer-

protein complexes focused at different locations of the conductivity gradient, allowing the detection and quantification of complexes. Though this approach achieved high sensitivity, the assay required separate off-chip incubation followed by on-chip signal enhancement and a total assay time of 60 min. The authors found the separation resolution to vary based on assay conditions. They suggested the addition of a spacer may better control the separation resolution between the two peaks.

In this chapter, we present a novel assay for ITP-based detection of a protein target with a SOMAmer probe. ITP is an electrophoretic technique that can selectively purify and preconcentrate reactants at a sharp interface, allowing isolation and concentration of low abundance probe-target complexes and increasing complex forming reaction kinetics.[92] ITP has been leveraged in the speed-up of reactions with protein targets. Khnouf et al.[56] used ITP to accelerate heterogeneous immunoassays in which antibodies were bound to magnetic beads or to the channel wall. Kawabata et al.[5] leveraged ITP for accelerated reaction and separation in an α–fetoprotein immunoassay. This assay was later developed into a commercial product by Wako Pure Chemical Industries and validated in clinical samples.[55] We note that, with the exception of the α–fetoprotein immunoassay, the use of ITP to accelerate reactions in complex samples has largely been limited to NAs rather than protein assays.[2,50] High protein content in samples like serum (60-80 g/L) can result in protein precipitation, non-specific interactions, and other deleterious effects. In this study, we briefly explore challenges of extending ITP to protein assays in complex samples.

In the assay reported here, we leverage the two standard modes of ITP: peak-mode and plateau-mode. Peak-mode usually occurs when analyte concentrations are several orders of magnitude smaller than those of the LE and TE buffers. In peak-mode, analytes focus at a sharp interface between the LE and TE, and have negligible effect on the local ionic conductivity in the channel.[28] Above a certain threshold concentration, the analyte eventually segregates into a plateau-like zone of constant concentration and increasing length.[93] Plateau-mode ITP has been leveraged to separate and indirectly detect non-fluorescent species.[38,94] We recently demonstrated an assay in which we integrated peak and plateau-mode ITP.[95] In the first stage, we used peak-mode ITP to preconcentrate and mix DNA probe and target molecules at a sharp interface. In the second stage, using a region with sieving matrix and an ionic spacer with mobility between that of the probe and target, we triggered plateau-mode ITP and separated the excess probe from the probe-target complex. We achieved a limit of detection of 220 fM, the highest reported sensitivity for free solution NA-based ITP assays.

We present an integrated assay to detect a low-mobility protein target using ITP and an ionic spacer. We know of no other work which has extended ITP-based reaction assays to non-focusing, low-mobility targets, in which higher-mobility probe molecules recruit target molecules into the ITP zone. Our assay is carried out in a microfluidic channel, allowing reaction of protein and SOMAmer and detection of the protein-SOMAmer complex on the same chip. We demonstrate the applicability of ITP-spacer assays to non-focusing targets in general. Additionally, we present a simple analytical model describing the reaction, as well as design considerations broadly applicable to ITP-spacer assays with low-mobility, non-focusing targets. We demonstrate a proof-of-

concept assay with C-reactive protein (CRP) as a clinically-relevant protein target. Lastly, we perform preliminary experiments to explore the extension our assay to detect CRP in a serum sample. We discuss challenges and recommendations for enhancing the performance of this assay in complex samples.

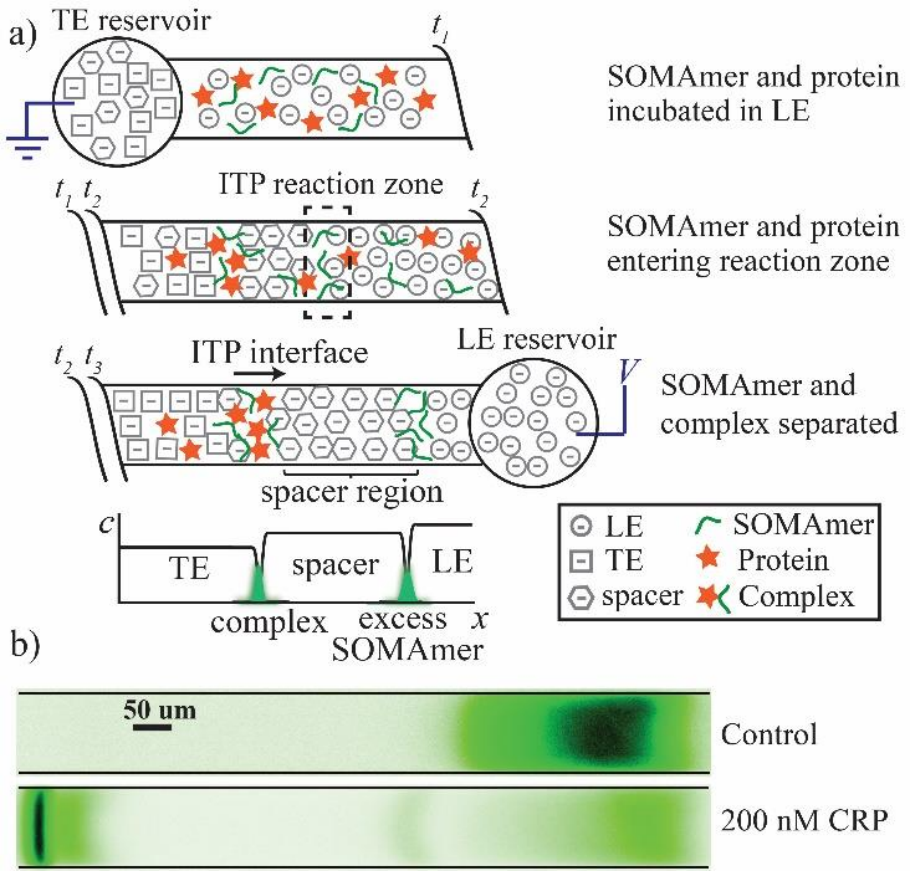

Figure 4.1. a) Schematic representation of the ITP-spacer assay. At t_1, the AlexaFluor 488-labeled SOMAmer reagent and the protein target are loaded in the LE buffer, while the TE and spacer ions are loaded into the TE reservoir. At t_2, ITP is initiated. Low-mobility complexes are formed by binding of SOMAmers and targets and then oversped by spacer molecules. At t_3, unreacted SOMAmer molecules are focused between the LE and spacer, whereas SOMAmer-target complexes are focused at the interface between the spacer and TE. b) Experimental visualization of the ITP-spacer assay in the detection region. In the negative control case, where only SOMAmer reagent is included, we observe only one ITP peak for free SOMAmer reagent. When 200 nM of CRP is included in the mixture, a second ITP peak forms at the trailing spacer-TE interface. This trailing peak represents the focused SOMAmer-target complex.

4.1.2 Principle of the assay

Figure 4.1 presents an overview of this assay. We inject the fluorescently-labeled SOMAmer and protein molecules in the channel, within the LE buffer. We then load the TE and spacer into the TE reservoir. Upon applying current, the LE, TE, spacer, SOMAmer reagent, and CRP target all begin to migrate towards the cathode (LE reservoir). An ITP peak consisting of SOMAmer forms immediately outside the TE reservoir. The high concentration of SOMAmer focused by ITP at the LE-spacer interface accelerates the second-order reaction kinetics between the SOMAmer and CRP in this region. Concurrently, SOMAmer and CRP molecules bind in the LE zone. As SOMAmer-CRP complexes form, they are overtaken by spacer molecules, which have higher mobility than that of the SOMAmer-CRP complex but lower than that of free SOMAmer. The complex refocuses at the spacer-TE interface, separating from the free SOMAmer and forming a trailing second peak, allowing detection of CRP in the labeled complex. Due to the large difference in mobility between the free SOMAmer and SOMAmer-CRP complex, no sieving matrix is needed in this assay. The simultaneous reaction and separation processes continue as the species migrate along the channel and reach the detection point where SOMAmer-CRP complex concentration is measured.

4.2 Theory

4.2.1 Initial placement of the probe in the channel

The placement of the target and probe molecules in the channel is an important decision in the assay design. When working with targets that have relatively low or unknown

mobilities (such as proteins), we generally recommend that the target be initially loaded into the LE. A target with a mobility lower than that of the TE and placed in the TE neither focuses in ITP nor encounters ITP-focused probes. Placing such a low-mobility target in the LE ensures that the target molecules encounter ITP-focused probe, even if the free target molecules do not focus in ITP.

The placement of the higher-mobility probe is more interesting. In this analysis, we only consider placing the probe molecules in either the LE or TE buffers. As described in the main text, the spacer molecules are included in the TE buffer. We note that it is possible to include probe molecules in both buffers. Given a maximum concentration of probe in both buffers, doing so can maximize the number of molecules entering the ITP zone and thus maximize reaction speed-up. However, probe molecules can be expensive and should thus only be placed where they will be most effective.

The key term influenced by the initial loading of the probe is the probe flux term. This term has a prefactor that depends on species' mobilities and buffer ion concentrations, and is denoted by $\eta_{P,LE}$ and $\eta_{P,spacer}$ when placed in the LE or spacer, respectively. $\eta_{P,LE}$ and $\eta_{P,spacer}$ are given by:

$$\eta_{P,LE} = 1 - \frac{\mu_P}{\mu_{LE}} \tag{4.1}$$

$$\eta_{P,spacer} = \left(\frac{\mu_P}{\mu_{spacer}} - 1 \right) \frac{\mu_{CI} - \mu_{LE}}{\mu_{CI} - \mu_{spacer}} \frac{\mu_{spacer}}{\mu_{LE}} \frac{c_{LE}}{c_{TE}^{well}} \tag{4.2}$$

A key parameter, therefore, in deciding on the placement of the probe, is the ratio between the two terms, defined as:

$$\phi = \frac{\eta_{P,LE}}{\eta_{P,spacer}} = \frac{(\mu_{LE} - \mu_P)(\mu_{CI} - \mu_{spacer})}{(\mu_P - \mu_{spacer})(\mu_{CI} - \mu_{LE})} \frac{c_{TE}^{well}}{c_{LE}} \quad (4.3)$$

For $\phi \approx 1$, the rate at which the probe enters the ITP zone is not greatly dependent on its initial placement. However, for $\phi >> 1$, placing in probe in the LE leads to a greater flux of probe into ITP. Similarly, for $\phi << 1$, reaction kinetics are improved by placing the probe in the TE. In Figure 4.2, we see the dependence of ϕ on the mobilities of the probe and spacer for equimolar concentrations of LE and TE. We applied eq 4.3 for the assay described in this chapter, using SPRESSO[75] to obtain the mobilities of the LE (μ_{LE} = -79 × 10^{-9} $m^2V^{-1}s^{-1}$), spacer (μ_{spacer} = -17 × 10^{-9} $m^2V^{-1}s^{-1}$), and counterion (μ_{CI} = 20 × 10^{-9} $m^2V^{-1}s^{-1}$), and an approximation of probe mobility based on published values (μ_P = -30 × 10^{-9} $m^2V^{-1}s^{-1}$).[46] Using equal TE and LE concentrations, we found that $\phi \approx 1.5$ for our assay chemistry. We note that a secondary advantage of placing the probe in the LE is the lack of background noise behind the trailing ITP peak, due to the continuous accumulation of fluorescent probe from the TE reservoir.

4.2.2 Modeling spacer assay reaction kinetics

We present an analysis of the reaction and separation processes which occur in an ITP-spacer assay with a non-focusing target, as well as recommendations on assay design. We begin with a simplified model of the probe-target reaction similar to the analysis of Bercovici and Han.[3] In this model, we assume that the dissociation constant K_d << 1 µM, such that dissociation rate k_{off} is much smaller than the characteristic association rate $k_{on}c_{P,0}$ where k_{on} is the association rate constant and $c_{P,0}$ is the initial probe concentration. We load both the probe (SOMAmer) and target (CRP) in the LE zone (Figure 4.1a). There are thus two regions where the probe-target reactions occur: in the

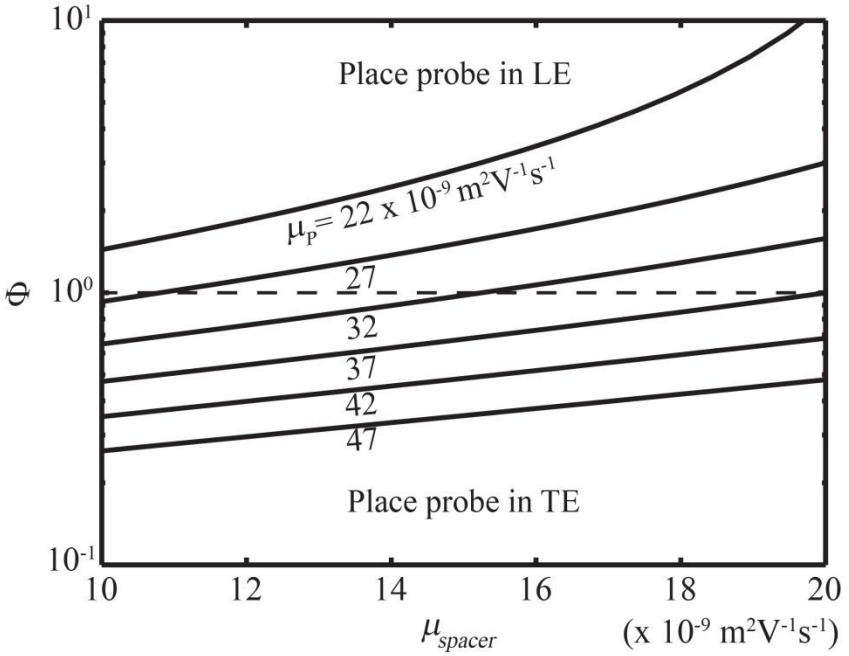

Figure 4.2. Results from the analytical modeling showing the ratio of probe flux to the ITP reaction zone from a starting position in the LE and TE, respectively. This ratio is plotted for various spacer and probe mobilities. We find that for values of $\phi >> 1$, including the probe in the LE results in greater flux into the ITP reaction zone and thus accelerated reaction kinetics. This effect is reversed for low values of ϕ. We conclude that, when the probe and spacer have similar mobilities, the probe should be placed in the LE. In this calculation, we assume equimolar LE and TE concentrations, as well as anE mobility of -79 x 10^{-9} m^2/V.s (that of the commonly used Cl^-) and a counterion mobility of 20 x 10^{-9} m^2/V.s (that of Imidazole, a common counterion).

LE zone (containing unfocused reactants) and in the ITP zone. The LE zone reactions

are given by:

$$\begin{cases} \dfrac{dc_P^{LE}}{dt} = -k_{on} c_P^{LE} c_T^{LE} \\ \dfrac{dc_T^{LE}}{dt} = -k_{on} c_P^{LE} c_T^{LE} \\ \dfrac{dN_{PT}^{LE}}{dt} = k_{on} c_P^{LE} c_T^{LE} V(t) \end{cases} \tag{4.4}$$

where $V(t) = A(L_0 - U_{ITP}t)$ is the time-dependent volume of the LE zone. U_{ITP} is the velocity of the ITP front, A is the channel's cross-sectional area, and L_0 is the length of the channel. As the ITP zone migrates through the channel, the volume of the LE zone continuously decreases. Reactions in the ITP zone are given by:

$$\begin{cases} \dfrac{dc_P^{ITP}}{dt} = -k_{on}c_P^{ITP}c_T^{ITP} + \dfrac{U_{ITP}}{\delta}\eta_{P,LE}c_P^{LE} \\ \dfrac{dc_T^{ITP}}{dt} = -k_{on}c_P^{ITP}c_T^{ITP} + \dfrac{U_{ITP}}{\delta}\eta_{T,LE}(c_T^{LE} - c_T^{ITP}) \\ \dfrac{dN_{PT}^{ITP}}{dt} = k_{on}c_P^{ITP}c_T^{ITP}(\delta A) \end{cases} \tag{4.5}$$

where $\eta_{P,LE} = 1 - \dfrac{\mu_P}{\mu_{LE}}$ and $\eta_{T,LE} = 1 - \dfrac{\mu_T}{\mu_{LE}}$

c_P and c_T represent the concentrations of probe and target, respectively. N_{PT} is the number of probe target complexes present. Superscripts "LE" and "ITP" designate the LE and ITP zones, respectively. δ represents the characteristic axial width of the ITP peak, and μ represents electrophoretic mobility. $\eta_{P,LE}$ and $\eta_{T,LE}$ represent the normalized difference in mobility between the LE and the probe and target, respectively. Here, the subscripts "P", "T", "PT", "LE", "TE", "spacer", and "CI" denote properties related to the probe, target, probe-target complex, LE, TE, spacer, and counterion, respectively. We note that all species mobilities refer to the mobility of that species in the buffer in which it is migrating (e.g. μ_T refers to the mobility of the target in the LE buffer).

Probe molecules continuously accumulate in the ITP zone at a rate proportional to the relative difference in mobility between the LE and the probe, $\eta_{P,LE}$. Target molecules do not focus in ITP, but instead enter the ITP zone from the LE and exit to the spacer and

TE zones. In addition to the fundamental requirements necessary for all ITP assays ($\mu_{LE} > \mu_{TE}$ in their respective zones), an ITP-spacer reaction-separation assay requires that $\mu_P > \mu_{spacer} > \mu_{PT} > \mu_{TE}$. In this analysis, we assume that $\mu_{TE} > \mu_T$, since the target does not focus in ITP.

4.2.3 Simplified model under abundant probe assumption

We present the simplified model reflecting the assumption that probe molecules are abundant relative to target molecules. In this case, we can neglect the reaction terms in the probe concentration equations. The result of this simplification propagates to the other equations describing the concentration of free target and the number of molecules of probe-target complex.

In the downstream LE region:

$$\begin{cases} c_{P,down} \approx c_P^0 \\ \dfrac{\mathrm{d}c_{T,down}}{\mathrm{d}t} = -k_{on} c_P^0 c_{T,down} \\ \dfrac{\mathrm{d}N_{PT,down}}{\mathrm{d}t} = k_{on} c_P^0 c_{T,down} A(L_0 - U_{ITP} t) \end{cases} \tag{4.6}$$

In the ITP zone:

$$\begin{cases} \dfrac{\mathrm{d}c_{P,ITP}}{\mathrm{d}t} = \dfrac{U_{ITP}}{\delta} \eta_{P,LE} c_P^0 \\ \dfrac{\mathrm{d}c_{T,ITP}}{\mathrm{d}t} = -k_{on} c_{P,ITP} c_{T,ITP} + \dfrac{U_{ITP}}{\delta} \eta_{T,LE} (c_{T,down} - c_{T,ITP}) \\ \dfrac{\mathrm{d}N_{PT,ITP}}{\mathrm{d}t} = k_{on} c_{T,ITP} c_{P,ITP} (\delta A) \end{cases} \tag{4.7}$$

4.2.4 Production of probe-target complex in the channel

In this section, we focus on the case where the probe is abundant with respect to the target, as this is often the most interesting regime for biomolecule detection assays. We therefore assume that $c_{P,0} >> c_{T,0}$, which simplifies the model presented above. We present the simplified model in the Section 4.2.3. During the assay, probe-target complexes form in the ITP and LE zones. As the ITP zones sweep through the channel, the formed probe-target complexes accumulate at the spacer-TE interface. The rate of product formation per unit volume is significantly higher in the ITP zone at the interface between the LE and spacer. However, the LE zone occupies a much larger volume than the ITP zone, and so its production of product cannot be neglected. We find that, for the current assay design and a wide range of assay parameters, the rates of complex formation in the LE and ITP zones are on the same order of magnitude and both should be considered. There exists an interesting trade-off between reducing assay time and producing a large number of probe-target complexes. We introduce the non-dimensional parameter λ to quantify this trade-off. λ relates the assay velocity, channel length, association on-rate, and initial probe concentration:

$$\lambda = \frac{L_0 k_{on} c_{P,0}}{U_{ITP}} \tag{4.8}$$

λ can be interpreted as a modified Damkohler number, relating the advection and the reaction rates. Under the simplifying assumptions listed above, λ incorporates several of the key variables influencing complex formation and determines the fraction of target molecules which are bound and can be detected at the end of the assay. In Figure 4.3, we visualize the relationship between complex formation and λ, which shows sigmoidal

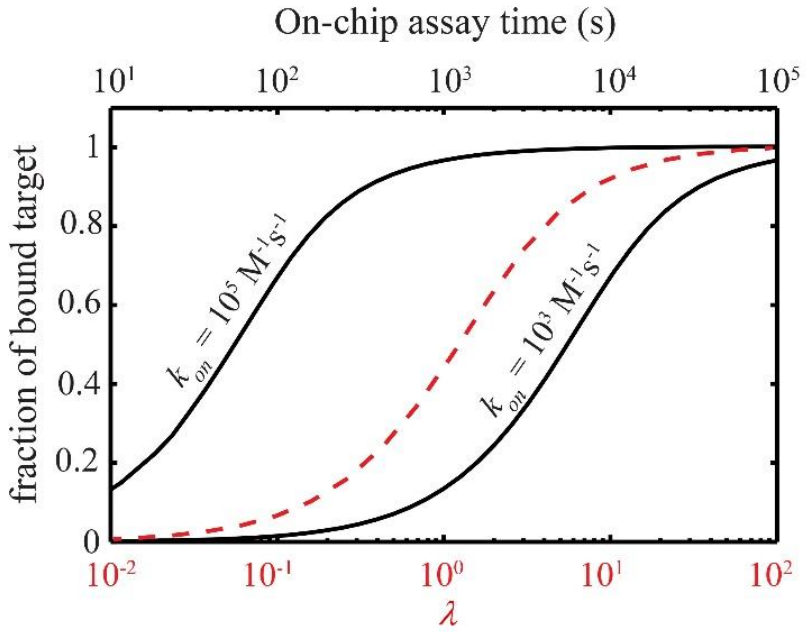

Figure 4.3. Results of analytical modeling determining the fraction of bound, detectable target at the end of the assay for the case with abundant probe. We show the ratio of target molecules which have formed a complex as a function of λ, ITP assay times, and k_{on} values. The dashed curve represents the bound target as a function of parameter λ (see eq 4.8). We find a sigmoidal shape and a region of assay times that maximizes complex formation while minimizing assay time. The assay temporal response curves over different values of k_{on} collapse into a single λ curve. We experimentally measure the assay time to be around 600 s in a 45 mm long channel. We use an initial SOMAmer concentration of 180 nM. We assume μ_{LE} = -79 x 10^{-9} $m^2V^{-1}s^{-1}$ (that of the commonly used Cl^-), μ_P = -30 x 10^{-9} $m^2V^{-1}s^{-1}$, and μ_T = -2 x 10^{-9} $m^2V^{-1}s^{-1}$, and an ITP zone width of 100 μm.

character. At low λ values, the free probes are swept away by the ITP zone before they have a chance to bind with target. Conversely, at high λ values, the reaction between probe and target molecules approaches equilibrium in the LE, minimizing the effect of ITP on reaction kinetics. The optimal region of operation is at the very beginning of the plateau at higher λ, which maximizes product formation while minimizing assay time.

4.2.5 Spacer zone length and complex accumulation

In order to be detected, probe-target complexes must be separated from excess probes and focused at a separate ITP interface. The probe-target complex forms in the LE and ITP reaction zones, is oversped by the LE and spacer molecules, and refocuses at the trailing spacer-TE interface. In this section, we present an analysis of the competing phenomena of spacer zone growth and complexes falling behind the spacer molecules and accumulating at the trailing interface. As discussed earlier, plateau ITP is triggered when the spacer reaches a threshold concentration, above which the spacer molecules cease to accumulate in a high-concentration peak and instead form a growing zone. This plateau concentration is given by Martin and Everaerts[32]:

$$c_{spacer}^{threshold} = c_{LE} \frac{\mu_{spacer}(\mu_{LE} - \mu_{CI})}{\mu_{LE}(\mu_{spacer} - \mu_{CI})} \frac{z_{LE}}{z_{spacer}} \tag{4.9}$$

where z indicates the molecule's ionic charge. We can decrease the time needed to induce plateau mode by loading a larger concentration of spacer into the TE reservoir and/or including a lower concentration of LE in the channel. Above the threshold concentration, the newly-formed spacer plateau zone grows proportionally to the influx of spacer molecules at the ITP interface. This rate is given by Martin and Everaerts [32,37]:

$$\frac{dL_{spacer}}{dt} = \frac{\mu_{LE}}{\mu_{TE}} \left[\frac{(\mu_{spacer} - \mu_{TE})(\mu_{spacer} - \mu_{CI})}{\mu_{spacer}(\mu_{LE} - \mu_{CI})} \right] \frac{c_{spacer}^{well}}{c_{LE}} V_{ITP} \tag{4.10}$$

L_{spacer} represents the length of the growing spacer zone and c_{spacer}^{well} denotes the concentration of the spacer species in the TE reservoir. The length of the LE-filled channel gives the upper bound for L_{spacer} while its lower limit is dependent on the ability

of the detector to distinguish between the LE-spacer and spacer-TE interfaces where the unbound and bound probes are focused respectively.

While the spacer zone grows in length as described above, the probe-target complex traverses the spacer zone and accumulates at the spacer-TE interface. The rate at which the probe-target complex migrates backwards (in the ITP frame of reference) towards the trailing ITP zone is given by

$$V_{spacer} - V_{PT} = V_{ITP}\left(1 - \frac{\mu_{PT}}{\mu_{spacer}}\right) \tag{4.11}$$

where V_{PT} and V_{spacer} are the velocities of the probe-target complex and spacer in the spacer zone. Therefore, in order to ensure that the probe-target complex is approaching the spacer-TE interface (eq 4.11) faster than the spacer zone is growing (eq 4.10), we consider the ratio of eqs 4.10 and 4.11. We define this ratio as:

$$\alpha = \frac{\mu_{TE}}{\mu_{LE}}\left(\frac{\mu_{spacer} - \mu_{PT}}{\mu_{spacer} - \mu_{TE}}\right)\left(\frac{\mu_{LE} - \mu_{CI}}{\mu_{spacer} - \mu_{CI}}\right)\frac{c_{LE}}{c_{spacer}^{well}} \tag{4.12}$$

For large values of α ($\alpha >> 1$), the rate of probe-target complex accumulation is significantly greater than the rate of growth of the spacer zone, and the large majority of complexes are focused at the spacer-TE interface for detection with relatively few left in the spacer zone. In practice, probe-target complex mobility may be difficult to determine for this calculation. NA-protein complexes, however, generally migrate at a lower mobility than the free NAs.[96,97] If probe-target complex mobility is unknown, we recommend using a high-mobility spacer, increasing LE concentration, or reducing the spacer reservoir concentration to increase the fraction of formed probe-target complexes that are focused at the trailing interface. Generally, a slower probe-target

complex results in faster accumulation (larger α values). In Table 4.1, we summarize the influence of several important parameters on the design of a high- performance ITP-spacer reaction-separation assay.

Table 4.1. Important parameters in ITP-spacer assay design

Parameter	Interpretation	Notes
μ_{LE}	Mobility of the LE ion	Choosing $\mu_{LE} >> \mu_T$ and $\mu_{LE} >> \mu_P$ maximizes flux of probe and target molecules into the ITP reaction zone.
μ_{spacer} c_{spacer}^{well}	Mobility of spacer ion and reservoir spacer concentration	Maximizing μ_{spacer} - μ_{TE} and c_{spacer}^{well} minimizes flux of probe-target complex molecules out of the ITP reaction zone.
λ	Ratio of convective to reactive timescales	When probe is abundant and $k_{off} << k_{on}$, λ collapses the effect of several assay parameters on complex production.
α	Ratio of complex accumulation rate to spacer zone growth rate	If $\alpha >> 1$, probe-target complexes reach the spacer-TE interface at a higher rate than the spacer molecules.

4.3 Materials and methods

4.3.1 Chip and Reagents

All experiments were performed on a 20 µm deep Crown glass NS-12A chip (Figure 4.4) from Caliper Life Sciences (Mountain View, CA). The channels are 90 µm wide and 20 µm deep. The SOMAmer/protein injection region between reservoir 4 and the cross junction is 45 mm in length. The detection point was located about 5 mm away from the cross-junction.

For ITP hybridization, we prepared an LE buffer consisting of 100 mM HCl, 200 mM Imidazole (pKa = 7.15), 1% (w/v) PVP, 0.02% (v/v) Tween-20, 6 mM $MgCl_2$, and 10 µM of the non-specific blocker, Z-block. PVP was used to suppress electroosmotic flow.

Tween-20 was included to increase protein solubility and minimize nonspecific adsorption of the protein target to the walls of the microfluidic channel. Mg^{2+} was used to ensure appropriate binding between the SOMAmer and the target protein. We use Imidazole as the counterion due to its pKa, which is close to physiological pH (~7.4), optimal for SOMAmer binding. Z-block is a synthetic oligodeoxynucleotide containing Benzyl-dU modified bases, synthesized at SomaLogic.[98] We include it in high concentrations to act as a competitive inhibitor of non-specific interactions. We mixed both the SOMAmer and CRP with the LE buffer. The TE consisted of 100 mM Tricine, 200 mM Imidazole, 0.5 mM HEPES, and 1% PVP. HEPES acted as a spacer in these experiments. We determined the appropriate spacer through an iterative process.

We prepared serum samples from whole blood samples donated in non-anticoagulated tubes by healthy donors to the Stanford Blood Center (Palo Alto, CA). The fresh human blood samples clotted for approximately an hour under room temperature. We then removed the clot by centrifuging at 1500*g* for 15 min. We collected and made aliquots of the resultant supernatant serum. Serum samples were then stored at -80 °C. We note that for experiments with serum sample, we used 0.2% (v/v) Triton X-100 as surfactant instead of Tween-20, due to decreased aggregate formation with Triton X-100.

We purchased HEPES, Tris, Imidazole, PBS, Tricine, Glycerol, Tween-20, and Triton X-100 from Sigma-Aldrich (St. Louis, MO). Magnesium Chloride was obtained from EMD Millipore (Gibbstown, NJ). Polyvinylpyrrolidone (PVP, MW = 1,000,000) was purchased from Polysciences, Inc. (Warrington, PA). Hydrochloric acid was procured from J.T. Baker (Avantor Performance from Mallinckrodt Chemicals (Avantor Performance Materials,

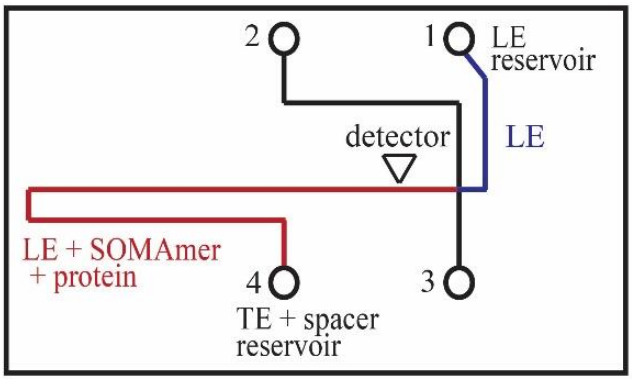

Figure 4.4. Design of the Caliper NS12 deep Crown glass chip. Prior to each run, we fill a section of the channel with pure LE buffer (blue) and another section with LE buffer mixed with SOMAmer and protein (red). The detection point is placed approximately 5 mm away from the cross junction, as shown above. ITP proceeds from reservoirs 4 to 1.

Center Valley, PA). AlexaFluor 488 labeled SOMAmer (AF488-SOMAmer) and Z-block were provided by SomaLogic, Inc. (Boulder, CO). C-reactive protein was obtained from US Biological (Salem, MA). SOMAmers were stored in a buffer consisting of 10 mM HCl and 20 mM Tris. The stock solutions were stored at -20°C, but a working stock was stored at 4°C and replaced every two days. CRP was stored in a solution consisting of 0.8x PBS (Phosphate buffered saline) and 50% (v/v) glycerol. Glycerol was used in order to prevent the protein from freezing while stored at -20°C, and its subsequent denaturation. Other solutions were stored at room temperature. All solutions were prepared in DNase/RNase-free distilled water (GIBCO Invitrogen, Carlsbad, CA).

4.3.2 Protocol and chip operation

Prior to and between each experiment, we prepared the channel with the following wash protocol: deionized water (DI) (1 min), 1 M NaOH (1 min), DI (1 min), 1 M HCl (1 min), and finally DI (1 min). We used this protocol to remove adsorbed proteins and

impurities from the channel. We then filled all reservoirs with LE buffer and applied vacuum at reservoir 2 (Figure 4.4) to fill the entire channel with LE. Prior to each run we mixed the SOMAmer in the LE buffer (and serum when working with the serum sample), and heated the solution at 95°C for 10 min and allowed it to cool to room temperature, as recommended by SomaLogic. This was done to refold the SOMAmer and dissociate any SOMAmer aggregates that may have formed during cold storage. We then centrifuged the solution at 6000 rpm for 10 seconds, and added CRP to it. This LE-SOMAmer-CRP solution was immediately transferred from the tube to reservoir 4. We then applied vacuum at reservoir 2 for 30 s to fill the section of the channel between reservoir 4 and the intersection with LE as well as the two analytes. We then rapidly rinsed the reservoir and replaced its contents with the TE buffer. Finally, we placed a positive electrode in reservoir 1 and ground in reservoir 4, and applied current (4 μA) to initiate ITP. As a result of the chemistry we used, the pH in ITP was between 7.2 and 7.7 depending on the zone.

4.3.3 Imaging system

For on-chip tracking of the ITP zone, we used an inverted epifluorescence microscope (Eclipse TE200, Nikon, Melville, NY) equipped with a 10x objective (PlanApo, Nikon, Melville, NY). We used a short-arc mercury lamp (102DH, Ushio, Tokyo, Japan) and a filter cube optimized for AF488 detection (C-124352, Chroma, Bellows Falls, VT). We recorded all images using a 1300 x 1030 CCD camera (Coolsnap, Roper Scientific, Trenton, NJ) controlled with Winview32. Obtained images were processed with MATLAB (R2011a, Mathworks, Natick, MA).

4.4 Results and discussion

4.4.1 Demonstration of assay with CRP as target

For this initial demonstration, we chose CRP as a clinically relevant protein target. CRP is a pentameric protein commonly used as an inflammation biomarker. Its circulating plasma levels in healthy individuals are less than 80 nM, but can exceed 2 μM in severe bacterial infections.[99] CRP is also associated with myocardial disease.[100,101] In its non-glycosylated form, CRP has a molecular weight of 115 kDa[102] and an isoelectric point of 5-6.[103] The mobility of CRP varies significantly based on a number of factors, including pH and Ca^{2+} concentration.[98] Since the pH in the channel is between 7.2-7.7, above its isoelectric point, CRP is negatively charged under our assay conditions and migrates towards the cathode. However, reported mobility values of CRP indicate that it migrates relatively slowly (its mobility is reported as -1×10^{-9} $m^2V^{-1}s^{-1}$ at pH = 8.6, for example[104]). We therefore do not expect CRP to focus in ITP at either the LE-spacer or spacer-TE interfaces. Furthermore, low protein mobility often leads to low probe-target complex mobility and consequent higher value of α (see eq 4.12), allowing the complex to traverse the spacer zone and focus at the spacer-TE interface.

In Figure 4.1b, we show experimental visualizations of SOMAmer fluorescence from the SOMAmer-CRP assay. In the negative control case, where no CRP is added, there is only one ITP peak, at the LE-spacer interface, corresponding to unbound SOMAmer. However, when CRP is added, a second peak forms at the spacer-TE interface, corresponding to SOMAmer-CRP complexes. We attribute the large axial width of the first ITP zone to the high concentration of Z-block (10 μM) used in the assay. Since Z-

block is an oligodeoxynucleotide, it has mobility similar to that of the SOMAmer, and thus focuses at the LE-spacer interface.

4.4.2 Effect of Z-block on non-specific interactions

Z-block is a synthetic oligodeoxynucleotide containing modified dU nucleotides synthesized at SomaLogic. Z-block is described briefly in Kraemer at al.[98] We used this reagent in our experiments in order to reduce non-specific interactions in the assay. To demonstrate its efficacy, we used bovine serum albumin (BSA) as a non-specific target with and without Z-block. We measured the ratio of bound SOMAmer to total SOMAmer, and plotted the results in Figure 4.5. We found a 50-fold reduction in non-specific binding between the CRP SOMAmer and BSA in the presence of 10 μM Z-block. We hypothesize that Z-block can play a significant role in the extension of this assay to complex samples with many proteins.

4.4.3 Fraction of focused SOMAmer in ITP

For the quantification experiments, we chose a probe concentration of 180 nM to minimize negative control signal (discussed below) and maximize fluorescent signal without saturating the detector. We measured the fluorescent signal at the detection point, located close to the cross junction. We chose this point due to constraints imposed by the channel geometry. We found that this location maximized the accumulated fluorescent signal, while avoiding the perturbation caused by the cross junction and subsequent channel bending between the junction and reservoir 1 (Figure 4.4). The number of focused unbound probe molecules at a given location along the channel is given by:

$$N_P(x) = \left(\frac{\mu_P - \mu_{LE}}{\mu_{LE}} \right) c_P^{LE} Ax \tag{4.13}$$

where x represents the axial location of the detection point along the channel. In this assay, the detection point, x_{det}, lies at approximately 90% of the injected plug length, L_0. For the low-target concentration case, the fraction of ITP-focused SOMAmers is estimated to be:

$$\frac{N_P(x_{\text{det}})}{N_{P,o}} \approx 0.9 \left(\frac{\mu_P - \mu_{LE}}{\mu_{LE}} \right) \approx 0.55 \tag{4.14}$$

We therefore estimate that we focused 55% of available SOMAmers based on our choice of detection point.

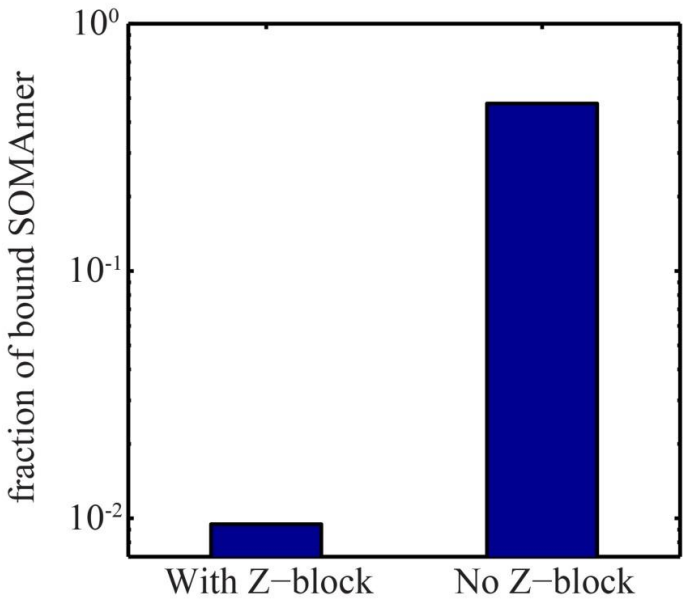

Figure 4.5. Quantification of the effect of Z-block on the non-specific interactions between SOMAmer and BSA. We performed two sets of experiments with 180 nM SOMAmer and 7.5 µM BSA. In the first set (left), we included 10 µM Z-block and found that the ratio of bound to total SOMAmer was 0.01. In the second set (right), we did not include any Z-block and found the same ratio to be 0.48, a 50-fold increase in non-specific interactions.

4.4.4 Fraction of target-bound SOMAmer

For each run, we measured the area-averaged fluorescent signal of the trailing ITP peak associated with the SOMAmer-CRP complex. We divided this value by the total fluorescent signal of the two ITP peaks. From this ratio obtained for each sample, we subtracted the same signal ratio obtained for the negative control (which includes only probe and no protein target). As a result, we accounted for both run-to-run variation in injected SOMAmer and false positive fluorescent signal from the negative control. Finally, we normalized this number by the difference obtained for the case with excess target concentration (2 µM CRP). The raw data is plotted in Figure 4.7 below. We include a bar graph of the raw data from the experiments we used to build the titration curve. We note that even at protein target concentrations exceeding the SOMAmer concentration 10-fold, the fraction of bound SOMAmer does not reach unity. With normalization, we obtain the fraction of hybridized SOMAmer:

$$f_{complex} = \frac{f_{p2}/f_{tot} - f_{c,p2}/f_{c,tot}}{f_{2uM,p2}/f_{2uM,tot} - f_{c,p2}/f_{c,tot}} \tag{4.15}$$

Here, f_{p2}, $f_{c,p2}$, and $f_{2uM,p2}$ denote the area-averaged fluorescent signal observed in the trailing peak of the sample, control, and 2 µM runs, respectively. f_{tot}, $f_{c,tot}$, and $f_{2uM,tot}$ denote the combined area-averaged fluorescent signal observed in both ITP peaks, in the sample, control, and 2 µM runs, respectively.

We performed the normalization above in order to account for various factors which prevent the bound fraction of SOMAmers from reaching unity even when CRP outnumbers SOMAmer 10-fold. Such factors include protein aggregate formation, which we observed in the ITP zone during the runs with 2 µM concentration of CRP.

We hypothesize that this is due to the combination of high initial concentration of CRP and the preconcentration effects of ITP, which lead to CRP molecules aggregating and crashing out of solution. Other factors include wall adsorption and photobleaching.

4.4.5 Titration curve and limit of detection

We built a titration curve using CRP as target and the CRP-specific SOMAmer as probe, shown in Figure 4.6. For all runs, we used a constant probe concentration of 180 nM and varied CRP concentration between 2 nM and 2 μM, performing 3 repetitions for each target concentration. In addition to the data points, we include a plot of the ITP hybridization model presented above (eqs 4.4 and 4.5). Because only the dissociation constant was known (K_d = 4 nM) rather than k_{on} or k_{off}, we use the kinetic on-rate as a free parameter to fit our model to the experimental data (we find $k_{on}= 3 \times 10^4$ $M^{-1}s^{-1}$). We find that the modified Damkohler number $\lambda \approx 3$ using the fitted value of k_{on}, placing the assay close to the optimal flat region shown in Figure 4.3. We achieve an LOD of 2 nM with a 2.5 decade dynamic range in a 10 min on-chip assay time. This result is comparable with Wang et al. who reported an LOD of 1 nM for their t-ITP and aptamer-based detection assay. Additionally, the reported LOD is well-within the clinically relevant range of CRP, though we again stress that this LOD applies to our assay in simple buffer, not in a complex sample.

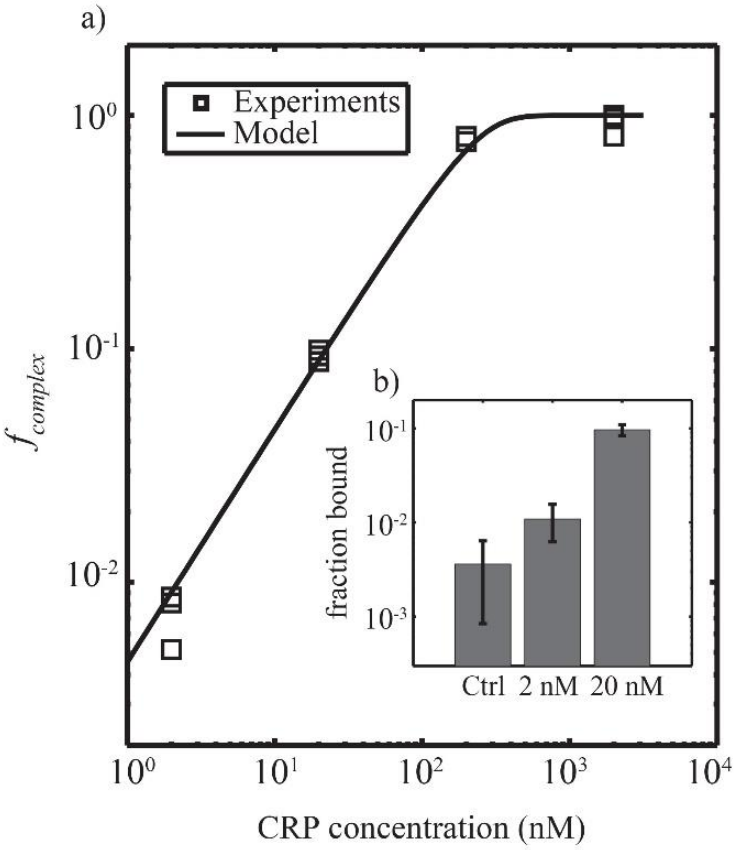

Figure 4.6. Experimental data of the ITP-spacer assay for the detection of CRP protein using CRP-specific SOMAmer. For all experiments, we fix the SOMAmer concentration at 180 nM. a) Titration curve showing the control-corrected fraction of SOMAmer hybridized with increasing CRP concentration (2 nM to 2 μM). The assay has a 2.5 decade dynamic range ($R^2 = 0.98$). We also include a prediction of the model, using k_{on} as a fitting parameter ($k_{on} = 3 \times 10^4$ $M^{-1}s^{-1}$). b) Limit of detection analysis that indicates a 2 nM limit of detection for this assay. The ratio of signal from the trailing peak to total signal is plotted for the negative control ($c_T = 0$) as well as the cases with two lowest CRP concentrations ($c_T = 2$ nM and 20 nM, respectively). Uncertainty bars represent 95% confidence on the mean.

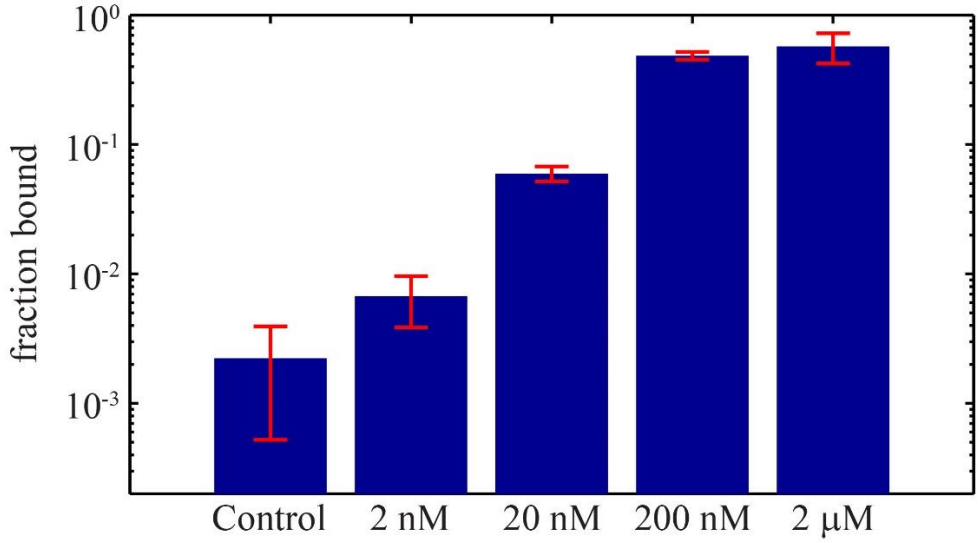

Figure 4.7. Raw data from the assay experiments for the detection of CRP protein using CRP-specific SOMAmer. For all experiments, we fix the SOMAmer concentration at 180 nM and vary CRP concentrations. Control here describes a buffer that contains no CRP protein. The fraction of bound SOMAmer does not reach unity even at the highest protein target concentrations. We attribute this to protein aggregate formation and other factors.

4.4.6 CRP detection in serum

We explore the applicability of the CRP assay to complex samples. To this end, we performed preliminary experiments on diluted human serum. In addition to its high protein content, serum contains several anions that are present in millimolar concentrations, and thus form plateau-mode zones in ITP.[105,106] These anions, which include phosphate, sulfate, bicarbonate, and uric acid, have a wide range of mobilities. As a result, we observed additional spacer zones even after removing the original spacer ion (HEPES) from the TE buffer. We diluted the serum sample 20-fold in LE buffer to minimize protein aggregates and obtain higher sensitivity and repeatability. In diluted serum with spiked CRP target, our assay achieved an LOD of 25 nM, approximately an order of magnitude loss in sensitivity (Figure 4.8). We assume negligible levels of CRP

naturally present in the serum samples. This limit of detection extrapolates to 500 nM in undiluted serum, a significant loss of clinical applicability for all but severe cases of inflammation. Clearly, additional work is required to extend our assay to clinical applications.

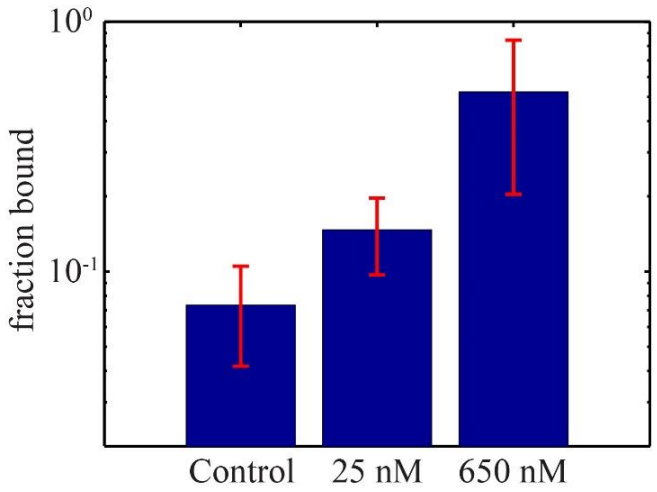

Figure 4.8. Experimental data from CRP assay in diluted serum sample. For all experiments, we use a SOMAmer concentration of 180 nM and vary CRP concentrations. We dilute serum samples 20-fold in LE buffer. We then spike CRP target into the mixture. We observe significantly higher background signal in the negative control case. We attribute this increase in signal to non-specific interactions between the SOMAmer and other serum proteins.

We also note that using 0.2% Triton X-100 led to decreased aggregate formation than 0.02% or 0.12% Tween-20. We hypothesize that this is due to Triton X-100 being a harsher detergent than Tween-20, and thus was more successful in solubilizing serum proteins. However, we still observed significant aggregates regardless of the surfactant chosen.

Extending this assay and other ITP reaction assays with proteins to a complex sample like serum presents several challenges. As mentioned above, the presence of several

ionic species in serum at high concentrations complicates an assay that is dependent on optimized buffer chemistry and species' mobilities. Another challenge is the abundance of other serum proteins, particularly albumin, which is present in very high concentration, and causes nonspecific binding to SOMAmer probes and other proteins; a well-known problem.[107,108] We hypothesize that non-specific binding between SOMAmers and proteins increased our background fluorescence while preventing binding of the SOMAmer to CRP. We note that the use of certain nonspecific competitors (such as Z-block) mitigates those effects (discussed in Section 4.4.2).

However, achieving specificity remains a difficult challenge. The high concentration of serum proteins also results in protein-protein interactions, leading to aggregate formation. We note that changing surfactant from Tween-20 to Triton X-100 reduced aggregate formation in our experiments. Additionally, protein mobility is highly dependent on the local ionic and chemical environment. Unlike NAs, proteins have a wide range of isoelectric points and mobilities, which further complicates assay design in complex samples.

4.5 Summary

We report here on our proof-of-concept effort towards extending ITP- and ionic spacer-based reaction and separation to the detection of protein targets. We introduce and discuss key parameters important in the design of an ITP based reaction-separation assay where a low-mobility, non-focusing target is recruited into ITP by a high-mobility probe. We then demonstrate our assay using the clinically relevant CRP protein. The assay is rapid, with 10 min off-chip heating plus 10 min on-chip ITP, and easy to

implement with few manual steps. To our knowledge, this is the first ITP-based assay to show simultaneous on-chip reaction and separation of an aptamer and its protein target. Finally, we explore the extension of our assay to diluted serum spiked with CRP, where we encounter and discuss several challenges, including the formation of additional spacer zones and loss of sensitivity.

The 2 nM LOD of the assay in clean buffer is acceptable for CRP detection, but needs to be improved for other clinically-relevant protein targets. Our current assay had an extrapolated LOD of 500 nM in undiluted serum, which diminishes its clinical applicability. We hypothesize that using a custom-designed chip with longer reaction zone or an aptamer with higher affinity would enhance sensitivity.

As discussed above, ITP assays accelerating NA reactions in complex samples have been successfully demonstrated and validated for several samples and applications. The narrow range of free-solution NA mobility[46] facilitates the exclusion of unwanted contaminants from the ITP zone. Proteins targets, however, present additional challenges for ITP assays. Overcoming these challenges will require careful target selection and buffer chemistry design. We present the work in this chapter as an entry into extending ITP-based spacer assays to the detection of proteins and other low- or unknown-mobility targets, and as a guide towards the design of such assays.

5 Size-based RNA fractionation using ITP and ionic spacer

The contents of this chapter are adapted from a conference proceeding submitted to MicroTAS 2016, and are reproduced here with minor modifications. The work described in this chapter was performed during a summer internship at Sandia National Laboratories in Livermore, CA, under the supervision of Robert J. Meagher.

5.1 Introduction

We have developed a rapid microfluidic technique for size-based RNA fractionation, an important step in RNA sequencing library preparation. Our assay leverages isotachophoresis (ITP) and an ionic spacer to preconcentrate RNA then create two RNA fractions based on a tunable cutoff size. We demonstrate this approach using synthetic DNA as well as an RNA ladder. Our assay requires less than 10 min, has minimal sample loss, and is easily tunable for user-specified cutoff sizes.

RNA transcripts circulating in blood and plasma have widespread utility as biomarkers of cancer, infection, and numerous other pathophysiological states.[109-112] Profiling of circulating RNAs by next-generation sequencing (NGS) techniques like RNA-Seq has immense potential to identify meaningful biomarkers for many diseases.[113,114] However, circulating RNA are typically <200nt, and include both "small" RNAs (such as microRNA and others) as well as "large" degraded mRNA and other species. Library preparation, sequencing, and bioinformatics analysis of "small" (<50 nt) and "large" (>100 nt) RNA differs significantly.[115,116] Therefore, though both fractions provide useful information, it is imperative to analyze them separately. Though there are several commercial size-selection kits for DNA fractionation,[117] we only know of Pippin Prep

kit to perform small RNA size-selection.[118] Pippin Prep retains RNA molecules less than 150-200 nt, a cutoff that is significantly larger than our intended application. Furthermore, larger RNA fragments are not preserved in this process.

The assay presented here addresses the need for rapid RNA size-selection by integrating ITP-based nucleic acid fractionation in a large-channel microfluidic device capable of processing 10 µL of sample. ITP is an electrophoretic technique that uses two buffer systems, a high-mobility leading electrolyte (LE) and a low-mobility trailing electrolyte (TE). When an electric field is applied, analytes which have mobilities intermediate to those of the LE and TE, focus at a sharp interface between the two.[27] In Chapters 3 and 4, we has demonstrated the use of high-concentration spacer ions, which have intermediate mobility and form a plateau zone, to create two ITP interfaces, and separate reaction products following ITP-based reaction.

In this chapter, we extend the spacer concept to perform size-based RNA fractionation in large volume microfluidic devices, as shown in Figure 5.1. Our channel consists of two regions; the first containing sample mixed in with TE and spacer ions, the second containing LE and sieving matrix. We use a sieving matrix to increase the difference in effective mobility between small and large RNA fragments.[46] In the first region, all RNA molecules, independent of size, focus in ITP ahead of both the spacer and TE ions. This is due to the largely size-independent electrophoretic mobility of nucleic acids in free-solution. Upon entering the second region, which contains the sieving matrix, spacer ions gradually overtake large RNA molecules but not smaller RNA, and form a zone separating the two RNA fractions based on size. We design the spacer ion and sieving matrix concentration to achieve a size cutoff of approximately 50-60 nt, and we

note that this approach is highly tunable for different size cutoffs. RNA molecules smaller than 50 nt focus at the LE-spacer interface, whereas those larger than 50 nt focus at the spacer-TE interface.

5.2 Materials and methods

5.2.1 Design of microfluidic device

We designed a microfluidic device capable of processing 10 µL of sample. We designed the device layers using AutoCAD software, and fabricated the poly(methyl methacrylate) (PMMA) device using a laser cutter. The device is composed of a reservoir layer, a channel layer, and a cover layer. We used pressure-sensitive double-sided adhesive tape to bond the three PMMA layers together and form leak-proof channels. The resulting channels are 2 mm in width, 0.2 mm in depth, and 20 mm in length. We added a slit in the top layer above the channel to facilitate creation of a distinct 10 µL sample zone, and an extraction reservoir to enable sample extraction following ITP. The chip layout is shown in Figure 5.2. We designed buffering reservoirs in order to ensure sufficient buffering capacity and prevent bubbles formed in the reservoir from entering the channel. These reservoirs consisted of 1 mL pipette tips filled with buffering TE and LE, a Pd electrode connected to an external voltage source, and a layer of solidified agarose, as shown in Figure 5.2c. Agarose creates a solid support layer at the bottom of the reservoir and prevents sample leakage.

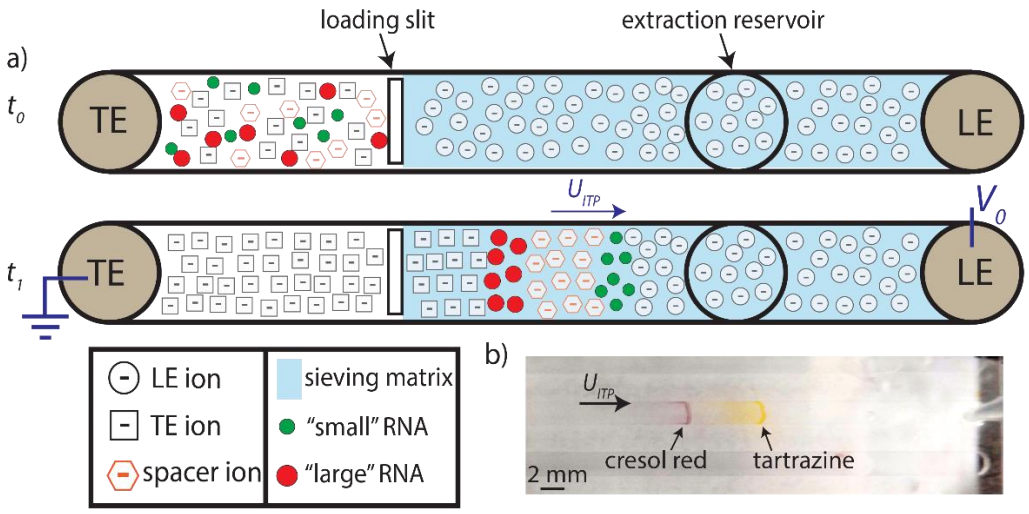

Figure 5.1. a) Schematic representation of the assay. At t_0, small and large RNA are mixed together with the TE and spacer ions. At t_1, ITP has been initiated, and the RNA fragments have entered the region containing sieving matrix. The sieving matrix greatly reduces the effective mobility of the large RNA fragments, allowing the spacer ions to overtake them while staying behind the small RNA. This creates two distinct ITP peaks, separated by a spacer zone of user-defined length. b) Experimental visualization of the ITP-spacer assay using Tartrazine and Cresol Red as ITP tracking dyes. Tartrazine, which has the higher mobility, focuses at the LE-spacer interface while Cresol Red focuses at the spacer-TE interface.

5.2.2 ITP chemistry

Our LE consisted of 30 mM HCl, 60 mM Tris, 1% PVP, 4M Urea, and 2.5% HEC. PVP was used to suppress electroosmotic flow. Urea is a denaturant, which helps reduce secondary structure in the longer RNA. fragments.[119] We chose HEC, a linear polymer, as our sieving matrix, due to its strong sieving capability and its moderately high viscosity (to reduce hydrodynamic flow). Our TE consisted of 30 mM HEPES, 60 mM Tris, 10 mM Aspartic Acid, and 1% PVP. Aspartic acid was used as a spacer in this assay, as it has intermediate mobility to the RNA fragments in the sieving matrix region.

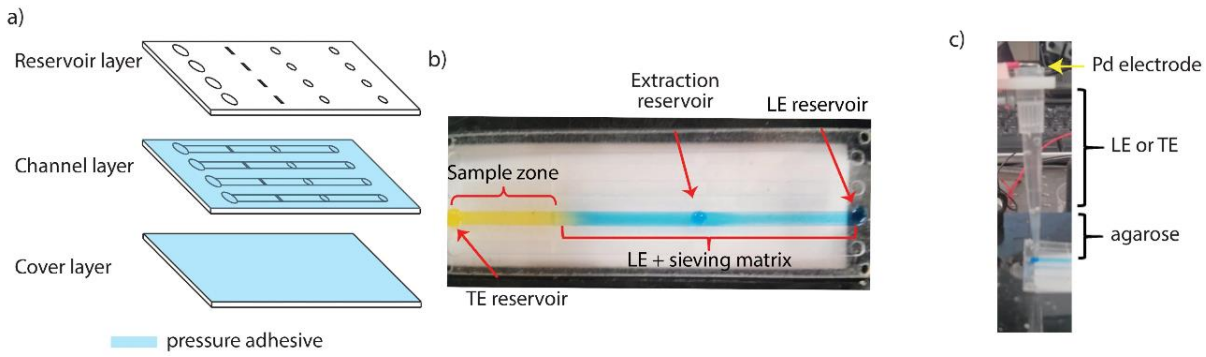

Figure 5.2. a) Schematic showing the three layers of the PMMA device. Pressure adhesive is used to bond the layers and create watertight channels. Top layer is the reservoir layer, the middle is the channel layer, and the bottom is the cover layer. b) Top-down view of the large volume microfluidic devices, highlighting the LE, TE, and extraction reservoirs, as well as the sample and LE zones. Channels are 2 mm in width, 0.2 mm in depth, and 2 cm in length. The sample zone (yellow) has a total volume of 10 µL. c) Buffering reservoir design consisting of a 1 mL pipette tip filled with LE or TE buffer and solidified agarose on the bottom to prevent leakage. A Pd electrode is connected to an external voltage source. This reservoir design allows sufficient buffering capacity and prevents bubbles from entering the channel.

5.2.3 Assay operation

We filled the channel using a 3-step process, shown in Figure 5.3: we first loaded the LE by slowly pipetting from the LE reservoir until buffer reached the extraction reservoir, then the loading slit. We then filled the rest of the channel by loading the TE, spacer, and sample from the TE reservoir. Finally, we loaded "clean" TE into the TE reservoir. After filling the channel and reservoirs, we brought the device into contact with the buffering reservoirs, and initiated ITP. We used Tartrazine and Cresol Red, common gel electrophoresis loading dyes, to track ITP progress. We found that Tartrazine, the faster of the two, focused at the LE-spacer interface, whereas Cresol Red focused at the spacer-TE interface. This allowed colorimetric tracking of ITP and bypassed the need for a fluorescent microscope or camera. The entire ITP process required approximately 10 min.

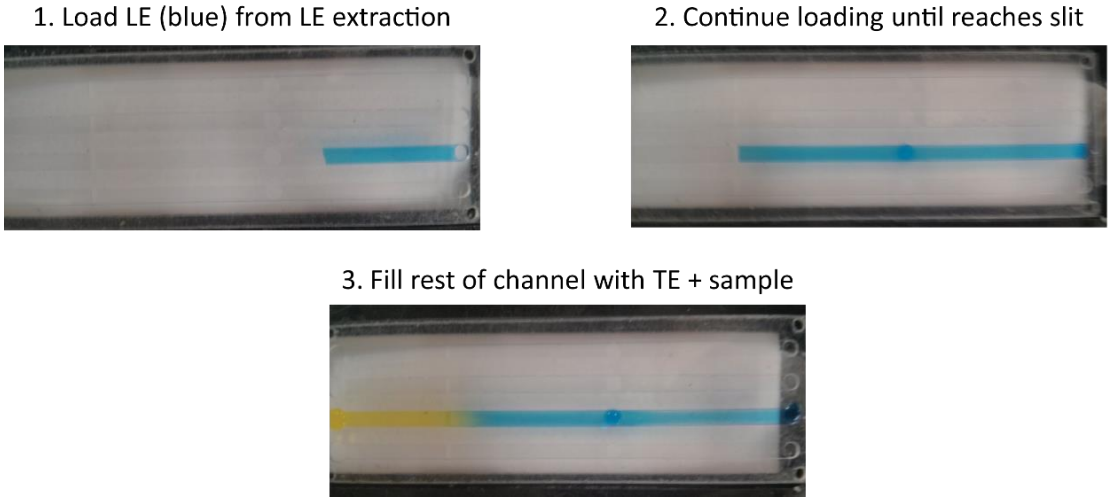

Figure 5.3. Loading protocol using 10 µL laser-cut PMMA chip. We initially load LE from LE reservoir, and allow it to fill through capillary wicking until it reaches extraction reservoir. We then dispense more LE from the extraction reservoir, allowing LE to further wick until reaching the loading slit. We then load a mixture of TE buffer, spacer ions, and sample (yellow) into the TE reservoir, and allow it to fill the rest of the channel. Finally, we load "clean" TE into the TE reservoir. After loading, we bring the device into contact with the buffering reservoir shown in Figure 1c, and initiate ITP separation. Following ITP, we extract both ITP-focused fractions from the extraction reservoir, using a pipette.

When the first ITP peak, represented by Tartrazine, reached the extraction reservoir, we pipetted 5 µL from the reservoir and then replaced 4 µL of the LE. As the second ITP peak, represented by Cresol Red, arrived at the reservoir, we pipetted 5 µL of the second fraction. For each experiment, we analyzed the pre-processed sample mixture and both extracted fractions from ITP using the small RNA assay on the Agilent Bioanalyzer. The Bioanalyzer is an electrophoretic system that provides quantitation and sizing information for nucleic acids and proteins.

5.3 Results and discussion

5.3.1 Demonstration of fractionation using DNA oligonucleotides

We first tested the ITP-spacer assay by using Tartrazine and Cresol Red, commonly-used gel electrophoresis loading dyes, as a colorimetric trackers of ITP peaks. We observed two clearly defined ITP peaks separated by a spacer zone, as shown in Figure 5.1b. We first demonstrated successful fractionation using a mixture of DNA oligonucleotides (20, 50, and 100 nt). As described above, we manually extracted 5 uL of each DNA fraction, and tested the contents of each using the small RNA assay on the Agilent Bioanalyzer, In Figure 5.4, we show the results of a typical experiment with DNA sample. We see that fraction 1 contains only 20 and 50 nt DNA fragments, and no 100 nt fragments. Fraction 2, on the other hand, mostly contains 50 and 100 nt fragments, though it also has a small amount of 20 nt fragment.

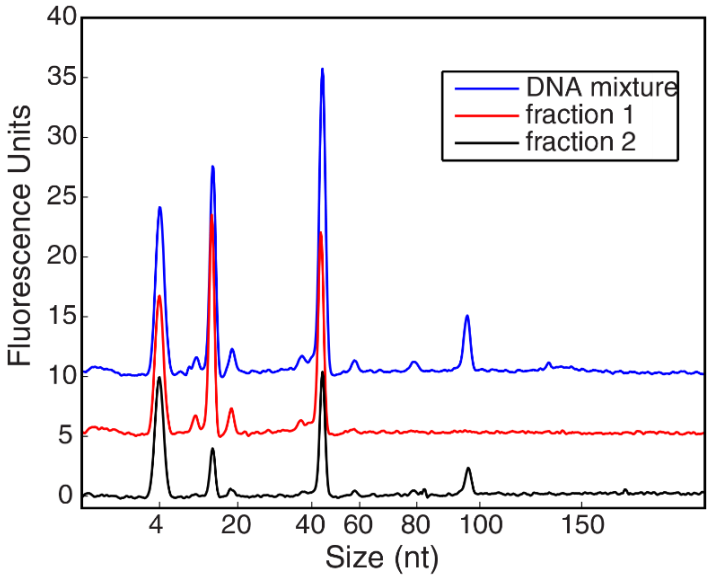

Figure 5.4. Results of a typical ITP-spacer experiment using a mixture of DNA oligonucleotides (20, 50, and 100 bp). We used aspartic acid as the spacer species, and 2.5% HEC as sieving matrix. Following ITP, we collected two fractions, and analyzed their contents, along with those of the pre-processed sample, using the Agilent Bioanalyzer. The spike at 4 nt represents a control peak and is not part of the DNA sample. We find that the majority of DNA content in the pre-processed DNA mixture was retained following ITP. Fraction 1 contained primarily 20 and 50 bp fragments, with no 100 bp. All extracted 100 bp fragments was found in fraction 2, which also contained the remaining 50 bp DNA and a small amount of 20 bp fragments.

5.3.2 Demonstration of fractionation using RNA mixture

Finally, we demonstrated the results of this assay using an RNA ladder containing various RNA fragment sizes in Figure 5.5. The results of these experiments with RNA sample were comparable to those using DNA. Compared to the pre-reaction mixtures, we found that ITP separation and extraction resulted in high yield with minimal sample loss. Our assay excluded large RNA from the first fraction, ensuring that the small RNAs were not "contaminated" with larger RNAs. While the second fraction was primarily composed of RNA fragments 50 bp or larger, it retained a small fraction of small RNA. As expected RNA fragments close to the cutoff size were found in both fractions. We believe that the presence of small RNA in the second fraction indicates that small RNA did not fully resolve and focus at the LE-spacer interface. We hypothesize that the assay's performance could be further improved with increasing separation channel length and further optimizing spacer and sieving matrix concentrations.

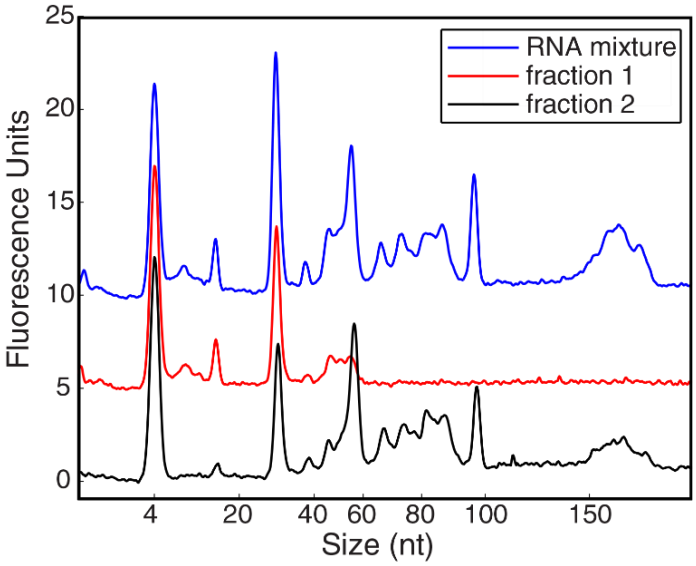

Figure 5.5. Results of a typical ITP-spacer experiment using a mixture of synthetic RNA fragments. We again used aspartic acid as the spacer species, and 2.5% HEC as sieving matrix. Following ITP, we collected two fractions, and analyzed their contents, along with those of the pre-processed mixture, using the Agilent Bioanalyzer. The spike at 4 nt represents a control peak and is not part of the RNA sample. Similar to experiments with DNA, we found that the majority of RNA content in the pre-processed RNA mixture was retained following ITP, indicating high extraction yield. Fraction 1 contained no RNA fragments larger than 50 bp and was thus purified of large RNA. While fraction 2 was primarily composed of RNA fragments 50 bp or larger, it retained a small fraction of small RNA. We hypothesize that small RNA did not fully resolve and focus at the LE-spacer interface, and that the assay's performance could be further improved with increasing separation channel length and further optimizing spacer and sieving matrix concentrations.

5.4 Summary

In this chapter, we presented an approach that leverages ITP and an ionic spacer to perform RNA and DNA fractionation. We designed a device that can process 10 µL of sample. We demonstrated this assay using synthetic DNA and RNA samples. This approach is fast (10 min separation), tunable, and retains both fragments for downstream processing. Our device design enables colorimetric tracking of ITP and bypasses the need for cameras or fluorescence microscopy. With additional optimization, we believe

that our assay could be a promising approach to rapid and effective size-based RNA fractionation in RNA-Seq library preparation workflows.

6 Purification and detection of bacteria in blood using ITP and RPA

The contents of this chapter are adapted from a manuscript which is currently under review in *Analytical Chemistry*, and are reproduced here with minor modifications.

6.1 Introduction

We present a new approach which enables lysis, extraction, and detection of inactivated *Listeria Monocytogenes* cells from blood using isotachophoresis (ITP) and recombinase polymerase amplification (RPA). We use an ITP-compatible alkaline and proteinase K approach for rapid and effective lysis. We then perform ITP purification to separate bacterial DNA from whole blood contaminants using a microfluidic device that processes 25 µL sample volume. Lysis, mixing, dispensing, and on-chip ITP purification are completed in a total of less than 50 min. We transfer extracted DNA directly into RPA master mix for isothermal incubation and detection, an additional 25 min. We first validate our assay in the detection of purified genomic DNA spiked into whole blood, and demonstrate a limit of detection of 16.7 fg/µL genomic DNA, the equivalent of 5 x 10^3 cells/mL. We then show detection of chemically-inactivated *L. Monocytogenes* cells spiked into whole blood, and demonstrate a limit of detection of 2 x 10^4 cells/mL. Our results suggest that ITP purification is compatible with RPA detection, and has potential to extend the applicability of RPA to whole blood.

Bacteremia is the presence of viable bacteria in the bloodstream, and this condition can be life-threatening.[120,121] The gold standard for bacteremia diagnosis is blood culture. Though capable of resolving very low bacterial counts, this method requires trained

personnel and specialized microbiology infrastructure, and typically takes several days to produce a result. The time-critical nature of certain bacterial infections makes bacterial cultures a suboptimal diagnostic approach.[122] Nucleic acid amplification has gained traction in bacterial infection detection. The most widespread and adopted technique is polymerase chain reaction (PCR). PCR is highly sensitive, capable of detecting as little as a single copy of a bacterial genome. However, PCR requires extensive sample preparation, and is highly vulnerable to inhibitors.[123,124]

Recombinase Polymerase Amplification (RPA) is an isothermal amplification technique that is a promising alternative to PCR.[125] RPA requires no thermal cycling and can be completed in less than 30 min. RPA is also likely more robust to inhibitors compared to PCR.[126] For example, Kersting et al.[127] demonstrated successful RPA in the presence of several known PCR inhibitors. Furthermore, RPA has been successfully demonstrated with minimal sample preparation in serum,[127] saliva,[128] and urine.[129]

Despite these advantages, RPA is incompatible with whole blood, an important matrix in infectious disease diagnostics. Kersting et al.[127] tested RPA in the presence of blood components like serum and hemoglobin, and showed successful amplification. However, experiments with whole blood were unsuccessful. They hypothesized that RPA inhibition was due to other blood components or the use of sodium fluoride (NaF) as anticoagulant. Rohrman et al.[130] discussed the inhibitory effect of large quantities of background DNA present in 50-100 µL of white blood cells, and suggested selective capture of target DNA would improve assay sensitivity. Though the inhibitory effect of blood on RPA is consistently observed, the full set of causes is not yet established.

In this chapter, we leverage isotachophoresis (ITP) purification to enhance RPA compatibility with blood. As discussed in Chapter 1, until somewhat recently, nucleic acid purification assays using ITP were limited to small volumes on the order of 100 nL, due to geometrical constraints of (convenient) commercially available chips. Marshall et al.[10] developed an injection-molded chip that processes 25 µL of sample, greatly increasing processed volume and yield. We use this device in our assay to increase sensitivity.

Borysiak et al.[62] recently developed an assay combining ITP and loop-mediated isothermal amplification (LAMP) for the detection of *E. Coli* bacteria in milk. They used electromigration and heat-induced pressure driven flow to direct purified DNA into an amplification reservoir. Their assay demonstrated two orders of magnitude improvement over tube-based LAMP assays in milk. We know of no other work that combines ITP with isothermal amplification. We know of no other microfluidic assay (e.g., ITP) for RPA for blood.

In this chapter, we combine rapid cell lysis, ITP purification, and RPA for the detection of inactivated *L. Monocytogenes* cells in whole blood. Presence of *L. Monocytogenes* cells in whole blood, known as Listeriosis, is a condition particularly hazardous for pregnant women and immunocompromised patients.[131] *L. Monocytogenes* is a gram-positive bacteria, and is difficult to lyse due to its thick peptidoglycan cell wall. This work differs from Borysiak et al., as we here address a more difficult to lyse gram-positive bacteria from a significantly more complex sample, blood. We also employ a different isothermal amplification technique, and for simplicity and speed use ITP for

all transport (e.g., no valving or pressure driven flows). Our results suggest that ITP purification can be integrated with RPA detection even for difficult-to-lyse species in whole blood.

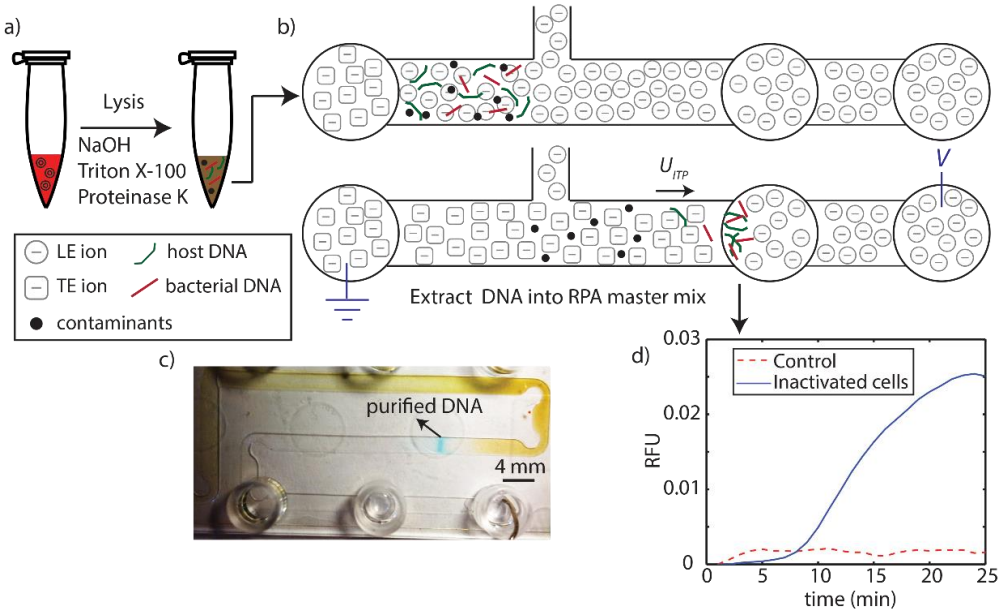

Figure 6.1. Schematic of ITP-RPA assay protocol summarizing lysis, extraction, and detection steps. a) We lyse whole blood spiked with *L. Monocytogenes* using NaOH, Triton X-100, and proteinase K. This method is rapid, extremely effective, and ITP-compatible. We quench the high pH (12.5-13) with LE buffer, then transfer and load the 25 µL mixture into the high-throughput microfluidic chip. b) We apply electric field and initiate constant-current ITP purification of bacterial DNA and host DNA from whole blood. The current ITP extraction requires about 40 min to complete. c) Image of ITP process in chip. The ITP zone (containing purified total nucleic acids) and its separation from contaminants in whole blood is clearly visible by eye. The ITP zone is tracked/visualized using AlexaFluor 647 as an ITP peak tracking dye. The contains channel with nominal widths of 2 mm, 0.15 mm depth, and a total channel length of 200 mm (see Marshall et al.[10]). d) After purified DNA reaches extraction reservoir, we pipette and transfer this fraction directly into standard RPA master mix. RPA is performed at 40°C for 25 min in a thermal cycler.

6.2 Materials and methods

A schematic of our protocol is shown in Figure 6.1. We performed two versions of the assay. First with a controlled experiment where we spiked *L. Monocytogenes* genomic

DNA into whole blood. The second where we spiked *L. Monocytogenes* inactivated cells into blood. In both cases, we chemically lysed the blood using the HotSHOT lysis method, which relies on high pH (12.5-13) for rapid and effective lysis.[132] We quenched and reduced this pH down to 8.1 with LE buffer, and loaded the 25 µL mixture into the microfluidic chip. We then applied electric field to initiate ITP. Following ITP purification, we pipetted the purified DNA from the extraction reservoir, and transferred directly to the RPA master mix for 25 min off-chip amplification with RPA.

6.2.1 Whole blood and *L. Monocytogenes* samples

Human blood samples from a healthy donor were collected in heparin tubes at the Stanford Blood Center. We prepared aliquots of 1 mL and stored them at -80°C. Purified *L. Monocytogenes* genomic DNA was purchased from ATCC (no. 19115D-5, ATCC, VA) and suspended in 1x Tris-EDTA buffer. Chemically-inactivated *L. Monocytogenes* cells were purchased from ZeptoMetrix (NY) and suspended in their proprietary Purified Protein Matrix.

6.2.2 Lysis protocol

We lysed 2.5 µL of whole blood with suspended genomic DNA or *L. Monocytogenes* cells with 2.5 µL lysis buffer consisting of 125 mM NaOH (Sigma-Aldrich, MO), 1% Triton X-100 (Sigma-Aldrich, MO), and 1 mg/mL Proteinase K (Invitrogen, CA). We incubated the mixture for 2 min at room temperature when using genomic DNA, and for 10 min at 65°C when using inactivated cells, as shown in Brewster and Paoli.[133] We then added 20 µL of 40 mM HCl, 50 mM Tris (Sigma-Aldrich, MO), 0.1% PVP (Sigma-

Aldrich, MO), and 1% Triton X-100 to reduce pH to ~ 8 and dilute the cell lysate mixture 10-fold.

6.2.3 Channel Preparation

Prior to first use, we rinsed the channel with methanol, deionized (DI) water, NaOH, and HCl for 2 min each. Following each experiment, we rinsed the channels with 10% bleach for 10 min to minimize cross-contamination between experiments. This was followed by rinses with DI water, NaOH, HCl, and then DI water again, each for 2 min. We then dried the channel under vacuum for 10 min. We note that these inter-experiment washes would not be required for implementation of the injection molded chip as a disposable device.

6.2.4 ITP extraction

We used a buffering LE (loaded into the LE reservoir) consisting of 200 mM HCl, 400 mM Tris, and 0.1% PVP (Sigma-Aldrich, MO). Our channel LE (loaded into the channel) consisted of 35 mM HCl, 70 mM Tris, and 0.1% PVP (Sigma-Aldrich, MO) (predicted pH = 8.1). Buffering TE consisted of 100 mM HEPES, 230 mM Tris, and 0.1% PVP (predicted pH = 8.2). At the start of each experiment, we loaded LE buffer into the extraction reservoir and allowed it to passively fill the separation channel. We then loaded the quenched lysate mixture into the TE reservoir and allowed it to fill the sample channel. Finally, we added 20 µL of buffering LE, channel LE, and buffering TE to each of the LE, extraction, and TE reservoirs, respectively.

Our microfluidic device is an injection molded (cyclic olefin copolymer (COC) material) chip, and is described in detail by Marshall et al.[10] Briefly:

- The chip footprint is 25 by 76 mm and contains channels with nominal widths of 2 mm, 0.15 mm depth, and a total channel length of 200 mm.
- The sample channel segment can has a loading volume of 25 µL and the separation channel a volume of 30 µL. Given the composition of our LE and TE buffers, this separation channel volume is sufficient to fully separate bacterial DNA from whole blood contaminants.
- The device contains an extraction reservoir that is separate from the LE buffering reservoir. This ensures that electrodes placed in the buffering LE reservoir do not come into contact with the sample, and that reactions occurring at the electrode do not interfere with composition of extracted sample.
- Capillary barriers are used to aid in sample loading and to create a sharp interface between the sample and separation channels. These barriers consist of steep flat-surface ramps that reduce the channel depth by half, before suddenly expanding back to full depth. This "ledge" creates an energetic barrier that stops the flow of a wicking liquid. We use this feature to first load clean LE from the buffering reservoir and fill the separation channel, but stop at the ledge. We then loaded the blood lysate sample from the TE reservoir, which wicked through the sample channel. The sample then reaches the ledge, and forms a liquid-to-liquid interface that overcomes the energetic barrier. Images and a more detailed discussion of the device are found in Marshall et al.[10]

We load buffering TE, buffering LE, and channel/separation LE are load into the TE, LE, and extraction reservoirs, respectively, as shown below. We applied 105 µA of

current using a Keithley 2410 current source (Keithley, OH) between the LE and TE reservoirs. We monitored ITP progress by using AlexaFluor 647 (Life Technologies, CA) simply as an ITP tracking dye. We performed experiments (not shown) to confirm the dye did not interfere with downstream RPA detection. In Figure 6.2, we show an image of the microfluidic device, with labeled reservoirs and channel sections.

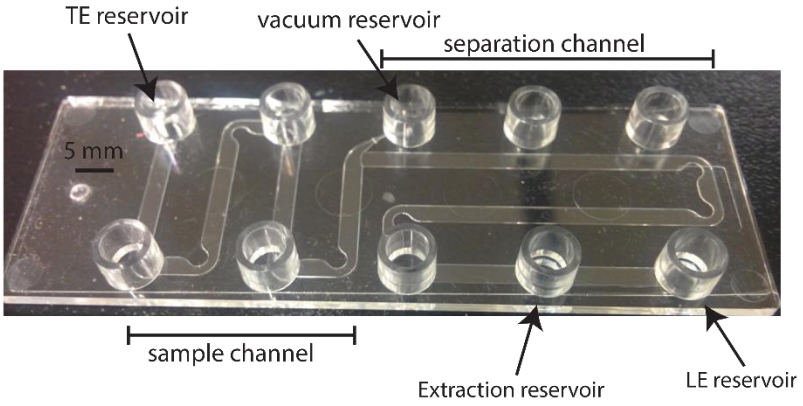

Figure 6.2. Image of the device used for ITP purification. The sample channel portion holds a total volume of 25 µL, while the separation channel portion can hold 30 µL. The device uses capillary barriers to aid in the loading and create a sharp interface between the channel and separation channels. A more detailed view and explanation of the device design can be found in Marshall et al.[10] We load buffering TE into the TE reservoir, buffering LE into the LE reservoir, and channel LE into the extraction reservoir, and apply vacuum as shown. The vacuum reservoir is also used to dry and rinse the channels between experiments.

6.2.5 RPA

We used off-chip RPA to demonstrate the compatibility of ITP purification with RPA detection. We added 5 µL of extracted DNA from ITP to RPA mastermix (TwistDx, Cambridge, UK). Mastermix includes a pellet containing enzymes, a rehydration buffer, and magnesium acetate to activate the enzymes. We used the TwistAmp exo +*ListeriaM* kit.[134] Primers and probe were provided as part of the kit from TwistDx. Sequences were published in Schuler et al.[135] Forward primer was TTCAATTTCATCCATGGCAC,

reverse primer was CTTTGTAACCTTTTCTTGGC, and the exo probe sequence was [FAM]ACGCCAATCGAAAAGAAACACGC[BHQ-1]. We performed RPA using a real-time PCR thermocycler (MiniOpticon, Bio-Rad, CA), set at 40°C for 25 min.

6.3 Results and discussion

6.3.1 Assay operation.

The ability to process a relatively large volume of sample is important in infectious disease detection assays, as bacterial or viral species are often present in trace amounts. As mentioned above, we used the chip of Marshall et al.[10] which is an injection-molded device that can process 25 µL of sample. We used this device in our experiments to increase our assay's extraction efficiency and sensitivity. Scaling up microfluidic systems implies several challenges, including Joule heating, limited buffering capacity, and increased susceptibility to hydrodynamic pressure effects.[79] As shown in Figure 6.1, the chip contains features designed to support pH buffering of large volumes.[81] A downstream-most reservoir accommodates a high-concentration (200 mM) Tris-HCl LE buffer (predicted pH = 8.1). After loading of sample channel section, the loading reservoir is filled with a high concentration (100 mM) TE buffer (predicted pH = 8.2). The LE loaded into the 30 µl separation channel has a concentration of 35 mM to achieve extraction time of approximately 40 min. In the Section 6.3.5, we analytically derive expected assay times. In their work, Marshall et al.[10] used Pluronic F-127, a temperature-sensitive gel that is liquid at cold temperatures but solidifies into a gel at room temperature, in their two buffering reservoirs in order to minimize pressure-driven flow. While elegant, this approach requires the presence of nearby refrigerator and swift

handling of the gel. We here successfully mitigated pressure-driven effects without Pluronic F-127, through careful loading and balancing volumes dispensed into the reservoirs.

6.3.2 Visualizations of ITP purification of bacterial DNA purification whole blood

Following lysis of spiked whole blood using NaOH, Triton X-100, and proteinase K, we quenched the mixture using LE buffer, down to pH 8.1. We then transferred this mixture into the microfluidic device described above. In Figure 6.3 we show images of the ITP purification process. We dispensed the quenched cell lysate mixture into the TE reservoir, and it passively wicked through the 25 µL portion of the channel. After loading the various LE and TE buffers in the appropriate reservoirs (see Section 6.2.4), we applied an electric field between the LE and TE reservoirs to initiate ITP and used AlexaFluor 647 to visualize the ITP peak and so track ITP progress (i.e., only indirect visualization of the zone containing DNA). As analytes progressed through the channel, genomic DNA separated from the contaminants found in whole blood. Eventually, purified DNA was fully separated and reached the extraction reservoir ahead of the contaminants. We manually extracted the DNA using a pipette, and transferred 5 µL of the mixture into the RPA master mix for amplification and detection. The entire process required approximately 40 min. We note that this purification time is constrained by the available power source and Joule heating, and theoretically could be further reduced.

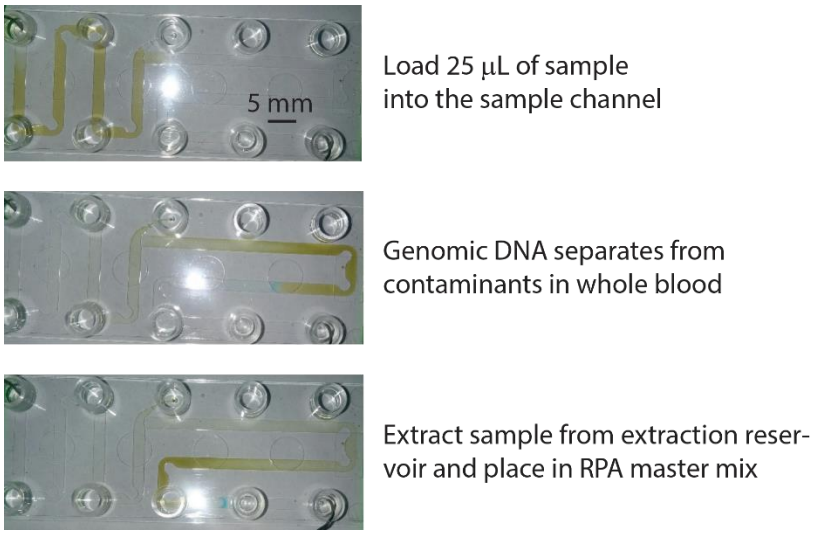

Figure 6.3. Images of an ITP experiment using whole blood. We first load 25 μL of sample into the sample channel. The sample is 10-fold diluted infected whole blood mixed with quenching LE buffer. We apply electric field between the TE and LE reservoirs, initiating ITP. We use AlexaFluor 647 as an ITP tracking dye. Genomic DNA begins to separate from the contaminants found in whole blood. Eventually purified genomic DNA reaches the extraction reservoir ahead of the contaminants. At that point, we manually extract DNA using a pipette, and place in the RPA master mix.

6.3.3 Lysis.

Gram-positive bacteria are harder to lyse than gram-negative species due to their thicker peptidoglycan wall. Methods such as gentle thermal lysis, detergent-based lysis, and even lysozyme lysis, are either ineffective or require overnight incubation.[136] We therefore used a more aggressive chemical method to lyse the *L. Monocytogenes* cells. We used an alkaline-based method (HotSHOT) which leverages high pH for rapid and effective lysis. This method was shown by Brewster and Paoli[133] to be highly effective in the extraction of genomic DNA for *L. Monocytogenes*, and shown by Rogacs et al.[70] to be ITP-compatible. We included proteinase K in our lysis buffer to aid in lysis and degrade DNA-binding proteins. Consistent with the findings of Persat et al.,[11] we found that using proteinase K was necessary for high extraction efficiency. Our lysis buffer

avoids chaotropic agents which are used in high ionic strengths (such as guanidine hydrochloride), and require significant dilution to integrate with ITP. We diluted the infected blood in our assay by 10-fold.

6.3.4 Effect of proteinase K on assay performance

Persat et al.[11] noted that proteinase K was necessary for successful nucleic acid purification from whole blood using ITP. Without using proteinase K, their assay's estimated extraction efficiency was on par with control experiments. They hypothesized that DNA binding proteins like histones significantly reduced DNA mobility and caused the complex to not focus in ITP. Proteinase K is a broad range protease, and nonspecifically degrades proteins. Proteinase K degrades DNA-binding proteins, thereby releasing DNA and allowing it to focus.

We experimentally demonstrated the effect of proteinase K on ITP purification and RPA detection, as shown in Figure 6.4. In these experiments, we spiked purified *L. Monocytogenes* genomic DNA into whole blood. We measured fluorescent signal after 15 min of RPA for both sets of experiments. RPA was unsuccessful when proteinase K was excluded from our lysis buffer. On the other hand, including 1 mg/mL proteinase K in our lysis buffer allowed for efficient degradation of proteins and focusing of DNA. Our findings are consistent with those of Persat et al.,[11] and further validate the importance of proteinase K in successful ITP purification of genomic nucleic acids from whole blood.

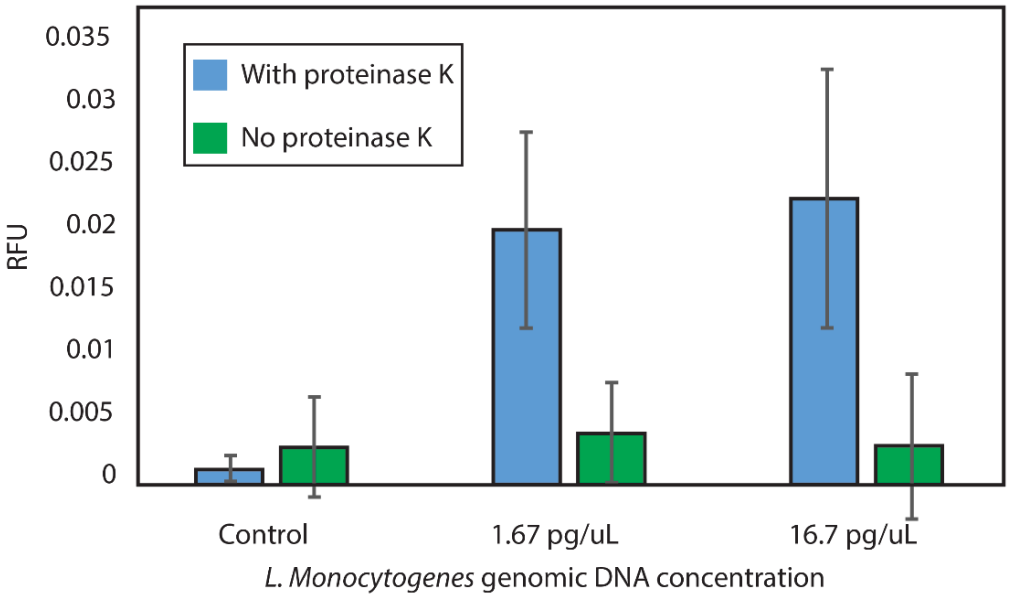

Figure 6.4. Experimental demonstration of the effect of proteinase K on ITP purification of spiked *L. Monocytogenes* genomic DNA in whole blood. We plot fluorescence measurements following 15 min of amplification with RPA. In experiments with proteinase K, we added 1 mg/mL proteinase K into the lysis buffer. Lysis in the presence of proteinase K resulted in significantly higher fluorescent signal, indicating successful ITP purification and RPA detection. On the contrary, excluding proteinase K resulted in no amplification. Together, these experiments demonstrate the importance of proteinase K on ITP purification of genomic DNA in whole blood. Uncertainty bars represent 95% confidence on the mean (as determined from Student's t-distribution). This result is consistent with the finding of Persat et al.[11] They hypothesized that proteinase K degrades DNA-binding proteins like histones, allowing DNA to focus in ITP. For experiments with proteinase K, these results are from N = 6, 7, and 6 repetitions, respectively. For experiments without proteinase K, these results are from N = 5, 10, and 3 repetitions, respectively.

6.3.5 Estimating ITP purification time

Electromigration velocity of a species migrating under an applied electric field is determined by the electrophoretic mobility of the species as well as the magnitude of the applied electric field. In the LE zone, this relation can be written as:

$$U_{ITP} = \mu_{LE} E^{LE}. \tag{6.16}$$

U_{ITP} is the observed velocity, μ_{LE} is the effective electrophoretic mobility of the LE, and E_{LE} is the electric field in the LE zone. We relate velocity to total channel length and total assay time by the simple relation,

$$U_{ITP} = \frac{L_{channel}}{t_{tot}}, \tag{6.17}$$

where $L_{channel}$ is the total length of the channel swept by ITP, and t_{tot} is the total ITP purification time. We only consider current in zones away from the ITP interface, and neglect bulk flow, and so can neglect advective and diffusive currents, and relate conductivity and electric field through Ohmic law:

$$j = \sigma^{LE} E^{LE}. \tag{6.18}$$

Here, j is current density. Conductivity in the LE zone is expressed by:

$$\sigma^{LE} = \sum_i \sum_{z=z_i}^{z_n} Fz\mu_{i,z} c_{i,z}, \tag{6.19}$$

where F is Faraday's constant, z is valence of a given ionization state of a species, $\mu_{i,z}$ is the electrophoretic mobility of species i at valence z, and $c_{i,z}$ is the concentration of species i at valence z. Here, we use monovalent LE (Cl^-) and counterion species (Tris). This allows us to recast eq 6.3 as:

$$\sigma = F\left(\mu_{LE} c_{LE} + \mu_{CI} c_{CI}\right), \tag{6.20}$$

where μ_{CI} is the electrophoretic mobility of the counterion, and c_{CI} is the concentration of the counterion. To satisfy electroneutrality, $c_{LE} = c_{CI}$, and we further simplify eq 6.4 as:

$$\sigma = Fc_{LE}\left(\mu_{LE} + \mu_{CI}\right). \tag{6.21}$$

For channels with constant cross-sectional areas, we substitute eqs 6.2 and 6.6 into eq 6.1, and algebraically manipulate to obtain:

$$t_{tot} = \frac{L_{channel} Fc_{LE}}{j}\left(\frac{\mu_{LE} + \mu_{CI}}{\mu_{LE}}\right) = \frac{\forall_{channel} Fc_{LE}}{I}\left(\frac{\mu_{LE} + \mu_{CI}}{\mu_{LE}}\right). \quad (6.22)$$

Here, I is the current in the channel and $\forall_{channel}$ is the total volume of channel swept by ITP. Using eq 6.7, we can calculate the expected ITP purification time. We estimate an LE concentration of approximately 50 mM in the sample channel (40 mM from the quenching buffer and approximately 10 mM from diluted blood) and 35 mM in the separation channel. The total channel volume is 60 µL, and we apply a constant current of 105 µA using a Keithley 2410 current source. We estimate the mobility of our LE (Cl^-) to be 79 x 10^{-9} $m^2V^{-1}s^{-1}$ and of our counterion (Tris) to be 11 x 10^{-1} $m^2V^{-1}s^{-1}$. We insert these values into eq 6.7 and find an expected assay time of just under 40 min, consistent with our experimental observations.

6.3.6 Detection of purified genomic DNA in whole blood.

We first demonstrated this assay using purified *L. Monocytogenes* genomic DNA spiked into whole blood. Figure 6.5 presents the results of these experiments. Our assay reliably detects as little as 16.7 fg/µL of genomic DNA in whole blood. This is a limit of detection (LOD) equivalent to 5 x 10^3 cells/mL (mL of original undiluted blood), or about 10-15 cells' worth of genomic DNA loaded into our microfluidic chip. For comparison, we performed control experiments using genomic DNA spiked into whole blood without ITP purification. RPA was severely inhibited by whole blood. This severe inhibition is consistent with previous efforts to apply RPA to blood in the literature.[127] Our results suggest that the current LOD is constrained by the throughput

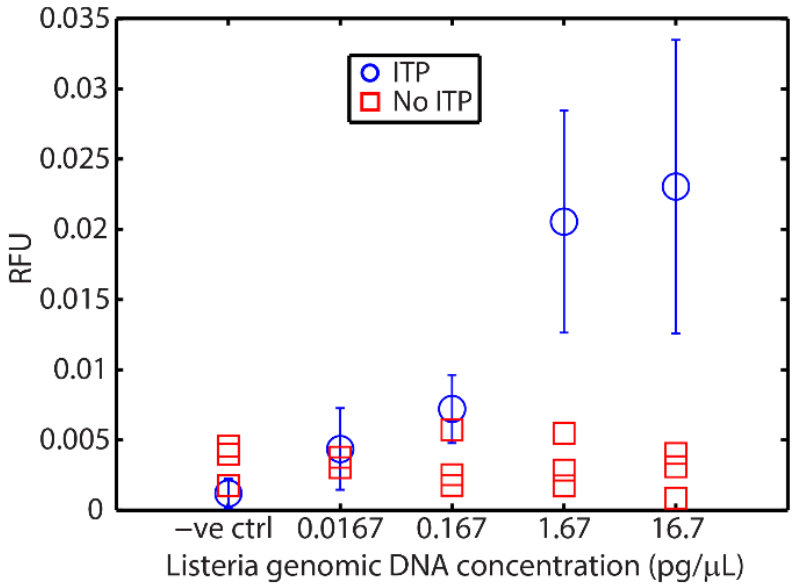

Figure 6.5. Results of our ITP-RPA assay using purified *L. Monocytogenes* genomic DNA spiked into whole blood. We measured fluorescence following 15 min of incubation. Our assay has a limit of detection of 16.7 fg/µL of spiked genomic DNA in 10-fold diluted whole blood, which corresponds to approximately 5 x 10^3 cells/mL. This is the equivalent of 10-15 cells' worth of DNA loaded into the channel. Error bars represent 95% confidence on the mean (from Student's t-distribution). We also plot the results from the corresponding experiments using 10-fold diluted whole blood without ITP purification. As expected, whole blood inhibits RPA (red squares). Results plotted are for N = 6, 5, 10, 7, and 6 repetitions, respectively, in order of increasing concentration.

of the current chip, and may be improved by using a device that can process more sample. Rohrman et al.[130] found in their experiments that background DNA found in white blood cells had an inhibitory effect on RPA detection. We have no evidence this is the case in our experiments, but hypothesize that sequence-specific target capture[49,54] could also improve sensitivity.

6.3.7 Detection of *L. Monocytogenes* cells in whole blood.

For safety concerns (and limitations of our lab), we tested our approach using chemically-inactivated *L. Monocytogenes* cells spiked into whole blood. These cells are

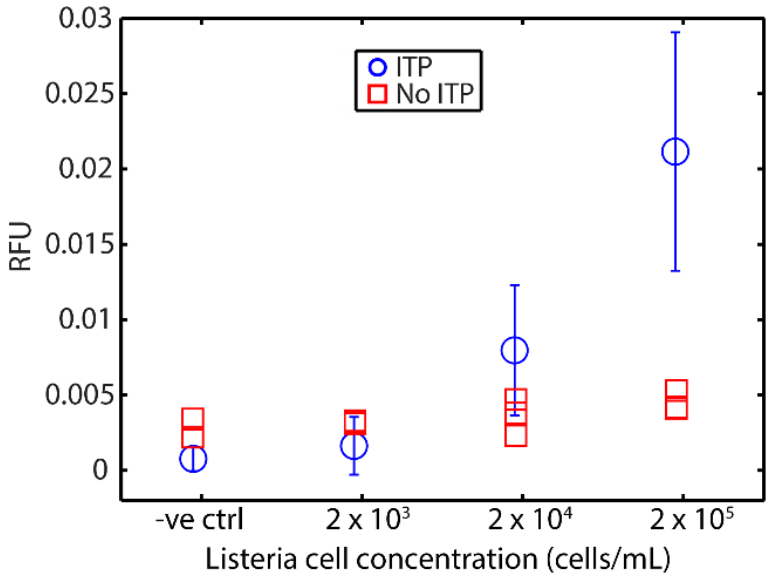

Figure 6.6. Results of our ITP-RPA assay using chemically inactivated *L. Monocytogenes* cells spiked directly into whole blood. Cells are inactivated at the surface and are thus non-infectious, but otherwise intact. We measured fluorescence (RFU) after 15 min of incubation. We demonstrate the compatibility of our approach with RPA detection from bacterial cells. Our assay (circles) LOD of about 2 x 10^4 cells/mL, which corresponds to about 50-60 cells loaded into our device. Uncertainty bars represent 95% confidence on the mean (Student's t-distribution). We also plot results from experiments without ITP purification. RPA is strongly inhibited by whole blood (red squares). The LOD using cells is approximately 4-fold worse than that of the experiments of Figure 6.5. We suspect this is due to incomplete lysis and perhaps potential losses due to contaminants (e.g., in the initial cell solution). Results plotted are from N = 5, 4, 8, and 7 repetitions, respectively, in order of increasing concentration.

rendered non-infectious by inactivation of proteins at the cell surface but are otherwise reported to be chemically intact.[137] Figure 6.6 shows our assay bacteria in blood had a limit of detection of 2 x 10^4 cells/mL (mL of original undiluted blood), which corresponds to about 50-60 cells loaded into the microfluidic device. The comparison with parallel experiments wherein RPA was performed without ITP show clearly that RPA is severely inhibited by whole blood. Our assay's LOD for the bacteria lysate DNA in in blood is approximately 4-fold worse than the genomic DNA in blood. We hypothesize two reasons for this. First, we suspect our lysis of this gram-positive

bacteria is incomplete. Second, we hypothesize that the cell solution (as received from ZeptoMetrix) may contain contaminants which may lower ITP extraction efficiency (e.g., anions which lower accumulation rate of DNA into ITP zone). We are confident that the LOD can be improved using a higher-throughput device (e.g., processing 200 µL samples versus the current 25 µL). Our results nevertheless suggest that ITP purification is compatible with RPA detection of gram-positive species from whole blood samples.

6.3.8 Toward RPA detection in a microfluidic reservoir

We report in this section on preliminary experiments toward exploring the feasibility of detection of on-chip RPA. To this end we performed a limited set of experiments where we purify DNA on-chip and elute the purified DNA ITP peak into a microfluidic reservoir. For convenience, we used for this feasibility experiment a commercially-available glass chips (NS12 Caliper chips, Perkin Elmer, CA). We achieved the required incubation temperature by placing an Indium-Tin-Oxide (ITO) heater equipped with a microcontroller (mTCII, Cell MicroControls, VA) under the microfluidic device, and set the temperature to 41 °C. We used an epifluorescent microscope equipped with a FITC filter cube, and connected to a coupled charge device (CCD) camera. Illumination was provided by a 100 W short-arc mercury lamp (102DH, Ushio, Japan). We acquired images of the reservoir at regular intervals of 30 s, and computed the fluorescence intensity using custom MATLAB (R2012a, Mathworks, MA) scripts.

In Figure 6.7a, we show images of the reservoir prior to and after RPA. We found that fluorescence increased significantly due to RPA, indicating successful amplification. In

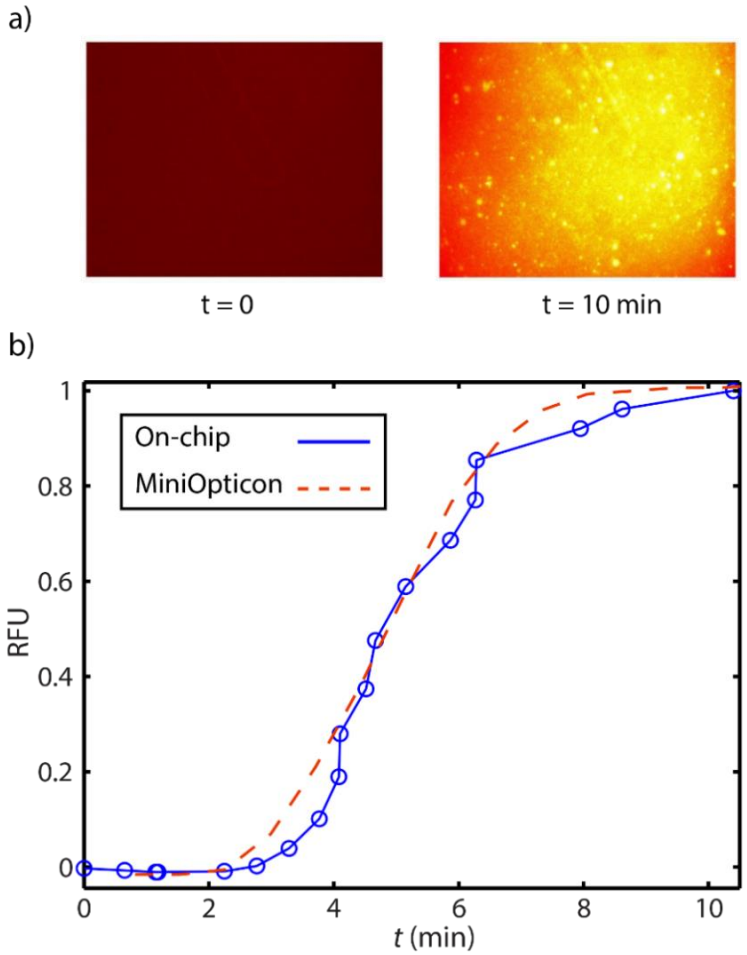

Figure 6.7. Feasibility demonstration of on-chip amplification using RPA. a) Images of fluorescence signal before and after RPA. Fluorescence increases significantly after amplification. We placed an Indium-Tin-Oxide (ITO) heater equipped with a microcontroller under the microfluidic device to provide suitable incubation temperature for RPA. b) Comparison of on-chip amplification with MiniOpticon thermal cycler, using 2.5 pg/µL purified *L. Monocytogenes* genomic DNA. We normalized each curve by its maximum value, and plot against amplification time. We find good agreement between the shape and time scale of both curves. This preliminary data suggests on-chip amplification may be a promising approach for further iterations of this work.

Figure 6.7b, we compare on-chip amplification with data obtained from MiniOpticon thermal cycler. For these experiments, we used 2.5 pg/µL purified *L. Monocytogenes* genomic DNA. We normalized each curve by its maximum value, and plot against amplification time. The two curves are very consistent confirming that RPA detection

on chip is feasible can be performed without the use of a dedicated real-time PCR machine. There remain several challenges with automating RPA detection on microfluidic devices. Evaporation, though not as significant as in PCR assays, remains an issue. Another is the need to add magnesium acetate immediately prior to initiating amplification. This issue may be addressed through custom lyophilized formulations in which the entire master mix is rehydrated immediately prior to amplification, similar to Borysiak et al.[62] Nevertheless, with further improvements, we believe that integrating ITP with on-chip RPA detection is promising and has potential in point-of-care (POC) applications, where limited resources necessitate increased device portability.

6.4 Summary

We demonstrated a novel assay for the lysis, extraction, and detection of *L. Monocytogenes* bacteria in whole blood. We used an ITP-compatible lysis method capable of lysing difficult-to-lyse, gram-positive bacteria. We performed two versions of the assay: First, an ITP purification of total DNA from whole blood starting with bacterial DNA spiked into whole blood, and, second, ITP purification starting with *L. Monocytogenes* spiked into whole blood. Our lysis, extraction, and on-chip purification is completed in a total of less than 50 min (about 40 min of that time on chip), and requires minimal user intervention. We then transferred purified DNA to a standard off-chip RPA assay. The LOD for bacterial DNA spiked into blood was 16.7 fg/μL (corresponding to about 5×10^3 bacterial cells per ml). The LOD for bacteria spiked into blood was 2×10^4 cells/mL. We attribute the latter higher LOD to imperfect lysing and perhaps lowering of ITP extraction efficiency. Assay sensitivity could be further

improved by improving lysis protocol, using a higher-throughput microfluidic device, or perhaps incorporating species-specific target capture/enrichment into the assay. Our assay is amenable to automation and may have potential for point-of-care applications. For example, we hypothesize that both lysis and RPA and detection can be performed within chip reservoirs using an integrated heater (and showed preliminary data in Section 6.3.8).

Our assay can be extended for the detection of other species, including gram-positive and gram-negative bacteria in whole blood. ITP purification has potential to expand the applicability of RPA to blood samples.

7 Conclusions, contributions, and recommendations

In this chapter, we summarize the main conclusions and contributions of the work presented in this dissertation. We also present recommendations for future work, including ideas that are significant extensions of this work.

7.1 Summary of major contributions

Accumulation and reaction rates in ITP

1. We developed an analytical model that intuitively describes accumulation and reaction rates to guide ITP assay design.
2. We introduced and discussed key parameters that guide the optimal design of ITP assays.
3. We analytically showed a quasi-equilibrium regime wherein reaction rates equal accumulation rates of reactants in ITP.

DNA detection using ITP and ionic spacer

1. We developed a two-stage hybridization assay that leverages ITP to enhance DNA hybridization kinetics and an ionic spacer to separate reaction products. Our approach is a liquid-phase separation method that is simple to implement in a microfluidic channel. Our technique produced two ITP-focused peaks, which is amenable to further downstream processing.
2. We demonstrated this approach using 26 nt DNA probe and 149 nt DNA target under relatively low stringency conditions. We achieved a 220 fM limit of detection (approximately 0.1 fg of DNA) within 10 minutes, with a linear dynamic range of nearly 4 orders of magnitude.

Protein detection using ITP and ionic spacer

1. We devised an approach to recruit non-focusing target into ITP using high-mobility SOMAmer probes. This extends ITP reaction assays to non-focusing targets such as other proteins and low-mobility species.
2. We developed a numerical and analytical model to describe ITP-spacer assays with a non-focusing target, and discuss key parameters in the design of such assay.
3. We characterized the sensitivity of our assay and achieved a clinically-relevant 2 nM limit of detection with 20 min assay time. We also explored the extension of this assay to diluted serum sample spiked with CRP, and discussed challenges and limitations of ITP-based protein assays in serum.

Size-based RNA fractionation using ITP and ionic spacer

1. We developed a rapid technique to perform size-based RNA fractionation by combining ITP with an ionic spacer in high-concentration sieving matrix. This is the first demonstrated size-based RNA fractionation in ITP.
2. We demonstrated this approach using synthetic DNA and RNA samples, and analyzed extracted fractions using commercial electrophoresis system.

Purification and detection of bacteria in blood using ITP and RPA

1. We demonstrated an approach that enables lysis, extraction, and detection of *L. Monocytogenes* cells using ITP and RPA detection. Our approach shows the potential for ITP purification to extend the applicability of RPA to whole blood samples.

2. We designed an ITP-compatible alkaline and proteinase K lysis buffer for rapid and effective lysis of inactivated *L. Monocytogenes* cells.
3. We first validated our assay using genomic DNA spiked into whole blood, then with inactivated *L. Monocytogenes* cells spiked into whole blood, and were able to detect as little as 2×10^4 cells/mL from whole blood.

7.2 Summary of conclusions

Accumulation and reaction rates in ITP

1. At sufficiently long times or high excess species concentration, reaction rate in ITP depends solely on the accumulation rate of the limiting species.
2. Under aggressive but experimentally achievable ITP buffer concentrations and mobilities, it is possible to improve accumulation rate by more than order of magnitude through optimal sample placement.
3. For large channels, sample depletion from well-stirred TE reservoir is significant and cannot be neglected.
4. For applications in which nucleic acids are placed in a sieving matrix, level of sieving and resulting change in effective electrophoretic mobility determines ideal sample placement.
5. Our model and analysis are applicable to both cationic and anionic peak-mode ITP assays, covering a wide range of species.

DNA detection using ITP and ionic spacer

1. The ITP-spacer technique is able to detect 3500-fold less target than probe, indicating that it is an effective strategy for background signal removal.

2. High-concentration linear polymer HEC is an effective sieving matrix, and 1.8% w/v was an effective compromise between fast resolution of peaks and reproducibility of the assay.
3. Theoretically, this approach should be able to resolve any amount of target present. Practically, it is limited by reaction kinetics as well as negative control signal, which we hypothesize is due to probe impurities.
4. This approach is easily tunable for the detection of targets of different sizes, by changing the type and concentration of sieving matrix, or the spacer species.

Protein detection using ITP and ionic spacer

1. Binding of SOMAmer probe to CRP target sufficiently increases CRP mobility to recruit it into ITP, while significantly slowing down SOMAmer mobility to create a large differential between mobility of unreacted and bound SOMAmer.
2. Mobility differential between unreacted and bound SOMAmer is sufficiently large to allow separation in free solution, without the use of a sieving matrix.
3. Under simplifying assumptions of probe concentration greatly exceeding target concentration, fraction of bound target is described by a modified Damköhler number that relates advection and reaction rates.
4. Titration experiments showed a limit of detection of 2 nM and a dynamic range of nearly 3 orders of magnitude. The limit of detection is well within the clinically-relevant range of CRP and demonstrates the potential of our assay.
5. Serum presents several challenges for protein detection using ITP and spacers, due to its high protein content and the presence of several anions that can form plateau mode zones in ITP.

Size-based RNA fractionation using ITP and ionic spacer

1. Buffering reservoirs consisting of a pipette tip filled with buffer and agarose to prevent leaking provide sufficient buffering capacity and prevent bubbles from entering channel.
2. Size cutoff can be turned by changing sieving matrix type and concentration as well as spacer species.
3. Our assay recovered majority of sample input and resulted in largely pure fractions, compatible with downstream analysis through Agilent Bioanalyzer.

Purification and detection of bacteria in blood using ITP and RPA

1. Consistent with previous observations, whole blood samples inhibit RPA. ITP purification enables successful amplification by excluding contaminants from extracted sample.
2. Alkaline and proteinase K lysis is compatible with ITP chemistry, and successful in lysis of inactivated *L. Monocytogenes* cells.
3. Proteinase K is essential for purification of genomic DNA from whole blood. When excluded from lysis buffer, no successful amplification was observed.
4. Lysis, extraction, and on-chip purification can be completed in a total of less than 50 min (about 40 min of that on chip), and requires minimal user intervention.
5. Our assay can be extended for the purification and detection of other bacterial species in whole blood.

7.3 Recommendations for future work

We here recommend future work including ideas for significant extensions of the current work.

Accumulation and reaction rates in ITP

1. We recommend extending the accumulation and reaction model to capture pH and ionic strength effects, further increasing its utility in ITP assay design.
2. Experimental validation of our accumulation and reaction model would assess its predictive power and potentially identify more interesting regimes where experiments deviate from analytical calculations.

DNA detection using ITP and ionic spacer

1. Extending our ITP and spacer approach for acceleration of DNA hybridization assays to detect 16S rRNA in urine would be important to assess the applicability of this technique to clinical samples, and its potential to enhance UTI detection.
2. Our assay suffered from a small amount of negative signal. We believe that sensitivity could further be improved by using probes of higher purity and longer channel lengths to allow more time for hybridization reactions.
3. Currently, TE buffer choices are made through trial and error. Designing a database with known DNA mobilities under different sieving conditions as well as TE mobilities at various pH levels, would greatly streamline buffer selection and enable more guided assay design.

Protein detection using ITP and ionic spacer

1. Applying our assay to a SOMAmer-protein pair with higher affinity than the CRP-SOMAmer and CRP target might result in higher sensitivity and better performance.
2. We believe that the performance of our ITP and spacer assay in serum is negatively affected by the high protein content of serum. We believe that we can improve its performance by integrating an on-chip albumin removal step, possibly through selective capture with antibodies or aptamers.

Size-based RNA fractionation using ITP and ionic spacer

1. With additional separation length and further optimization of sieving matrix and spacer, we believe that our size-based RNA fractionation approach could result in entirely pure fractions.
2. We recommend further study of manual pipette extraction, and evaluation of its efficiency and yield.

Purification and detection of bacteria in blood using ITP and RPA

1. Using a microfluidic device that can process a large volume (200 μL or more) of sample and further optimizing lysis protocol would improve the sensitivity of our integrated ITP-RPA assay by one or more orders of magnitude.
2. Currently, lysis and RPA are performed off-chip. However, both steps could conceivably be performed in microfluidic reservoirs. Integrating lysis, ITP purification, and RPA detection on a microfluidic chip would greatly improve the applicability of our assay to point-of-care settings.

3. We believe our integrated ITP-RPA assay can be extended for the purification and detection of other bacterial and viral species in whole blood. For example, the assay could be used for multiplexed detection of several bacterial or viral species by using RPA probes that fluoresce in different wavelengths.
4. ITP can be leveraged to accelerate enzymatic reactions, such as RPA itself, or other amplification steps, and further reduce assay times.

We hope that this work and these recommendations inspire future researchers to continue exploring ITP and its distinct advantages in the context of bioanalytical assays.

REFERENCES

(1) Persat, A.; Santiago, J. G. *Anal. Chem.* **2011**, *83*, 2310-6.

(2) Bercovici, M.; Kaigala, G. V.; Mach, K. E.; Han, C. M.; Liao, J. C.; Santiago, J. G. *Anal. Chem.* **2011**, *83*, 4110-7.

(3) Bercovici, M.; Han, C. M.; Liao, J. C.; Santiago, J. G. *Proc Natl Acad Sci U S A* **2012**, *109*, 11127-32.

(4) Han, C. M.; Katilius, E.; Santiago, J. G. *Lab Chip* **2014**, *14*, 2958-67.

(5) Kawabata, T.; Wada, H. G.; Watanabe, M.; Satomura, S. *Electrophoresis* **2008**, *29*, 1399-406.

(6) Park, C. C.; Kazakova, I.; Kawabata, T.; Spaid, M.; Chien, R. L.; Wada, H. G.; Satomura, S. *Anal Chem* **2008**, *80*, 808-14.

(7) Schwartz, O.; Bercovici, M. *Anal Chem* **2014**, *86*, 10106-13.

(8) Marshall, L. A.; Wu, L. L.; Babikian, S.; Bachman, M.; Santiago, J. G. *Anal Chem* **2012**, *84*, 9640-5.

(9) Stellwagen, N. C.; Stellwagen, E. *J Chromatogr A* **2009**, *1216*, 1917-29.

(10) Marshall, L. A.; Rogacs, A.; Meinhart, C. D.; Santiago, J. G. *J Chromatogr A* **2014**, *1331*, 139-42.

(11) Persat, A.; Marshall, L. A.; Santiago, J. G. *Anal Chem* **2009**, *81*, 9507-11.

(12) Landegren, U.; Kaiser, R.; Caskey, C. T.; Hood, L. *Science* **1988**, *242*, 229-37.

(13) Gooding, J. J. *Electroanalysis* **2002**, *14*, 1149-1156.

(14) Fitts, R.; Diamond, M.; Hamilton, C.; Neri, M. *Appl Environ Microbiol* **1983**, *46*, 1146-51.

(15) Surinova, S.; Schiess, R.; Huttenhain, R.; Cerciello, F.; Wollscheid, B.; Aebersold, R. *J Proteome Res* **2011**, *10*, 5-16.

(16) Gerszten, R. E.; Carr, S. A.; Sabatine, M. *Clin Chem* **2010**, *56*, 194-201.

(17) Mariella, R., Jr. *Biomed Microdevices* **2008**, *10*, 777-84.

(18) Acinas, S. G.; Sarma-Rupavtarm, R.; Klepac-Ceraj, V.; Polz, M. F. *Appl Environ Microbiol* **2005**, *71*, 8966-9.

(19) Teles, F. R. R.; Fonseca, L. R. *Talanta* **2008**, *77*, 606-623.

(20) Hegde, P.; Qi, R.; Abernathy, K.; Gay, C.; Dharap, S.; Gaspard, R.; Hughes, J. E.; Snesrud, E.; Lee, N.; Quackenbush, J. *Biotechniques* **2000**, *29*, 548-50, 552-4, 556 passim.

(21) Cheung, V. G.; Morley, M.; Aguilar, F.; Massimi, A.; Kucherlapati, R.; Childs, G. *Nat Genet* **1999**, *21*, 15-9.

(22) Shi, T.; Fillmore, T. L.; Sun, X.; Zhao, R.; Schepmoes, A. A.; Hossain, M.; Xie, F.; Wu, S.; Kim, J. S.; Jones, N.; Moore, R. J.; Pasa-Tolic, L.; Kagan, J.; Rodland, K. D.; Liu, T.; Tang, K.; Camp, D. G., 2nd; Smith, R. D.; Qian, W. J. *Proc Natl Acad Sci U S A* **2012**, *109*, 15395-400.

(23) Liotta, L. A.; Petricoin, E. F. *Clin Chem* **2010**, *56*, 1641-2.

(24) Jayasena, S. D. *Clin Chem* **1999**, *45*, 1628-50.

(25) Chen, Y.; Guo, Z.; Wang, X.; Qiu, C. *J Chromatogr A* **2008**, *1184*, 191-219.

(26) Jung, B.; Bharadwaj, R.; Santiago, J. G. *Anal Chem* **2006**, *78*, 2319-27.

(27) Everaerts, F. M.; Beckers, J. L.; Verheggen, T. P. E. M. *Isotachophoresis : theory, instrumentation, and applications*; Elsevier Scientific Pub. Co.: Amsterdam ; New York, 1976, p xiv, 418 p.

(28) Khurana, T. K.; Santiago, J. G. *Anal. Chem.* **2008**, *80*, 6300-7.

(29) Rogacs, A.; Marshall, L. A.; Santiago, J. G. *J Chromatogr A* **2014**, *1335*, 105-20.

(30) Chen, C. H.; Lin, H.; Lele, S. K.; Santiago, J. G. *Journal of Fluid Mechanics* **2005**, *524*, 263-303.

(31) MacInnes, D. A.; Longsworth, L. G. *Chemical Reviews* **1932**, *11*, 171-230.

(32) Martin, A. J. P.; Everaert.Fm. *Proceedings of the Royal Society of London Series a-Mathematical and Physical Sciences* **1970**, *316*, 493-&.

(33) Kohlrausch, W. *Verhandlungen Der Deutschen Gesellschaft Fur Kreislaufforschung* **1951**, *17*, 303-305.

(34) Alberty, J. *Klin Wochenschr* **1950**, *28*, 786-7.

(35) Jovin, T. M. *Biochemistry* **1973**, *12*, 871-9.

(36) Bercovici, M.; Kaigala, G. V.; Santiago, J. G. *Anal Chem* **2010**, *82*, 2134-8.

(37) Bercovici, M.; Kaigala, G. V.; Backhouse, C. J.; Santiago, J. G. *Anal Chem* **2010**, *82*, 1858-66.

(38) Chambers, R. D.; Santiago, J. G. *Anal Chem* **2009**, *81*, 3022-8.

(39) Jacroux, T.; Bottenus, D.; Rieck, B.; Ivory, C. F.; Dong, W. J. *Electrophoresis* **2014**, *35*, 2029-38.

(40) Stover, F. S. *J Chromatogr* **1988**, *445*, 417-23.

(41) Thormann, W.; Arn, D.; Schumacher, E. *Electrophoresis* **1985**, *6*, 10-18.

(42) Oshurkova, O. V.; Gorshkov, A. I. *Uspekhi Khimii* **1993**, *62*, 774-787.

(43) Bahga, S. S.; Chambers, R. D.; Santiago, J. G. *Anal Chem* **2011**, *83*, 6154-62.

(44) Bahga, S. S.; Han, C. M.; Santiago, J. G. *Analyst* **2013**, *138*, 87-90.

(45) Qu, Y.; Marshall, L. A.; Santiago, J. G. *Anal. Chem.* **2014**, *86*, 7264-8.

(46) Stellwagen, N. C.; Gelfi, C.; Righetti, P. G. *Biopolymers* **1997**, *42*, 687-703.

(47) Goet, G.; Baier, T.; Hardt, S. *Lab Chip* **2009**, *9*, 3586-93.

(48) Tyagi, S.; Kramer, F. R. *Nat Biotechnol* **1996**, *14*, 303-8.

(49) Garcia-Schwarz, G.; Santiago, J. G. *Anal. Chem.* **2012**, *84*, 6366-9.

(50) Garcia-Schwarz, G.; Santiago, J. G. *Angew Chem Int Ed Engl* **2013**, *52*, 11534-7.

(51) Karsenty, M.; Rubin, S.; Bercovici, M. *Anal Chem* **2014**, *86*, 3028-36.

(52) Shintaku, H.; Palko, J. W.; Sanders, G. M.; Santiago, J. G. *Angew Chem Int Ed Engl* **2014**, *53*, 13813-6.

(53) Shkolnikov, V.; Santiago, J. G. *Anal. Chem.* **2014**, *86*, 6220-8.

(54) Shkolnikov, V.; Santiago, J. G. *Anal. Chem.* **2014**, *86*, 6229-36.

(55) Kagebayashi, C.; Yamaguchi, I.; Akinaga, A.; Kitano, H.; Yokoyama, K.; Satomura, M.; Kurosawa, T.; Watanabe, M.; Kawabata, T.; Chang, W.; Li, C.; Bousse, L.; Wada, H. G.; Satomura, S. *Anal Biochem* **2009**, *388*, 306-11.

(56) Khnouf, R.; Goet, G.; Baier, T.; Hardt, S. *Analyst* **2014**, *139*, 4564-71.

(57) Moghadam, B. Y.; Connelly, K. T.; Posner, J. D. *Anal Chem* **2015**, *87*, 1009-17.

(58) Catsimpoolas, N.; Kenney, J. *Biochim Biophys Acta* **1972**, *285*, 287-92.

(59) Bier, M.; Cuddeback, R. M.; Kopwillem, A. *J Chromatogr* **1977**, *132*, 437-50.

(60) Caslavska, J.; Gebauer, P.; Thormann, W. *Electrophoresis* **1994**, *15*, 1167-75.

(61) Schoch, R. B.; Ronaghi, M.; Santiago, J. G. *Lab Chip* **2009**, *9*, 2145-52.

(62) Borysiak, M. D.; Kimura, K. W.; Posner, J. D. *Lab Chip* **2015**, *15*, 1697-707.

(63) Kondratova, V. N.; Serd'uk, O. I.; Shelepov, V. P.; Lichtenstein, A. V. *Biotechniques* **2005**, *39*, 695-9.

(64) Kondratova, V. N.; Serdyuk, O. I.; Shelepov, V. P.; Potapova, G. I.; Likhtenshtein, A. V. *Dokl Biochem Biophys* **2005**, *402*, 200-3.

(65) Baumler, H.; Donath, E.; Krabi, A.; Knippel, W.; Budde, A.; Kiesewetter, H. *Biorheology* **1996**, *33*, 333-51.

(66) Smith, B. A.; Ware, B. R.; Weiner, R. S. *Proc Natl Acad Sci U S A* **1976**, *73*, 2388-91.

(67) Physicians, A. C. o., 2015.

(68) Opel, K. L.; Chung, D.; McCord, B. R. *J Forensic Sci* **2010**, *55*, 25-33.

(69) Marshall, L. A.; Han, C. M.; Santiago, J. G. *Anal Chem* **2011**, *83*, 9715-8.

(70) Rogacs, A.; Qu, Y.; Santiago, J. G. *Anal Chem* **2012**, *84*, 5858-63.

(71) Tsui, N. B. Y.; Ng, E. K. O.; Lo, Y. M. D. *Clinical Chemistry* **2002**, *48*, 1647-1653.

(72) Rubin, S.; Schwartz, O.; Bercovici, M. *Physics of Fluids* **2014**, *26*.

(73) Garcia-Schwarz, G.; Bercovici, M.; Marshall, L. A.; Santiago, J. G. *Journal of Fluid Mechanics* **2011**, *679*, 455-475.

(74) Persat, A.; Santiago, J. G. *Curr Opin Colloid Interface Sci* **2016**.

(75) Bercovici, M.; Lele, S. K.; Santiago, J. G. *J Chromatogr A* **2009**, *1216*, 1008-18.

(76) Bahga, S. S.; Bercovici, M.; Santiago, J. G. *Electrophoresis* **2010**, *31*, 910-9.

(77) Persat, A.; Chambers, R. D.; Santiago, J. G. *Lab Chip* **2009**, *9*, 2437-53.

(78) Bocek, P.; Gebauer, P.; Dolnik, V.; Foret, F. *J Chromatogr* **1985**, *334*, 157-95.

(79) Marshall, L. *Designing automated systems for sample preparation of nucleic acids using isotachophoresis*. Stanford University2013.

(80) Saifer, A.; Corey, H. *J Biol Chem* **1955**, *217*, 23-30.

(81) Persat, A.; Suss, M. E.; Santiago, J. G. *Lab Chip* **2009**, *9*, 2454-69.

(82) Ellington, A. D.; Szostak, J. W. *Nature* **1990**, *346*, 818-22.

(83) Tuerk, C.; Gold, L. *Science* **1990**, *249*, 505-10.

(84) Gold, L.; Ayers, D.; Bertino, J.; Bock, C.; Bock, A.; Brody, E. N.; Carter, J.; Dalby, A. B.; Eaton, B. E.; Fitzwater, T.; Flather, D.; Forbes, A.; Foreman, T.; Fowler, C.; Gawande, B.; Goss, M.; Gunn, M.; Gupta, S.; Halladay, D.; Heil, J.; Heilig, J.; Hicke, B.; Husar, G.; Janjic, N.; Jarvis, T.; Jennings, S.; Katilius, E.; Keeney, T. R.; Kim, N.; Koch, T. H.; Kraemer, S.; Kroiss, L.; Le, N.; Levine, D.; Lindsey, W.; Lollo, B.; Mayfield, W.; Mehan, M.; Mehler, R.; Nelson, S. K.; Nelson, M.; Nieuwlandt, D.; Nikrad, M.; Ochsner, U.; Ostroff, R. M.; Otis, M.; Parker, T.; Pietrasiewicz, S.; Resnicow, D. I.; Rohloff, J.; Sanders, G.; Sattin, S.; Schneider, D.; Singer, B.; Stanton, M.; Sterkel, A.; Stewart, A.; Stratford, S.; Vaught, J. D.; Vrkljan, M.; Walker, J. J.; Watrobka, M.; Waugh, S.; Weiss, A.; Wilcox, S. K.; Wolfson, A.; Wolk, S. K.; Zhang, C.; Zichi, D. *PLoS One* **2010**, *5*, e15004.

(85) Rohloff, J. C.; Gelinas, A. D.; Jarvis, T. C.; Ochsner, U. A.; Schneider, D. J.; Gold, L.; Janjic, N. *Mol. Ther. Nucleic Acids* **2014**, *3*, e201.

(86) German, I.; Buchanan, D. D.; Kennedy, R. T. *Anal. Chem.* **1998**, *70*, 4540-5.

(87) Pavski, V.; Le, X. C. *Anal. Chem.* **2001**, *73*, 6070-6.

(88) Zhao, Q.; Li, X. F.; Le, X. C. *Anal. Chem.* **2008**, *80*, 3915-20.

(89) Wang, L.; Ma, W.; Chen, W.; Liu, L.; Ma, W.; Zhu, Y.; Xu, L.; Kuang, H.; Xu, C. *Biosens. Bioelectron.* **2011**, *26*, 3059-62.

(90) Wang, J.; Zhang, Y.; Okamoto, Y.; Kaji, N.; Tokeshi, M.; Baba, Y. *Analyst* **2011**, *136*, 1142-7.

(91) Cheow, L. F.; Han, J. *Anal. Chem.* **2011**, *83*, 7086-93.

(92) Garcia-Schwarz, G.; Rogacs, A.; Bahga, S. S.; Santiago, J. G. *J Vis Exp* **2012**, e3890.

(93) Martin, A. J.; Everaerts, F. M. *Anal. Chim. Acta.* **1967**, *38*, 233-7.

(94) Khurana, T. K.; Santiago, J. G. *Anal. Chem.* **2008**, *80*, 279-86.

(95) Eid, C.; Garcia-Schwarz, G.; Santiago, J. G. *Analyst* **2013**, *138*, 3117-20.

(96) Hellman, L. M.; Fried, M. G. *Nat. Protoc.* **2007**, *2*, 1849-61.

(97) Ruscher, K.; Reuter, M.; Kupper, D.; Trendelenburg, G.; Dirnagl, U.; Meisel, A. *J. Biotechnol.* **2000**, *78*, 163-70.

(98) Kraemer, S.; Vaught, J. D.; Bock, C.; Gold, L.; Katilius, E.; Keeney, T. R.; Kim, N.; Saccomano, N. A.; Wilcox, S. K.; Zichi, D.; Sanders, G. M. *PLoS One* **2011**, *6*, e26332.

(99) Clyne, B.; Olshaker, J. S. *J. Emerg. Med.* **1999**, *17*, 1019-25.

(100) Ridker, P. M.; Haughie, P. *J. Investig. Med.* **1998**, *46*, 391-5.

(101) de Beer, F. C.; Hind, C. R.; Fox, K. M.; Allan, R. M.; Maseri, A.; Pepys, M. B. *Br. Heart J.* **1982**, *47*, 239-43.

(102) Pepys, M. B.; Hirschfield, G. M. *J. Clin. Invest.* **2003**, *111*, 1805-12.

(103) Lee, M. H.; Lee, D. H.; Jung, S. W.; Lee, K. N.; Park, Y. S.; Seong, W. K. *Nanomedicine* **2010**, *6*, 78-83.

(104) Potempa, L. A.; Maldonado, B. A.; Laurent, P.; Zemel, E. S.; Gewurz, H. *Mol. Immunol.* **1983**, *20*, 1165-75.

(105) Krebs, H. A. *Annu Rev Biochem* **1950**, *19*, 409-30.

(106) Psychogios, N.; Hau, D. D.; Peng, J.; Guo, A. C.; Mandal, R.; Bouatra, S.; Sinelnikov, I.; Krishnamurthy, R.; Eisner, R.; Gautam, B.; Young, N.; Xia, J.; Knox, C.;

Dong, E.; Huang, P.; Hollander, Z.; Pedersen, T. L.; Smith, S. R.; Bamforth, F.; Greiner, R.; McManus, B.; Newman, J. W.; Goodfriend, T.; Wishart, D. S. *PLoS One* **2011**, *6*, e16957.

(107) Travis, J.; Pannell, R. *Clin. Chim. Acta.* **1973**, *49*, 49-52.

(108) Steel, L. F.; Trotter, M. G.; Nakajima, P. B.; Mattu, T. S.; Gonye, G.; Block, T. *Mol. Cell. Proteomics* **2003**, *2*, 262-70.

(109) Baumberger, C.; Kinloch-de-Loes, S.; Yerly, S.; Hirschel, B.; Perrin, L. *AIDS* **1993**, *7 Suppl 2*, S59-64.

(110) El-Hefnawy, T.; Raja, S.; Kelly, L.; Bigbee, W. L.; Kirkwood, J. M.; Luketich, J. D.; Godfrey, T. E. *Clin. Chem.* **2004**, *50*, 564-73.

(111) Kopreski, M. S.; Benko, F. A.; Gocke, C. D. *Ann N Y Acad Sci* **2001**, *945*, 172-8.

(112) Mitchell, P. S.; Parkin, R. K.; Kroh, E. M.; Fritz, B. R.; Wyman, S. K.; Pogosova-Agadjanyan, E. L.; Peterson, A.; Noteboom, J.; O'Briant, K. C.; Allen, A.; Lin, D. W.; Urban, N.; Drescher, C. W.; Knudsen, B. S.; Stirewalt, D. L.; Gentleman, R.; Vessella, R. L.; Nelson, P. S.; Martin, D. B.; Tewari, M. *Proc Natl Acad Sci U S A* **2008**, *105*, 10513-8.

(113) Li, Y.; Elashoff, D.; Oh, M.; Sinha, U.; St John, M. A.; Zhou, X.; Abemayor, E.; Wong, D. T. *J Clin Oncol* **2006**, *24*, 1754-60.

(114) Wang, Z.; Gerstein, M.; Snyder, M. *Nat Rev Genet* **2009**, *10*, 57-63.

(115) McCoy, R. C.; Taylor, R. W.; Blauwkamp, T. A.; Kelley, J. L.; Kertesz, M.; Pushkarev, D.; Petrov, D. A.; Fiston-Lavier, A. S. *PLoS One* **2014**, *9*, e106689.

(116) Landgraf, P.; Rusu, M.; Sheridan, R.; Sewer, A.; Iovino, N.; Aravin, A.; Pfeffer, S.; Rice, A.; Kamphorst, A. O.; Landthaler, M.; Lin, C.; Socci, N. D.; Hermida, L.;

Fulci, V.; Chiaretti, S.; Foa, R.; Schliwka, J.; Fuchs, U.; Novosel, A.; Muller, R. U.; Schermer, B.; Bissels, U.; Inman, J.; Phan, Q.; Chien, M.; Weir, D. B.; Choksi, R.; De Vita, G.; Frezzetti, D.; Trompeter, H. I.; Hornung, V.; Teng, G.; Hartmann, G.; Palkovits, M.; Di Lauro, R.; Wernet, P.; Macino, G.; Rogler, C. E.; Nagle, J. W.; Ju, J.; Papavasiliou, F. N.; Benzing, T.; Lichter, P.; Tam, W.; Brownstein, M. J.; Bosio, A.; Borkhardt, A.; Russo, J. J.; Sander, C.; Zavolan, M.; Tuschl, T. *Cell* **2007**, *129*, 1401-14.

(117) SageScience.

(118) Munafo, D.; Sadaf, H.; Ettwiller, L.; Langhorst, B.; Dimalanta, E.; Stewart, F.; Boles, C. *New England BioLabs* **2014**.

(119) Fischer, S. G.; Lerman, L. S. *Proc Natl Acad Sci U S A* **1983**, *80*, 1579-83.

(120) Bearman, G. M.; Wenzel, R. P. *Arch Med Res* **2005**, *36*, 646-59.

(121) Seifert, H. *Clin Infect Dis* **2009**, *48 Suppl 4*, S238-45.

(122) Reimer, L. G.; Wilson, M. L.; Weinstein, M. P. *Clin Microbiol Rev* **1997**, *10*, 444-65.

(123) Schrader, C.; Schielke, A.; Ellerbroek, L.; Johne, R. *J Appl Microbiol* **2012**, *113*, 1014-26.

(124) Bessetti, J. *Promega Corporation Profiles in DNA* **2007**.

(125) Piepenburg, O.; Williams, C. H.; Stemple, D. L.; Armes, N. A. *PLoS Biol* **2006**, *4*, e204.

(126) Lillis, L.; Siverson, J.; Lee, A.; Cantera, J.; Parker, M.; Piepenburg, O.; Lehman, D. A.; Boyle, D. S. *Mol Cell Probes* **2016**, *30*, 74-8.

(127) Kersting, S.; Rausch, V.; Bier, F. F.; von Nickisch-Rosenegk, M. *Malar J* **2014**, *13*, 99.

(128) Abd El Wahed, A.; El-Deeb, A.; El-Tholoth, M.; Abd El Kader, H.; Ahmed, A.; Hassan, S.; Hoffmann, B.; Haas, B.; Shalaby, M. A.; Hufert, F. T.; Weidmann, M. *PLoS One* **2013**, *8*, e71642.

(129) Krolov, K.; Frolova, J.; Tudoran, O.; Suhorutsenko, J.; Lehto, T.; Sibul, H.; Mager, I.; Laanpere, M.; Tulp, I.; Langel, U. *J Mol Diagn* **2014**, *16*, 127-35.

(130) Rohrman, B.; Richards-Kortum, R. *Anal. Chem.* **2015**, *87*, 1963-7.

(131) Swaminathan, B.; Gerner-Smidt, P. *Microbes Infect* **2007**, *9*, 1236-43.

(132) Rudbeck, L.; Dissing, J. *Biotechniques* **1998**, *25*, 588-90, 592.

(133) Brewster, J. D.; Paoli, G. C. *Anal Biochem* **2013**, *442*, 107-9.

(134) TwistAmp® exo +ListeriaM Quick Guide. http://www.twistdx.co.uk/images/uploads/docs/QG_EXOLIST_online_RevB.pdf

(135) Schuler, F.; Schwemmer, F.; Trotter, M.; Wadle, S.; Zengerle, R.; von Stetten, F.; Paust, N. *Lab Chip* **2015**, *15*, 2759-66.

(136) Hoffman, L.; Jarvis, B. W. **2003**.

(137) NATtrol - Molecular Controls - ZeptoMetrix Corporation. http://www.zeptometrix.com/store/nattrola-molecular-controls/

A Design notes for design of ITP experiments

ITP assay design involves the careful balancing of several parameters. LE and TE buffers and concentrations, channel geometry, pH levels, and other factors all influence assay outcomes, and must be selected carefully. Below we summarize these factors and their impact on ITP assay design. We add a few pieces of advice specific to the design of anionic ITP assays involving biological sample species.

Leading ion: LE is typically chosen to be a high-mobility species that readily separates from sample and TE species. When sample species are mixed into the LE buffer, it is advantageous to choose an LE with high mobility in order to rapidly resolve the different species. LE also contributes to the properties of the adjusted TE (ATE) zone, which in turn affects sample focusing. Chloride is a commonly-used LE for anionic ITP applications, due to its high mobility and its compatibility and presence in many biological samples.

Trailing ion: TE is typically chosen to be a weak acid, with mobility that is highly dependent on the intended application. When sample ions are mixed into the TE, choice of TE has significant consequence on ITP focusing rates. TE's with low mobility will focus sample species at a higher rate, but are also more likely to focus contaminant species. At higher mobilities, TE's will exclude most contaminants but will also focus sample at a lower rate. Furthermore, sample dispersion is often observed when TE mobility is very close to that of the sample.

Channel dimensions: Channel geometry plays a significant role in the design of an ITP experiments. In finite injection mode, channels with small dimensions can process small sample volumes. In infinite injection, small channels are characterized by low extraction efficiencies. Furthermore, channels with width or height of less than 20 μm are susceptible to clogging when working with cell-containing samples. Larger channel volumes result in increased extraction efficiency and sample processing volume. However, larger dimensions introduce new issues to be addressed. In devices with large channel-to-reservoir volumes, buffering capacity becomes more challenging, requiring higher concentration of reservoir LE and TE buffers. Joule heating is also a bigger challenge at larger channel volumes, which limits applied voltage or current. For more rigorous discussion of the effects of channel dimensions on ITP assays, we refer interested readers to Marshall's dissertation.[1]

Initial LE and TE concentrations and ionic strength: LE and TE concentrations can greatly influence ITP assays. Separation capacity, the amount of charge a channel can hold, is proportional to the ion concentration in the channel. This is key for evaluating the ability of an ITP system to effectively separate ions, and is discussed in greater detail in Rogacs et al.[2] Furthermore, Bahga et al.[3] observed that low ionic strength resulted in reduced separation and peak resolution. However, high ionic strength reduces observed electrophoretic mobility, an effect that is more strongly experienced by polyionic species like nucleic acids and proteins.[4]

For semi-infinite injection mode ITP, sample focusing rate is maximized at high LE concentration and low TE concentration. We recommend that this ratio is maximized while maintaining buffering capacity of TE reservoir.

pH: Selection of pH in ITP experiments is largely tied to the choice of counterion. pH greatly affects mobility of TE, LE, and sample species.[5] In Figure A.1, we show the dependence of commonly used TE species on pH. We also include sample MATLAB code for calculating the electrophoretic mobility of a mono or di-valent weak acid as a function of pH. When working with complex biological samples, biological compatibility should be considered at low and high pH values. For instance, proteins have very low solubility at pH levels near their isoelectric points, and might aggregate and interfere with ITP processes. pH also impacts electroosmotic flow (EOF) mobility for glass and other surfaces.[6]

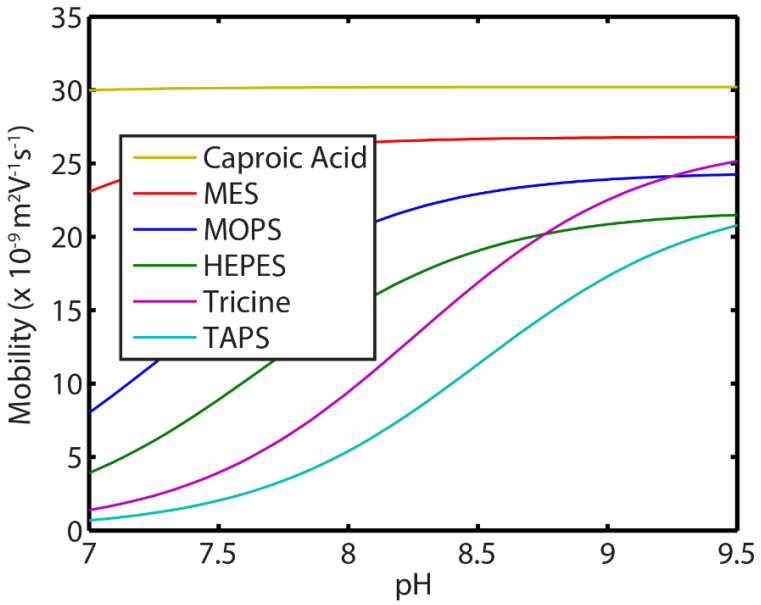

Figure A.1. Mobility of weak acids depends heavily on buffer pH. We show how pH affects predicted electrophoretic mobility of several commonly-used weak-acid TE species. Choice of TE and resulting pH are coupled and important to consider in the design of ITP assays.

Spacer ion: For ITP assays that also include a spacer ion, the spacer's mobility should be chosen such that it rapidly separates from both the buffer in which it is initially incubated (LE or TE buffers) and the two resulting ITP fractions.

In Table A.1, we summarize effect of various ITP design parameters on sample focusing in ITP, and add some considerations that determine the range of allowable values.

Table A.1. Effect of design parameters on ITP assays.

Parameter	**Effect on ITP focusing**	**Considerations at low values**	**Considerations at high values**
LE mobility (μ_{LE})	↑	Sample species resolve at low rates.	
TE mobility (μ_{TE})	↓	Must be sufficiently high to exclude contaminants.	Sample focusing rate will be lower, sample dispersion may occur.
Ionic strength	↓	Low separation and peak resolutions are observed at low ionic strengths.	High ionic strength reduces observed mobility. This effect is stronger for polyionic species (like nucleic acids and proteins), which reduces focusing in ITP.
Cross-sectional area (A)	↑	Low extraction efficiency and increased potential for obstruction of channel.	Buffering capacity of LE and TE buffers becomes a significant constraint. Joule heating is another significant issue.
Ratio of LE and TE concentrations (c_{LE}/c_{TE})	↑	Low sample accumulation rates, resulting from lower sample concentration in adjusted TE zone.	Buffering capacity of TE reservoir.
pH	↑ (Anionic ITP)	In anionic ITP, sample species may become positively charged and not focus in ITP. Compatibility with biological species, protein aggregation.	Compatibility with biological species.

Sample MATLAB code for TE mobility vs pH

```
close all

%TE's (in that order): MOPS, HEPES, MES, TAPS, Tricine,Caproic Acid
mob_full = [24.4 21.8 26.8 22.9 26.6 30.2];
valence= [1 1 1 1 1 1];
pKa = [7.31 7.66 6.21 8.51 8.26 4.86];

pH_i = 6; pH_f = 10;

for i = 1:length(mob_full)
    [pH(i,:) mob_pH(i,:)] =
mobility_vs_pH(mob_full(i),valence(i),pKa(i), pH_i, pH_f);
end

figure
plot(pH(1,:),mob_pH(1,:))
hold all
for i = 2:size(pH,1)
    plot(pH(i,:), mob_pH(i,:))
end
plotCE()
legend('MOPS','HEPES','MES','TAPS','Tricine','Caproic Acid')
xlabel('pH');ylabel('Mobility');


function [pH mob_pH] = mobility_vs_pH(mob_full,valence,pKa,pH_i,pH_f)

pH = linspace(pH_i,pH_f,100);
mob_pH = [];

if valence == 1
    for i = 1:size(pH,2)
        mob_pH(i) = mob_full(1)/(1+10^(pKa(1)-pH(i)));
    end
elseif valence == 2
    for i = 1:size(pH,2)
        mob_pH(i) = mob_full(1)+mob_full(2)*10^(pH(i)-pKa(2))/(1 +
10^(pH(i)-pKa(2))+10^(pKa(1)-pH(i)));
    end
else
    disp('Valence is not 1 or 2');
end

end
```

REFERENCES

(1) Marshall, L. *Designing automated systems for sample preparation of nucleic acids using isotachophoresis*. Stanford University2013.

(2) Rogacs, A.; Marshall, L. A.; Santiago, J. G. *J Chromatogr A* **2014**, *1335*, 105-20.

(3) Bahga, S. S.; Bercovici, M.; Santiago, J. G. *Electrophoresis* **2010**, *31*, 910-9.

(4) Persat, A.; Chambers, R. D.; Santiago, J. G. *Lab on a Chip* **2009**, *9*, 2437-2453.

(5) Persat, A.; Suss, M. E.; Santiago, J. G. *Lab on a Chip* **2009**, *9*, 2454-2469.

(6) Milanova, D.; Chambers, R. D.; Bahga, S. S.; Santiago, J. G. *Electrophoresis* **2012**, *33*, 3259-62.

B Design notes for ITP-spacer assays

Assays that couple ITP preconcentration with spacer ions and sieving matrices for separation, like the work presented in Chapters 3 and 5, require the careful balancing of several additional parameters. Here we briefly discuss a few important and tunable design factors in ITP-spacer assays.

Sieving matrix type and concentration. Selecting an appropriate sieving matrix is a very important and difficult decision in assay design. A selected sieving matrix needs to have good sieving performance, be compatible with the intended sample, easy to load into microfluidic channels, and not interfere with ITP dynamics. Effect of sieving matrix on sample mobility could be difficult to predict a priori. For nucleic acids, however, several publications have characterized the effect of different sieving matrices and sieving matrix concentrations on observed electrophoretic mobility. We recommend that users interested in the design of such assays refer to existing literature to help guide their sieving matrix selection.[1-3]

In Figure B.1, we show the performance of the assay we presented in Chapter 3 for different concentrations of PVP sieving matrix. At low sieving matrix concentrations (5%), the two peaks are not resolved in the available separation channel length. At higher PVP concentrations (8%), we see good resolution between the two peaks. We note that at high sieving matrix concentration, solutions becomes significantly more viscous and thus harder to pipette and load into microfluidic devices. We recommend using the lowest concentration of sieving matrix that achieves the desired fractionation.

Spacer ion concentration. As discussed in Chapter 1, in plateau-mode ITP, the length of sample zone grows in length, not concentration. Therefore, tuning the amount of

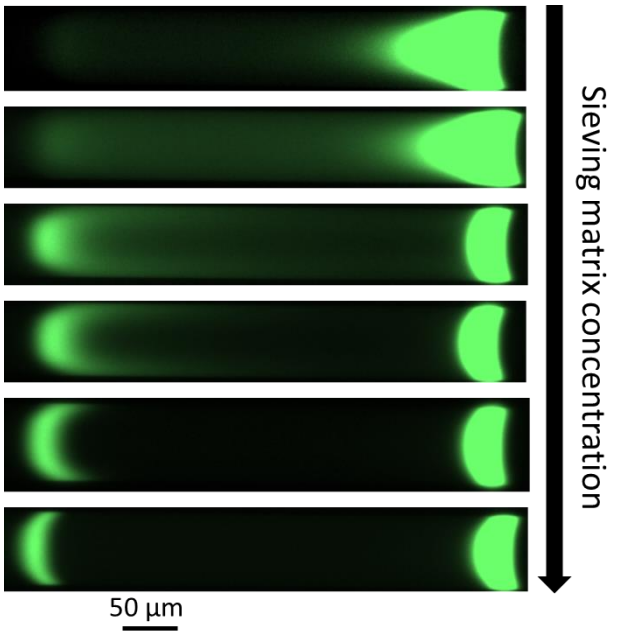

Figure B.1. Sieving matrix concentration affects resolution of peaks in ITP-spacer assays. We show results from assay presented in Chapter 3 using different concentrations of PVP as sieving matrix (5% to 8%). At low PVP concentration, almost no separation is observed between the two peaks. In contrast, at high PVP concentration, the two peaks are clearly resolved, indicating significantly improved sieving performance.

spacer ion added changes the length of the spacer zone. As the length of the spacer zone changes, the length of separation channel required to resolve the two peaks changes as well, as does the resolution of the peaks. Balancing the rates of spacer zone growth and peak resolution is described in Chapter 4, and particularly eqs 4.10-4.12. In Figure B.2, we show how changing the concentration of MOPS (the spacer ion used in Chapter 3), changes observed spacer zone length.

Choice of spacer and TE ions. The choice of spacer ion is particularly difficult and highly tied to the choice and concentration of sieving matrix. In Chapter 3, the spacer

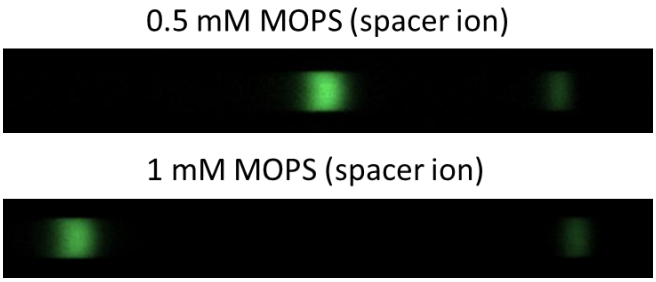

Figure B.2. Tuning spacer ion concentration also tunes the resulting spacer zone length. As discussed in Chapter 1, sample zone in plateau-mode ITP grows in length with additional sample. Spacer zone length affects the separation channel length required to fully fractionate the two peaks. Therefore, available channel geometry should be considered when choosing initial spacer ion concentration.

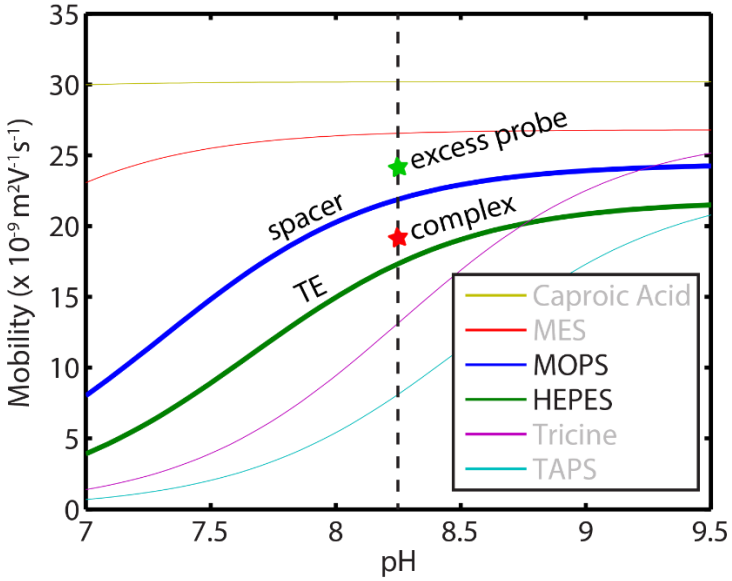

Figure B.3. Choice of spacer ion is challenging and must meet several criteria. We show how mobility of commonly-used weak-acid species varies with pH, and highlight MOPS and HEPES, which were chosen as spacer and TE ions, respectively, for the work presented in Chapter 3. Choice of spacer ion is highly coupled to sieving matrix used, and to the pH level of the LE and TE zones. It also has to meet several mobility criteria to both focus and separate the reactants and reaction products.

is also highly dependent on the sample ions being separated, as well as the expected pH of the LE and TE zones. As with choosing sieving matrix, we recommend consulting

existing literature (if any exists) for guidance on the expected electrophoretic mobility of sample ions.

In Table B1, we summarize the characteristics of the ITP-spacer assays presented in chapter 3, 4, and 5. We used SPRESSO software to simulate ITP experiments and obtain pH in the adjusted TE (ATE) and LE zones as well as TE and spacer mobilities. For all assays, the spacer was initially mixed into the TE, so we show its mobility in the ATE zone.

Table B1. Summary of assays presented in Chapters 3, 4, and 5 of this dissertation. All mobilities are in units of 10^{-9} $m^2V^{-1}s^{-1}$.

Chapter	Species separated	Sieving matrix	TE (mobility in ATE)	Spacer (mobility in ATE)	ATE pH	LE pH
3	27 nt ssDNA 27 nt + 149 nt ssDNA	1.8% HEC	HEPES (16)	MOPS (19)	8.5	8.2
4	unreacted SOMAmer SOMAmer + protein	None	Tricine (10)	HEPES (13.5)	7.9	7.1
5	Mixture of ssDNA and RNA	2.5% HEC	HEPES (17.5)	Aspartic acid (28)	8.4	8.1

REFERENCES

(1) Stellwagen, N. C.; Gelfi, C.; Righetti, P. G. *Biopolymers* **1997**, *42*, 687-703.

(2) Bunz, A. P.; Barron, A. E.; Prausnitz, J. M.; Blanch, H. W. *Industrial & Engineering Chemistry Research* **1996**, *35*, 2900-2908.

(3) Song, J. M.; Yeung, E. S. *Electrophoresis* **2001**, *22*, 748-754.

C Voltage and current monitoring during ITP experiments

ITP assays are typically performed under constant voltage or constant current. The rates of many ITP processes are proportional to applied current, making analysis easier when constant current is applied. There are, however, situations in which constant voltage is preferred, such as equipment and packaging limitations and precision levels. For further discussion on constant voltage vs constant current, we refer interested readers to Rogacs et al..[1] In Figure C1 below, we show sample results for an ITP assay performed at constant voltage, and one at constant current.

Constant voltage experiments are characterized by decreasing observed current, as low-conductivity TE buffer continuously replaces high-conductivity LE buffer. In the channel, decreased current results in continuously decreasing ITP velocity. Towards the end of the experiment, the curve flattens and reaches a plateau, indicating that the experiment is near end. In constant current experiments, voltage continuously increases linearly, again as low-conductivity TE replaces high-conductivity. Here, however, ITP velocity and many other processes proceed at a constant rate. We note that nearly zero current in constant voltage experiments or rapidly increasing and device threshold voltages in constant current experiments indicate an open circuit. This may be due to electrodes not making contact with the buffer reservoirs or to evaporation, drying, or blockage in the channel. We recommend that the power source be immediately turned off before further investigation.

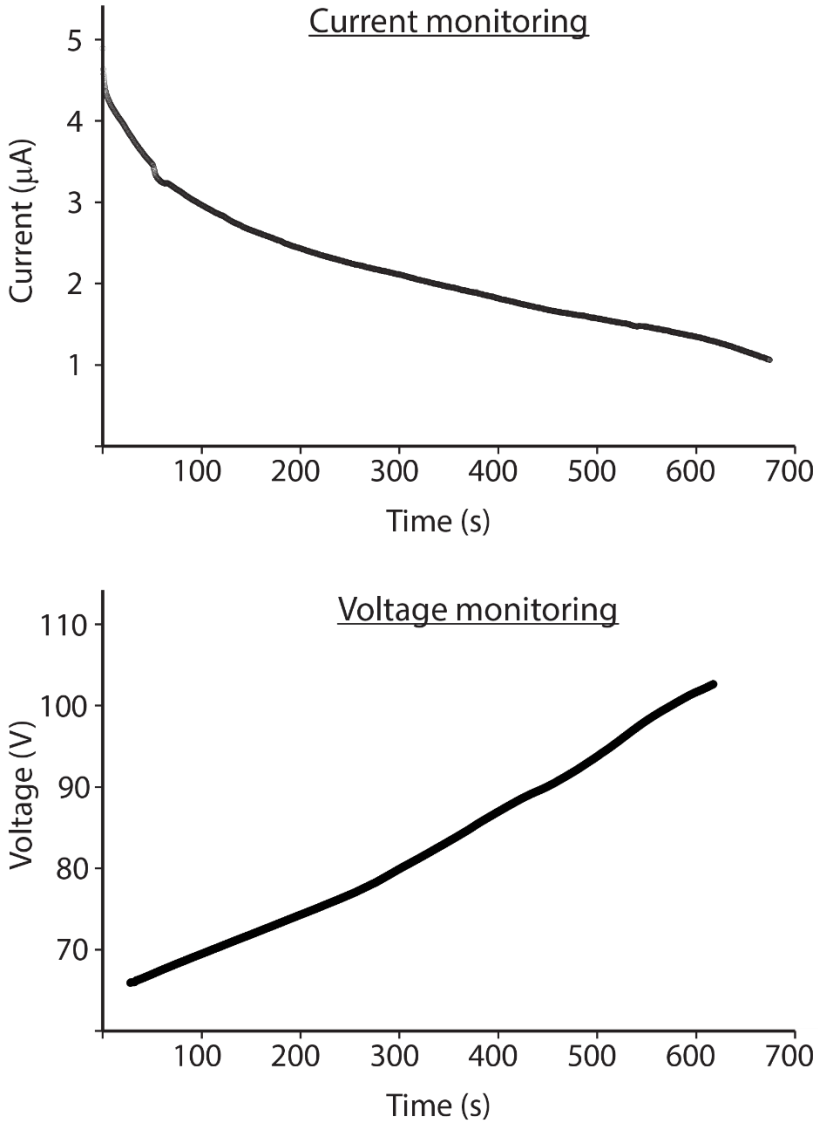

Figure C1. Voltage and current monitoring in ITP experiments. In the top plot, we monitor current for ITP experiments performed at constant voltage. In the bottom plot, we monitor voltage for constant current ITP experiments. Both plots were obtained using MATLAB script for data acquisition from Keithley 2410 power sources.

Monitoring voltage and current using MATLAB

It is possible and often advantageous to use MATLAB to monitor voltage and current in order to track ITP assay progress. We typically use Keithley or Labsmith power sources, which both come with API's that are compatible with MATLAB scripts. The

earliest versions of voltage and current monitoring MATLAB scripts were written by Moran Bercovici, and have since been adapted and modified for different applications. We recommend interested users to refer to manufacturers' websites and technical support resources for the latest resources on integrating power source equipment with MATLAB and other software monitoring tools.

REFERENCES

(1) Rogacs, A.; Marshall, L. A.; Santiago, J. G. *J Chromatogr A* **2014**, *1335*, 105-20.

D Strategies for successful ITP experiments

Strategies for reducing electroosmotic flow (EOF)

It is often desirable to suppress the effects of EOF in ITP experiments. In anionic ITP, EOF acts in the direction opposite to sample migration. If untreated, EOF often reverses the direction of ITP progress and complete disrupts ITP assays. As a result, several methods have been designed to effectively suppress EOF effects. We highlight several of the most commonly used methods. In Table D1, we summarize these methods and include references for further exploration.

- **PVP**. One of the most effective and commonly used methods to suppress EOF is through the use of non-ionic polymer polyvinylpyrrolidone (PVP). PVP vey effectively suppresses EOF at various concentrations, and is highly compatible with ITP chemistries as well as most biological samples. The Santiago group has often used 1% PVP as a typical EOF suppression method, though several papers have included significantly lower concentrations (highlighted in Table D1). Shintaku et al.[1] observed that PVP conentrations above 0.4% caused significant sieving when genomic DNA was present. Milanova et al.[2] found that increasing PVP concentration beyond 0.5% produced negligible improvement in EOF suppression.
- **Pluronic F-127**. Pluronic is a temperature-sensitive polymer that is liquid at cold temperatures but solidifies into a gel at room temperature and higher. While effective at both sieving and suppressing EOF,[3,4] using Pluronic requires experienced, rapid handling.

- **Sigmacote**. Sigmacote is a silanizing agent that can be used to pretreat glass microchannels. We highlight that Sigmacote cannot be included in LE or TE buffer, unlike PVP. A thorough protocol, such as that outlined by Persat et al.,[5] should be followed for optimal results.
- **EOTrol**. Though no published ITP assays have used EOTrol as a primary EOF suppression method, we nevertheless used it several times to reduce EOF, to good success.
- **Other sieving matrices**. We note that polymers and other sieving matrices will also affect EOF, to varying levels. We recommend consulting the literature for more information on EOF suppression performance of particular sieving matrices.
- **Buffer pH**. Milanova et al.[2] found that pH impacts the effect of PVP on EOF. Specifically, they found that PVP was much more effective at low pH (6.6) than at high pH (10.3). Furthermore, at high pH, increasing PVP concentration resulted in no observable improvement in EOF suppression.

Table D.1 Summary of EOF suppression methods in ITP assays by the Santiago group. We include selected references for further discussion.

EOF suppression method	Selected references
Sigmacote	5,6
Pluronic F-127	3,4,7
PVP, 1%	8-14
PVP, <0.5%	1,15-17

Channel conditioning prior to and between ITP experiments

The most commonly used method for channel conditioning and rinsing is serial washes with 1M NaOH, 1M HCl, and 1M DI water. We recommend washing for 2 minutes for clean buffers, and more for complex buffers. We also recommend washing with 10% bleach between runs to minimize cross-contamination when working with biological samples. When working with PDMS devices, include Triton X-100 (0.1% or higher) in all wash buffers in order to minimize bubble formation in the hydrophobic PDMS channels.

If clogging is observed between experiments, we recommend vacuuming from nearby reservoirs using water, NaOH, and HCl in succession to help dislodge the clogging specimen. Emptying the channel and vacuuming with air may also be effective.

Strategies for reducing surface adsorption

Sample adsorption to channel walls is a persistent problem in ITP assays that involve biological specimen. Both nucleic acids and proteins can adsorb to surfaces, significantly reducing extraction efficiency. When working with complex samples like serum or blood, adsorption is particularly prevalent. We recommend a few strategies to minimize sample adsorption.

- When possible, we suggest limiting the number of experiments performed on a single device. We have observed that treating surfaces with chemicals like Sigmacote or EOTrol helps to minimize adsorption when working with serum samples.

- Adding nonionic surfacants like Tween-20 or Triton X-100 solubilizes proteins, preventing their aggregation and reducing their likelihood to adsorb to channel surfaces.
- Adding Bovine Serum Albumin (BSA) is another commonly-used approach to reduce nucleic acid adsorption to channel walls. This approach is only compatible with a subset of assays, as BSA itself may focus in ITP.
- Members of our lab have found that using PDMS instead of glass microchannels significantly reduces nucleic acid adsorption. We note that this is not widely accepted in the literature.
- Thoroughly rinsing channels between uses is the simplest and possibly most effective method to rid the walls of biological debris. In our experience, repeated and extended washes with 1M NaOH and 1M HCl are often sufficient to maintain high performance and greatly prolong the lifetime of a microfluidic device.

REFERENCES

(1) Shintaku, H.; Palko, J. W.; Sanders, G. M.; Santiago, J. G. *Angew Chem Int Ed Engl* **2014**, *53*, 13813-6.

(2) Milanova, D.; Chambers, R. D.; Bahga, S. S.; Santiago, J. G. *Electrophoresis* **2012**, *33*, 3259-62.

(3) Schoch, R. B.; Ronaghi, M.; Santiago, J. G. *Lab Chip* **2009**, *9*, 2145-52.

(4) Marshall, L. A.; Rogacs, A.; Meinhart, C. D.; Santiago, J. G. *J Chromatogr A* **2014**, *1331*, 139-42.

(5) Persat, A.; Marshall, L. A.; Santiago, J. G. *Anal. Chem.* **2009**, *81*, 9507-11.

(6) Marshall, L. A.; Han, C. M.; Santiago, J. G. *Anal Chem* **2011**, *83*, 9715-8.

(7) Qu, Y.; Marshall, L. A.; Santiago, J. G. *Anal. Chem.* **2014**, *86*, 7264-8.

(8) Rogacs, A.; Qu, Y.; Santiago, J. G. *Anal. Chem.* **2012**, *84*, 5858-63.

(9) Bercovici, M.; Kaigala, G. V.; Mach, K. E.; Han, C. M.; Liao, J. C.; Santiago, J. G. *Anal. Chem.* **2011**, *83*, 4110-7.

(10) Eid, C.; Garcia-Schwarz, G.; Santiago, J. G. *Analyst* **2013**, *138*, 3117-20.

(11) Eid, C.; Palko, J. W.; Katilius, E.; Santiago, J. G. *Anal. Chem.* **2015**, *87*, 6736-43.

(12) Bahga, S. S.; Han, C. M.; Santiago, J. G. *Analyst* **2013**, *138*, 87-90.

(13) Persat, A.; Chivukula, R. R.; Mendell, J. T.; Santiago, J. G. *Anal Chem* **2010**, *82*, 9631-5.

(14) Persat, A.; Santiago, J. G. *Anal. Chem.* **2011**, *83*, 2310-6.

(15) Bercovici, M.; Han, C. M.; Liao, J. C.; Santiago, J. G. *Proc Natl Acad Sci U S A* **2012**, *109*, 11127-32.

(16) Kuriyama, K.; Shintaku, H.; Santiago, J. G. *Electrophoresis* **2015**, *36*, 1658-62.

(17) Han, C. M.; Katilius, E.; Santiago, J. G. *Lab Chip* **2014**, *14*, 2958-67.

E Designing oligonucleotide target for RPA experiments

Here, we describe an approach to design representative synthetic oligonucleotide targets for recombinase polymerase amplification (RPA). We used the TwistAmp exo+ *ListeriaM* kit from TwistDx.[1] This kit came with pre-designed primers and a probe, with sequences given in:[2]

Forward primer: CGCCTGCAAGTCCTAAGACGCCAATCGAAAAGAAAC

Reverse primer: CTGCATCTCCGTGGTATACTAATACATTGTTTTTA

Probe: CGAAAAGAAACACGCGGATGAAATCGATAAG[FAM][THF][BHQ-1]ATACAAGGATTGGA

This kit seeks to detect the virulent *hly* gene, which is unique to hazardous Listeria strains. Using FASTA, we find the partial sequence of the gene, and highlight the primer (yellow) and probe (blue) sequences.

Partial *hly* gene nucleotide sequence:

http://www.ncbi.nlm.nih.gov/nuccore/345287428?from=2180&to=3769&sat=4&sat_key=61906099&report=fasta

ATGAAAAAAATAATGCTAGTTTTTATTACACTTATATTAATTAGTCTACCA
ATTGCGCAACAAACTGAAGCAAAGGATGCATCTGCATTCAATAAAGAAAA
TTCAATTTCATCCATGGCACCACCAGCATCTCCGCCTGCAAGTCCTAAGAC
GCCAATCGAAAAGAAACACGCGGATGAAATCGATAAGTATATACAAGGAT
TGGATTACAATAAAAACAATGTATTAGTATACCACGGAGATGCAGTGACA
AATGTGCCGCCAAGAAAAGGTTACAAAGATGGAAATGAATATATCGTTGT

GGAGAAAAAGAAGAAATCCATCAATCAAAATAATGCAGACATCCAAGTTG
TAAATGCAATTTCGAGCCTAACTTATCCAGGTGCTCTCGTAAAAGCGAATT
CGGAATTAGTAGAAAATCAACCAGATGTTCTCCCTGTAAAACGTGATTCAT
TAACACTTAGCATCGATTTGCCAGGAATGACTAA

Using this information, we designed an oligonucleotide target, synthesized by Integrated DNA Technologies, with the following sequence:

CGCCTGCAAGTCCTAAGACGCCAATCGAAAAGAAACACGCGGATGAAATC
GATAAGTATATACAAGGATTGGATTACAATAAAAACAATGTATTAGTATA
CCACGGAGATGCAG

REFERENCES

(1) TwistAmp® exo +ListeriaM Quick Guide. http://www.twistdx.co.uk/images/uploads/docs/QG_EXOLIST_online_RevB.pdf

(2) Schuler, F.; Schwemmer, F.; Trotter, M.; Wadle, S.; Zengerle, R.; von Stetten, F.; Paust, N. *Lab on a Chip* **2015**, *15*, 2759-2766.